2016-03-01

Evaluation of Passive Force on Skewed Bridge Abutments with Controlled Low-Strength Material Backfill

Kevin Bjorn Wagstaff
Brigham Young University - Provo

Evaluation of Passive Force on Skewed Bridge Abutments with Controlled Low-Strength Material Backfill

Kevin Bjorn Wagstaff

A thesis submitted to the faculty of
Brigham Young University
in partial fulfillment of the requirements for the degree of

Master of Science

Kyle M. Rollins, Chair
Kevin W. Franke
W. Spencer Guthrie

Department of Civil Engineering

Brigham Young University

March 2016

ABSTRACT

Evaluation of Passive Force on Skewed Bridge Abutments with Controlled Low-Strength Material Backfill

Kevin Bjorn Wagstaff
Department of Civil Engineering, BYU
Master of Science

Although its use has become more widespread, controlled low-strength material, or CLSM, has fallen through the crack between geotechnical engineering and materials engineering research. The National Ready Mix Association states that CLSM is not a low strength concrete, and geotechnical engineers do not consider it as a conventional aggregate backfill. The use of CLSM as a bridge abutment backfill material brings up the need to understand the passive force versus backwall displacement relationship for this application.

To safely account for forces generated due to seismic activity and thermal expansion in bridge design, it is important to understand the passive force versus backwall displacement relationship. Previous researchers have pointed out the fallacy of designing skewed bridges the same as non-skewed bridges. They observed that as the bridge skew angle increases, the peak passive force is significantly diminished which could lead to poor or even unsafe performance. The literature agrees that a displacement of 3-5% of the wall height is required to mobilize the peak passive resistance. The shape of the passive force displacement curve is best represented as hyperbolic in shape, and the Log Spiral method has been confirmed to be the most accurate at predicting the peak passive force and the shape of the failure plane. All of the previous research on this topic, whether full-scale field tests or large-scale laboratory tests, has been done with dense compacted sand, dense granular backfill, or computer modeling of these types of conventional backfill materials. However, the use of CLSM is increasing because of the product's satisfactory performance as a conventional backfill replacement and the time saving, or economic, benefits.

To determine the relationship of passive force versus backwall displacement for a CLSM backfilled bridge abutment, two laboratory large-scale lateral load tests were conducted at skew angles of 0 and 30°. The model backwall was a 4.13 ft (1.26 m) wide and 2 ft (0.61 m) tall reinforced concrete block skewed to either 0 or 30°. The passive force-displacement curves for the two tests were hyperbolic in shape, and the displacement required to reach the peak passive resistance was approximately 0.75-2% of the wall height. The effect of skew angle on the magnitude of passive resistance in the CLSM backfill was much less significant than for conventional backfill materials. However, within displacements of 4-5% of the backwall height, the passive force-displacement curve reached a relatively constant residual or ultimate strength. The residual strength ranged from 20-40% of the measured peak passive resistance. The failure plane did not follow the logarithmic spiral pattern as the conventional backfill materials did. Instead, the failure plane was nearly linear and the failed wedge was displaced more like a block with very low compressive strains.

Keywords: CLSM, backfill, passive force, abutment, backwall, residual strength

ACKNOWLEDGEMENTS

First, I thank the members of my graduate advisory committee, Kyle M. Rollins, W. Spencer Guthrie, and Kevin W. Franke. I am grateful for their extensive efforts in reviewing this thesis and helping me complete the project. I thank Kevin W. Franke for teaching me in Introductory and Advanced Soil Mechanics. His classes encouraged me to pursue a geotechnical project. I thank W. Spencer Guthrie for allowing me to use his laboratory and equipment and for aiding me in analyzing my gathered data. It was a blessing for me to be able to work with Kyle M. Rollins. I am thankful for the engineering knowledge he has passed on to me and even more for his great example of leadership, hard work, and dedication.

I thank my wife, Rachel, for her support throughout the process involved in completing this thesis. Her support and encouragement were invaluable. I also acknowledge the professionalism of the BYU laboratory technician staff. Dave Anderson, Rodney Mayo, and their student staff of Rawley Selk and Kyle Chavez were indispensable in the set-up, instrumentation, and completion of the laboratory tests. Special thanks to Rawley and Kyle for their help in the back-breaking, hand-blistering removal of the CLSM backfill for both tests. Also, a special thanks to Landon Kinney who partnered with me in this project for the first few months until being reassigned. His help and contributions made this thesis possible to complete.

Funding for this study was provided by an FHWA pooled-fund study supported by departments of transportation from the states of California, Minnesota, Montana, New York, Oregon, Utah, and Wisconsin. Utah served as the lead agency with David Stevens as the project manager. This support is gratefully acknowledged; however, the opinions, conclusions and recommendations in this paper do not necessarily represent those of the sponsoring organizations.

TABLE OF CONTENTS

LIST OF TABLES

LIST OF FIGURES

1 INTRODUCTION

Lateral earth pressure is an essential parameter to understand for the safe design of retaining walls, basement walls, anchor blocks, laterally loaded pile caps, and bridge abutment backwalls (Das 2014). The lateral earth pressures stabilize these structures and resist their movement and rotation. Passive lateral earth pressures are generated when structural elements are forced into the backfill material supporting them. In bridge design, an important parameter is the passive force-displacement relationship at the abutment backwall-backfill interface. This relationship provides an estimate of the amount of passive resistance supplied by the backfill material for a given amount of backwall displacement.

When thermal expansion or seismic loadings cause the backwall to displace into the backfill, the backfill is required to produce adequate support in the form of passive resistance. The bridge design practices currently in use assume that the peak passive force is the same for skewed bridges as for those that are non-skewed (AASHTO 2011). Research and field tests have clearly pointed out that this assumption is not valid. The previous observations and test results have shown that skewed bridges do not perform as well as non-skewed bridges when subjected to loads due to earthquakes (Elnashi 2010, Toro 2013) or thermal expansion (Sandford and Elgaaly 1993). All prior research on the passive force-displacement relationship has been done on abutments with a conventional sand or gravel backfill. The purpose of this research is to define the passive force-displacement relationship for bridge abutments using a backfill consisting of

controlled low-strength material (CLSM) and to assess the effect of bridge skew angle on that relationship.

1.1 Background

Previously, large-scale lateral load tests have been performed (Duncan and Mokwa 2001, Rollins and Sparks 2002, Rollins and Cole 2006, Lemnitzer et al. 2009) for the purpose of analyzing the passive force versus backwall displacement relationship for dense sand and gravel backfill against non-skewed bridge abutments. These tests evaluated the results of using the three most common passive earth pressure theories to calculate the peak passive pressure. They are the Coulomb (Coulomb 1776), Rankine (Rankine 1857), and Log Spiral (Terzaghi 1943) theories. The results from Duncan and Mokwa (2001), Rollins and Cole (2002), Rollins and Sparks (2006), and Lemnitzer et al. (2009) agree that the peak passive pressure generated in the backfill is most correctly predicted using the Log Spiral method. Rollins and Sparks (2006) noted that the Rankine method significantly underestimates the peak passive pressure, and the Coulomb method overestimates it. Furthermore, it was observed that the peak passive pressure was fully mobilized when the backwall longitudinal displacements were in the range of 3-5% of the backwall height (Rollins and Cole 2006). Duncan and Mokwa (2001) further concluded that the passive force versus longitudinal displacement relationship could be described using a hyperbolic shape. To make the design process simpler, most bridge design specifications use a bi-linear passive force versus longitudinal displacement relationship (AASHTO 2011, CalTrans 2010).

As mentioned previously, the bridge design practices currently in use assume that the peak passive force is the same for skewed bridges as for those that are non-skewed (AASHTO 2011).

Research and field tests have clearly pointed out that this is not the case. Several lateral load tests were done on skewed abutment backwalls to evaluate the effect of skew angle on the peak passive resistance (Rollins and Jessee 2012, Marsh 2013, Franke, 2013, Rollins et al. 2015). Also, numerical models were created to predict the outcomes of future lateral load tests with skewed abutments (Shamsabadi et al. 2006). In-service bridges were analyzed under thermal expansion and after earthquakes. The load tests and numerical models confirmed that the peak passive resistance was significantly reduced as the skew angle increased. It was also concluded that skewed bridges do not perform as well as non-skewed bridges when subjected to loads due to earthquakes (Elnashi 2010, Toro et al. 2013) or thermal expansion (Sandford and Elgaaly 1993, Steinberg et al. 2004). However, it was found that the displacement required to mobilize the peak passive resistance was still 3-5% of the wall height.

The previous research described above was performed using conventional sand and gravel backfill materials. However, CLSM has begun to be used as a cost effective and time saving replacement for these backfill materials on bridge abutment applications. No research has previously been done in regard to the passive force-displacement relationship for CLSM backfill. Using CLSM as a backfill has attractive possibilities, but the passive force-displacement relationship needs to be characterized for safe and efficient abutment design when using CLSM as the backfill material.

1.2 Research Objectives

The objectives of this research investigation are as follows:

1. Define bridge abutment passive force-deflection relationships for CLSM backfill from large-scale laboratory testing.

2. Determine the influence of skew angle on the passive resistance of CLSM backfill.
3. Develop simple design models based on laboratory tests and numerical simulations.
4. Characterize the strength behavior of CLSM.
5. Examine the failure plane shape for the lateral load tests on CLSM.

1.3 Order of Presentation

This section outlines the order of this thesis. First, the literature review describes the current state of knowledge with regards to the use and characteristics of CLSM. It also assesses the current state of knowledge of the passive force-displacement relationship for skewed and non-skewed bridge abutments. Finally, it describes the need for new research with regard to using CLSM as a bridge abutment backfill material. Next, the test layout and procedures and CLSM backfill properties are described. Following the test description, the test results are given in the order of passive force-displacement curves, backwall movement and rotation, variation of forces with skew angle, failure surface geometries, and backfill surface heave. The test results are then compared with numerical models to analyze the results. Finally, conclusions from the tests and numerical models are discussed and the need for additional research is outlined.

2 LITERATURE REVIEW

This chapter addresses the current state of knowledge relating to the passive force-deflection relationship for skewed bridge abutments using controlled low-strength material (CLSM) backfill. First, CLSM is defined and its properties and applications are discussed. Second, passive earth pressure theories are outlined. Third, non-skew passive force-deflection tests are presented. Fourth, the forces developed within a skewed bridge abutment structure are illustrated. Fifth, the results of passive force-deflection tests with skewed abutment backwalls are analyzed. Finally, the chapter concludes by discussing the current limitations in the state of knowledge on this subject and how they are to be incorporated into this study.

2.1 Controlled Low-Strength Material (CLSM)

CLSM is a self-leveling and self-consolidating cementitious fill typically used as an alternative to conventionally compacted aggregate backfill. It is also known as flowable fill, unshrinkable fill, liquid dirt, controlled density fill (CDF), and various other trademark names. It has been used in the construction industry since the 1960s (PCA 2015) on applications such as pipeline backfill, but it is currently used in backfill, pavement bases, structural bases, utility embedment, void fill, trenching, and repair fill applications (Puppala et al. 2007). There are many advantages to using CLSM fill on a project, and the American Concrete Institute (1999) summarizes these in Table 2-1.

Table 2-1. Cited Advantages of Controlled Low-Strength Materials (ACI 1999).

Readily available	Using locally available materials, ready-mixed concrete suppliers can produce CLSM to meet most project specifications.
Easy to deliver	Truck mixers can deliver specified quantities of CLSM to job site whenever material is needed.
Easy to place	Depending on type and location of void to be filled, CLSM can be placed by chute, conveyor, pump, or bucket. Because CLSM is self-leveling, it needs little or no spreading or compacting. This speeds construction and reduces labor requirements.
Versatile	CLSM mixtures can be adjusted to meet specific fill requirements. Mixes can be adjusted to improve flowability. More cement or fly ash can be added to increase strength. Admixtures can be added to adjust setting times and other performance characteristics. Adding foaming agents to CLSM produces lightweight, insulating fill.
Strong and durable	Load-carrying capacities of CLSM are typically higher than those of compacted soil or granular fill. CLSM is also less permeable, thus more resistant to erosion. For use as permanent structural fill, CLSM can be designed to achieve 28-day compressive strength as high as 8.3 MPa (1200 psi).
Allows fast return to traffic	Because many CLSMs can be placed quickly and support traffic loads within several hours, downtime for pavement repairs is minimal.
Will not settle	CLSM does not form voids during placement and will not settle or rut under loading. This advantage is especially significant if backfill is to be covered by pavement patch. Soil or granular fill, if not consolidated properly, may settle after a pavement patch is placed and forms cracks or dips in the road.
Reduces excavation costs	CLSM allows narrower trenches because it eliminates having to widen trenches to accommodate compaction equipment.
Improves worker safety	Workers can place CLSM in a trench without entering the trench, reducing their exposure to possible cave-ins.
Allows all-weather construction	CLSM will typically displace any standing water left in a trench from rain or melting snow, reducing need for dewatering pumps. To place CLSM in cold weather, materials can be heated using same methods for heating ready-mixed concrete.
Can be excavated	CLSM having compressive strengths of 0.3 to 0.7 MPa (50 to 100 psi) is easily excavated with conventional digging equipment, yet is strong enough for most backfilling needs.
Requires less inspection	During placement, soil backfill must be tested after each lift for sufficient compaction. CLSM self-compacts consistently and does not need this extensive field testing.
Reduces equipment needs	Unlike soil or granular backfill, CLSM can be placed without loaders, rollers, or tampers.
Requires no storage	Because ready-mixed concrete trucks deliver CLSM to job site in quantities needed, storing fill materials on site is unnecessary. Also, there is no leftover fill to haul away.
Makes use of coal combustion product	Fly ash is by-product produced by power plants that burn coal to generate electricity. CLSM containing fly ash benefits environment by making use of this industrial product material.

CLSM is a versatile product with a wide range of strengths and characteristics dependent on the application and mix design. It is made by mixing various amounts of portland cement, fine aggregate, coarse aggregate, and water, but some mix designs include fly ash or other industrial by-products and various admixtures to reduce the cement required. For a mix design including

fly ash with a targeted 28-day compressive strength of 75-150 psi (517-1034 kPa), the cement content is only 3-5 % by weight. A typical cement content for structural concrete is 10-15%, but fly ash or other cementitious substitutions can replace up to 50% of the cement. The American Concrete Institute (ACI) considers flowable fill as a low-strength material as long as the compressive strength is less than 1,200 psi (8270 kPa) (FHWA 1997, Gabr and Bowders 2000). However, lower strengths are often required to ensure that the fill can be excavated without excessive effort. As described in Table 2-1, CLSM can be placed with a chute, conveyor, pump, or bucket, and it requires little spreading or compacting when at the appropriate slump. In contrast, placement and compaction of a conventional backfill requires large amounts of energy from heavy equipment and personnel. Furthermore, CLSM is typically cured in the ambient environment (ACI 1999), whereas structural concrete typically requires some type of cover or moisturizing equipment to properly cure to its design strength.

2.1.1 Physical Properties

The majority of the benefits of CLSM come from its properties of flowability and excavatability. These two properties allow it to be a versatile and effective fill material in lieu of conventional aggregate backfill when conditions make standard compaction methods difficult or impossible.

2.1.1.1 Flowability

As its name implies, flowable fill is able to flow into, around, and between areas that would be difficult to consolidate and compact were conventional aggregate backfill to be used (Türkel 2007). This ease of placement is what helped initiate the use of CLSM as an effective backfill for utility lines, trenches, abandoned tunnels and manholes, and other difficult-to-reach

void spaces (ACI 1999). In some instances, flowable fill is the only possible alternative to achieve the desired results. The flowability is measured using the slump test according to ASTM C143 standards where the slump is specified to be 6-8 in. (150-200 mm) in order for the CLSM to consolidate under gravity flow only (FHWA 1997). Another test that is performed to measure flowability is the ASTM D6103 flow cone test. The fresh CSLM is placed into a 6 in. (0.15 m) tall, 3 in. (0.076 m) diameter cylinder, and the top is leveled off with a trowel. The cylinder is quickly lifted upwards, and the diameter of the spread-out CLSM specimen is measured. To have appropriate flowability and self-leveling capability, the diameter of the CLSM spread when emptied from the flow cone must be 8 in. (200 mm) as a minimum (FHWA 1997, Howard and Hitch 1998).

2.1.1.2 Excavatability

The excavatability of CLSM allows for the material to be excavated with relative ease, either by hand or using machinery, after placement, unlike typical structural concrete mixtures. The compressive strength of flowable fill material is specified to be in the range of 20-1200 psi (140- 8270 kPa), but the upper range is only used for applications where the fill is not likely to be removed. At strengths higher than approximately 300 psi (2070 kPa), excavation becomes akin to removing structural concrete. For this reason, many state DOT specifications call for CLSM mix designs with a design 28-day compressive strengths much less than this. The Portland Concrete Association (2015) states that the upper compressive strength limit for excavatable CLSM fill is 200 psi (1380 kPa). The Utah Department of Transportation (UDOT) and the National Ready Mixed Concrete Association specify a maximum compressive strength of 150 psi (1035 kPa) (NRMCA 2015) to keep CLSM fill excavatable. Finally, Howard and Hitch (1998) state that the maximum 28-day compressive strength should be less than 100 psi for

CLSM fill that will be excavated in the future. Though the specifications differ, they give a range of strengths that are assumed to be the upper limits of excavatability. Figure 2-1 shows a bar chart of the upper and lower specified unconfined compressive strength (UCS) limits for CLSM in the states sponsoring this study.

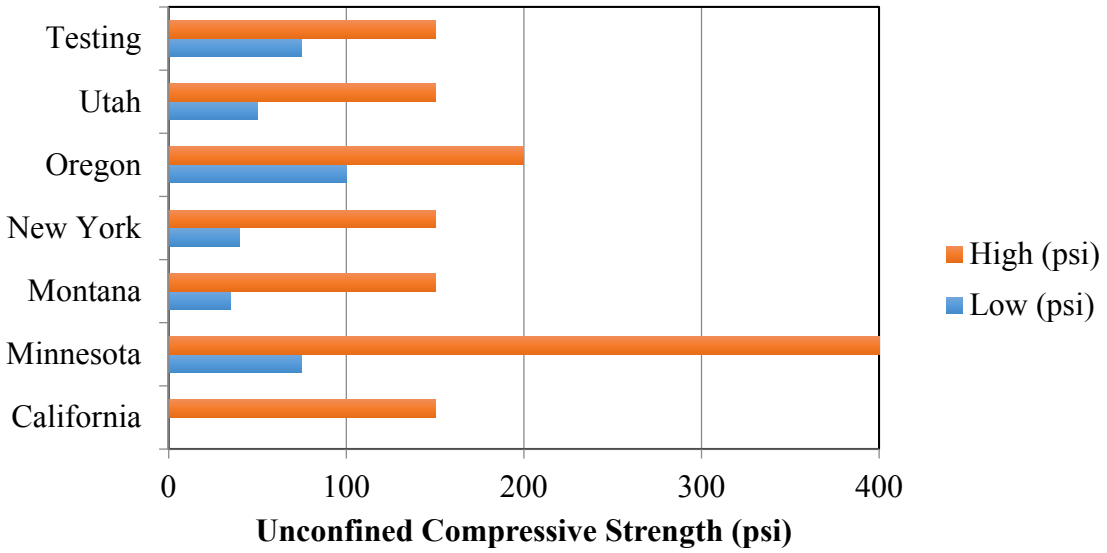

Figure 2-1. Limits of CLSM strengths for sponsor states.

2.1.2 Engineering Properties

The performance of CLSM lies between conventional aggregate backfill and structural concrete in most of the measured engineering properties. The cement content gives it higher strengths than aggregate backfill, but for most CLSM mix designs the cement content is much lower than that typically used for structural concrete and therefore yields lower strengths. Several of the engineering properties of CLSM are discussed in the following sections. The properties

that will be discussed are UCS, unit weight, hardening time, permeability, bleeding and shrinkage, bearing strength, modulus of subgrade reaction, and shear strength.

2.1.2.1 Unconfined Compressive Strength

The UCS of CLSM is tested in accordance with ASTM D4832 standards. Depending on the mix design and the desired application, the compressive strength can be as high as 1200 psi (8270 kPa). Depending on the type of aggregate used, conventionally compacted aggregate backfill can be compared to compressive strengths of 50-100 psi (345-690 kPa) (Rajendran 1994), but not in an unconfined state. CLSM can have compressive strength similar to that of regular aggregate backfill, but most mix designs and applications specify strengths that can be much greater. The difference in strengths is generally dependent on the cementitious material content of the mix design (Rajendran 1994). Higher cement content gives it higher strength, but some mix designs replace a portion of cement with fly ash to increase the workability. As mentioned before, 1200 psi (8270 kPa) is the industry threshold for the compressive strength of CLSM, whereas structural concrete is normally specified for strengths in the range of 3,000-4,000 psi (20.7-27.6 MPa).

The strains required to reach the peak passive force for conventional backfill material in bridge abutment applications has been agreed to be approximately 3-5% of the abutment backwall height. However, research on soil-cement used in deep mixing applications has shown that these strains are much lower for stabilized or cemented materials. In a UCS test, strains of less than 1% were generally exhibited at the peak UCS for soil-cemented materials (Filz et al. 2015, Kitazume and Terashi 2013). These smaller strains were attributed to the higher stiffness caused by the cementitious material. These materials are very similar in nature to CLSM.

2.1.2.2 Unit Weight

The unit weight, or density, of the in-place CLSM is quite similar to that of in-situ aggregate backfill but lower than that of conventional concrete (145 lb/ft^3 or 22.8 kN/m^3). The in-place unit weight depends on the weight of the filler or aggregate material. Typical mix designs using fly ash as the filler material have a unit weight of about 90-120 lb/ft^3 (1500-1900 kg/m^3); however, with the aid of foaming agents, CLSM densities have been lowered to 20 lb/ft^3 (325 kg/m^3) when reduced weight is required (PCA 2015). In contrast, the unit weight of conventional aggregate backfill with sand filler content is normally in the range of 115-145 lb/ft^3 (1900-2350 kg/m^3) (FHWA 1997).

2.1.2.3 Hardening and Curing Time

CLSM mixes containing 5% cement harden enough to support the weight of an average person within 1-4 hours. Within 24 hours, construction equipment is usually able to move across the CLSM without causing apparent damage to the CLSM surface (FHWA 1997). Increasing the cement content can also speed up the setting time of the CLSM. However, ambient temperature and water content in the surrounding soil can affect the setting time of the CLSM. In colder and wetter environments, the time to harden or set can be greatly increased (Schmitz et al. 2004).

Curing of CLSM is generally monitored using the same procedures applied to structural concrete. The 7-day strength of test cylinders gives an early strength estimate, and the 28-day strength is measured just as with structural concrete. However, the CLSM strength typically continues to increase over time, so the long-term strength should be monitored. This is especially the case when slow-reacting fly ash is included in the mix design. CLSM is generally cured

without any plastic sheeting or curing techniques (FHWA 1997). However, it should be insulated if exceedingly hot or cold temperatures will cause issues before it can set (Rajendran 1994).

2.1.2.4 Permeability

The permeability of CLSM mixes is dependent upon the amount of fly ash and cement content. In mixes with high fly ash content, the hydraulic conductivity values range from $2.8x10^{-3}$-$2.8x10^{-4}$ ft/day (10^{-6}-10^{-7} cm/sec), which would be similar to a compacted clay (Gabr and Bowders 2000). The low end of the range of permeability is in mixes with higher cement and fly ash content. Mixes with lower fly ash content have higher hydraulic conductivity values in the range of $2.8x10^{-1}$-$2.8x10^{-6}$ ft/day (10^{-4}-10^{-6} cm/sec), which is more typical of a compacted sandy silt (FHWA 1997).

2.1.2.5 Bleeding and Shrinkage

Bleeding and shrinkage is possible in CLSM mixtures with high water content. When the bleed water evaporates, lateral and vertical shrinkage can occur. This may be manifested on the surface by shrinkage cracks in the flowable fill. With cracks at the surface, water infiltrating the fill and creating freeze-thaw problems is the major concern. However, once the fill has set, no shrinkage or settlement will occur within the CLSM itself (FHWA 1997).

2.1.2.6 Bearing Strength

The bearing strength of the CLSM fill is directly related to the UCS. For example, a mix design with a 28-day UCS of 150 psi (1035 kPa) typically has a bearing strength of approximately 10 tons/ft^2 (9000 kg/m^2) (FHWA 1997). This is approximately three times greater than a well compacted aggregate backfill material.

2.1.2.7 Modulus of Subgrade Reaction

The modulus of subgrade reaction for most soils used in a rigid pavement design usually ranges from 50-300 lb/in^3 (8.2 to 49.2 N/cm^2) and is about 500 lb/in^3 (82 N/cm^2) for a quality granular subbase material (FHWA 1997). In contrast, the modulus of subgrade reaction for flowable fill is approximately 5000 lb/in^3 (820 N/cm^2). This high modulus makes it a suitable road base material.

2.1.2.8 Shear Strength

In triaxial shear strength testing, CLSM fill has shown internal friction angles ranging from 20-30° (FHWA 1997). The FHWA (1997) also reported cohesion of approximately 30-35% of the UCS. However, other researchers have found different results for the angle of shearing resistance because of the highly variable mix designs. Howard and Hitch (1998) found the friction angle to be a minimum of 38° at 16 hours for their CLSM mix design. They also stated that the cohesion increased from 0.2-6.3 psi (0.0014-0.043 MPa) from the 16-hour mark to 28 days. However, the angle of shearing resistance has been found to be in the range of 43-54° at 7 days, and the cohesion ranged from 5.4-7 psi (0.037-0.048 MPa) (Türkel 2007). According to Türkel (2007), the friction angles of CLSM are similar to those of medium-sized gravelly soil. The variations in the values found by these researchers are due to the different mix designs that were used in each study and the amount of time that each specimen was allowed to cure.

Another product very similar to CLSM is the deep-mixed soil-cement used in soil stabilization applications. This material is simply the native soil material mixed with a stabilizing agent consisting of typically lime or cement. Filz et al. (2015) reported that the cohesion value is generally estimated as 0.7 times 50% of the UCS. The authors stated that the 50% of the UCS

accounts for the shear strength of the material, and the 0.7 factor provides the mass strength in terms of the small-sample strength. The design process also assumes a friction angle of 0°. It was also commented that the shear strength of the soil-cement was unaffected by the consolidation pressure applied in the tests. (Filz et al. 2015, Kitazume and Terashi 2013). Filz et al. (2015) proposed a strength failure envelope with example values shown in Figure 2-2. The tension in the direct tension Mohr's circle for the soil-cement material was said to be estimated as 0.12*UCS (Filz et al. 2015).

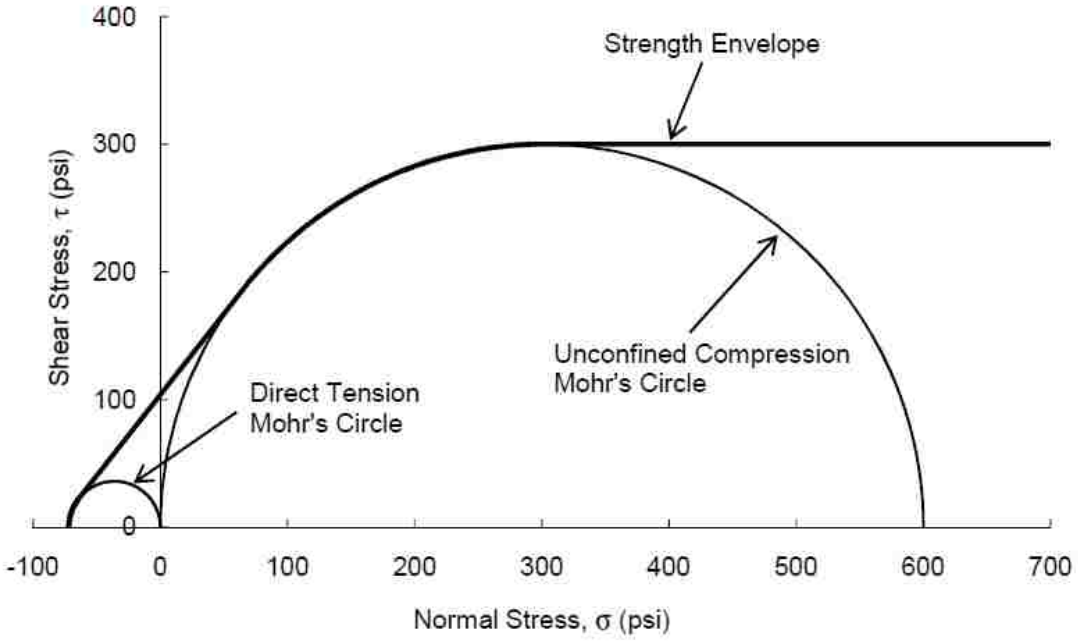

Figure 2-2. Proposed example strength envelope for deep-mixed soil-cement including tension (Filz et al. 2015).

2.1.3 Economic Benefits

The major cause of the increase in use of CLSM in recent years is the economic benefit available. CLSM is more expensive per cubic yard than conventional aggregate backfill material, but it only requires the use of a ready mix truck to place the fill into the desired volume. With the highly fluid CLSM, the ready mix truck can dispense the material very quickly. Within a few hours, traffic or previous activity can resume over the CLSM fill. Though the aggregate backfill material is cheaper than CLSM fill, the equipment, manpower, and time required for its proper installation and compaction are enough to make CLSM fill an economically viable alternative.

Furthermore, the improper compaction and placement of compacted aggregate fill can cause serious damage to structures, roadways, or utilities from large settlements. The self-consolidating CLSM fill is not prone to significant settlement so utility and structural damage due to settlement is less likely to occur (PCA 2015). The bump that is commonly felt before and after crossing a bridge can be virtually eliminated with no settlement, and pavement reconstruction costs can be reduced (Wilson 1999). These potential savings from avoiding repair and replacement work increase the potential economic benefits.

2.2 Passive Earth Pressure Theories

Lateral earth pressures are an essential parameter to understand for the safe design of retaining walls, basement walls, anchor blocks, laterally loaded pile caps, and bridge abutment backwalls (Das 2010). As shown in Figure 2-3, the lateral earth pressures stabilize these structural elements and resist their movement. The two types of lateral earth pressures are the active and passive cases. Passive lateral earth pressures are generated when structural elements are forced into the surrounding material by seismic loadings, thermal expansion, or simply as

part of their intended design. This research addresses laterally loaded abutment backwalls being displaced into a backfill material, so only the passive earth pressure theories are discussed.

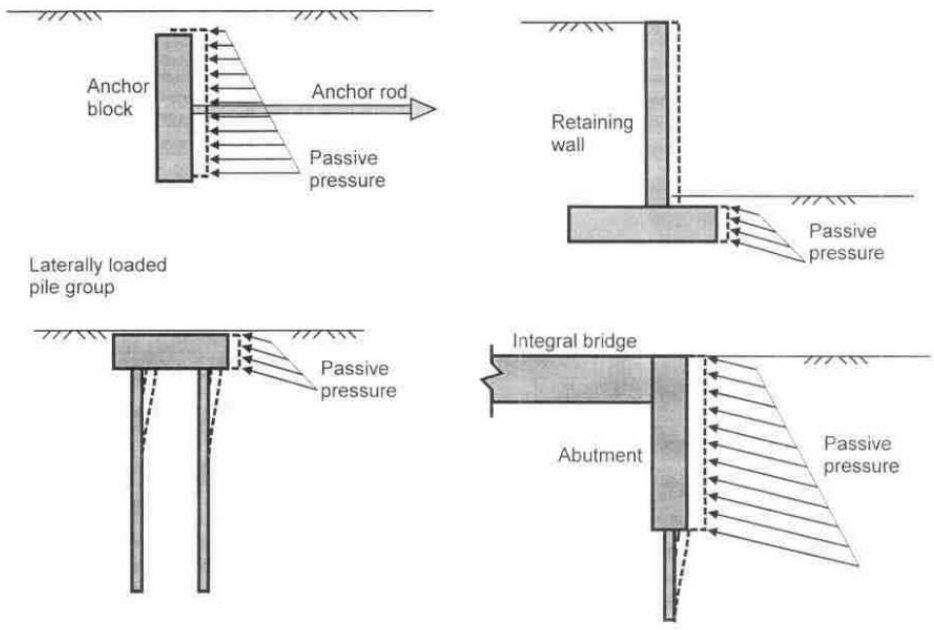

Figure 2-3. Passive earth pressure illustrations (Duncan and Mokwa 2001).

There are three commonly evaluated passive earth pressure theories used to estimate the passive earth pressures exerted on a structure. The two most commonly used in practice are the Coulomb theory (1776) and the Rankine theory (1857). Both of these theories are explained in nearly every soil mechanics textbook. The third commonly used method is known as the Log Spiral theory (Terzaghi 1943). The Log Spiral theory most accurately represents the passive earth pressures but is utilized less in practice because of its complexity and the time and effort required for its use (Duncan and Mokwa 2001). The equation for peak passive pressure per unit of wall width, P_p, reduces to the same form in all three theories and is given in Equation 2-1 as

$$P_p = \frac{1}{2} K_p \gamma H^2 + 2\sqrt{K_p} c' H \quad (2\text{-}1)$$

where

$K_p = passive\ earth\ pressure\ coefficient$,

$\gamma = moist\ unit\ weight\ of\ the\ soil$,

$H = backfill\ height$, and

$c' = soil\ cohesion$.

In cemented materials, the strength is likely to be determined by the cohesion in the specimen, and the friction angle is assumed to be zero. With a friction angle of zero for the backfill, the passive earth pressure coefficient, K_p, is equal to 1 according to all three theories. This is the case for this thesis, as a cemented CLSM backfill is used. For this case, Equation 2-1 can be simplified to Equation 2-2 to obtain the peak passive pressure P_p as

$$P_p = \frac{1}{2} \gamma H^2 + 2c' H \quad (2\text{-}2).$$

The variations in Coulomb, Rankine, Terzaghi, and many other researchers' theories are mainly reflected in their different approaches for estimating the passive earth pressure coefficient, K_p. The following sections describe the different ways that these common theories estimate K_p.

2.2.1 Coulomb and Rankine Theories

The Coulomb and Rankine passive earth pressure theories vary in that the Coulomb theory typically overestimates passive pressures while the Rankine theory usually gives very conservative estimates of passive earth pressures. The difference stems from the fact that Rankine's theory uses the Mohr-Coulomb failure criteria and does not consider the interface

friction between the structure and the backfill (Das 2010). This interface friction tends to increase the passive pressure, so disregarding it typically leads to a conservative passive force prediction.

Both the Coulomb and Rankine theories derive equations for the passive earth pressure coefficient, K_P. As was mentioned previously, Coulomb's equation considers wall friction whereas Rankine's does not. The Coulomb theory is also used in situations with an inclined wall and irregularly sloped backfill conditions. The Coulomb and Rankine solutions are shown in Equation 2-3 and Equation 2-4, respectively.

$$K_P = \frac{sin^2(\beta - \phi')}{sin^2\beta \sin(\beta+\delta')\left[1-\sqrt{\frac{\sin(\phi'+\delta')\sin(\phi'+\alpha)}{\sin(\beta+\delta')\sin(\beta+\alpha)}}\right]^2} \quad (2\text{-}3)$$

$$K_P = \frac{\cos\alpha + \sqrt{\cos^2\alpha - \cos^2\phi'}}{\cos\alpha - \sqrt{\cos^2\alpha - \cos^2\phi'}} \quad (2\text{-}4)$$

where

$\beta = inclination\ of\ backwall\ from\ vertical$,

$\phi' = effective\ soil\ friction\ angle$,

$\delta' = wall\ friction\ angle$, and

$\alpha = inclination\ from\ horizontal\ of\ the\ backfill.$

Both theories assume a planar or linear failure surface that starts at the bottom of the wall and progresses at an angle up to the backfill surface. This angle is defined by Rankine to be inclined 45°- $\phi/2$ from the horizontal as shown in Figure 2-4. The Coulomb theory uses an

iterative process involving force polygons to determine the angle of inclination. Graphical solutions to determine this angle were developed by Culmann (1875), but it can now be done quickly and easily with a computer (Das 2010). With the assumption of a linear failure surface, both theories tend to be inaccurate when the wall friction, δ, is greater than 40% of the internal friction angle, ϕ (Duncan and Mokwa 2001).

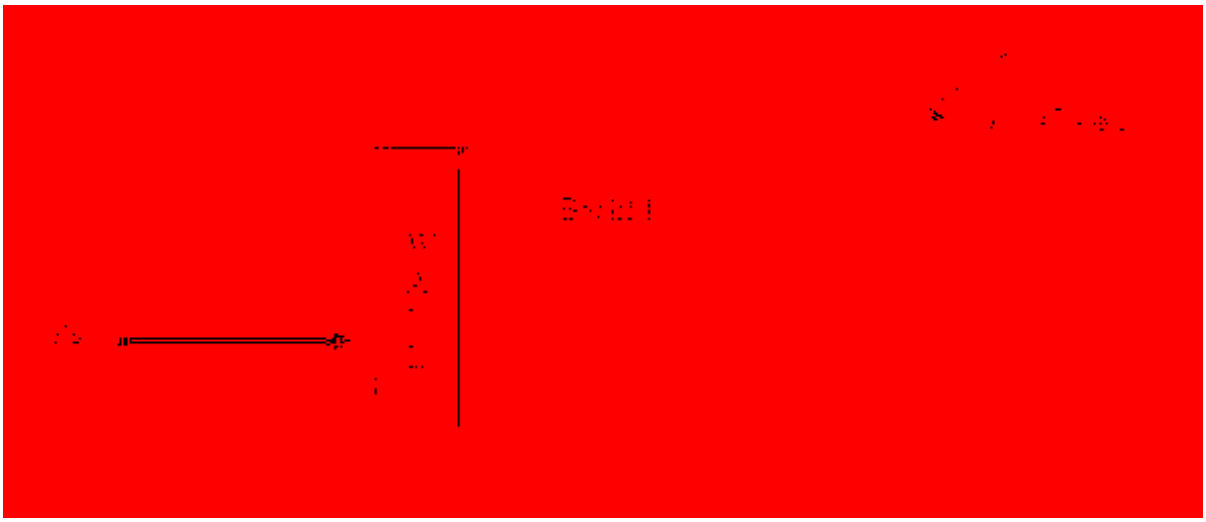

Figure 2-4. Rankine failure plane portrayal.

2.2.2 Log Spiral Theory

The Log Spiral theory has been commonly regarded as the best method for correctly predicting the passive earth pressure coefficient, K_p (Duncan and Mokwa 2001). Several researchers have developed different methods for determining K_p, and they typically report that their results are in agreement with the Log Spiral method (Kumar and Subba Rao 1997, Zhu and Qian 2000, Soubra 2007). The Log Spiral approach is much more complicated than the Coulomb and Rankine theories and is, consequently, less commonly used. The theory uses a limit

equilibrium approach like the Coulomb theory, so it is also an upper bound estimate (Kumar and Rao 1997).

The log-spiral-shaped failure wedge is not considered to be linear as the Coulomb and Rankine theories suggest. Terzaghi (1943) suggests a failure wedge with two distinct failure zones. The first is the Prandtl zone, which has the shape of a logarithmic spiral, and the second is the Rankine zone, which follows the linear failure surface that the Rankine theory predicts. Figure 2-5 shows the assumed log-spiral-shaped failure wedge.

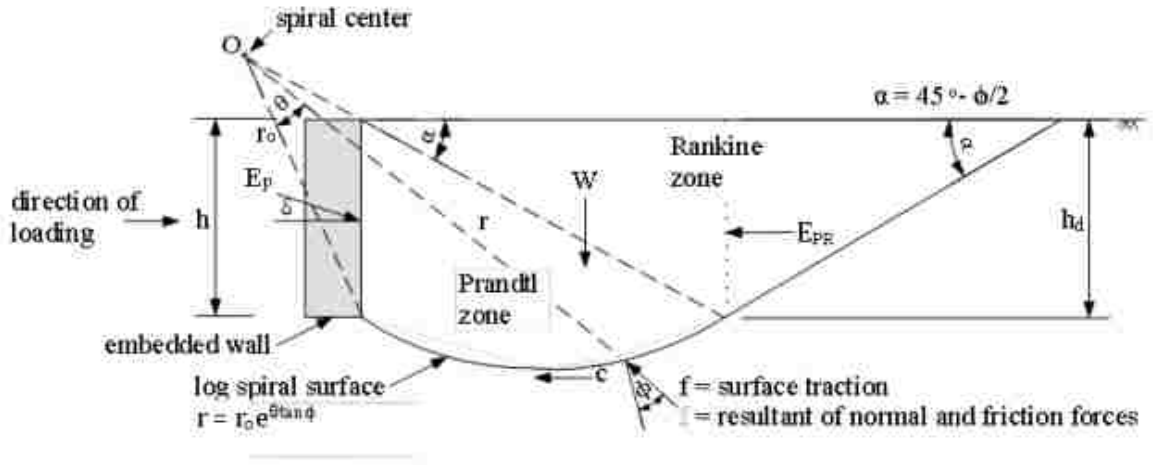

Figure 2-5. Log Spiral failure geometry [(Marsh, 2013) adapted from Terzaghi (1943)].

The process involved in the Log Spiral theory is to iteratively determine the mathematical center of the logarithmic spiral that will minimize the passive force calculated (Marsh 2013). This can be a very complex process, and there have been several different methods produced to complete the iterations quickly. There are three general ways that the Log Spiral theory is

typically employed (Duncan and Mokwa 2001). First, there are many tables and charts developed by Caquot and Kerisel (1948) that can be found in NAVFAC (1982) to quickly find the K_P value for simple conditions in cohesionless soil. Second, there is a graphical method that was established and is fully explained by Terzaghi (1943) and Terzaghi et al. (1996). However, these solutions can be very tedious. Finally, the solution can be determined using numerical analyses on a computer. Duncan and Mokwa (2001) created a numerical analysis program called PYCAP that can quickly and easily calculate the passive earth force. Its limitations are that it refers to a vertical wall and horizontal backfill with uniform surcharge (Duncan and Mokwa 2001). Despite its limitations, it makes the time and effort required to complete the iterative process of the Log Spiral theory much more manageable. A similar program known as ABUT was developed by Shasabadi et al. (2006) and produces K_p values similar to those from Duncan and Mokwa (2001).

The curved failure surface predicted by the Log Spiral theory is much more probable for conditions when the wall friction, δ, is greater than 40% of the angle of internal friction of the backfill, ϕ (Duncan and Mokwa 2001). For values of $\delta/\phi < 0.4$, the K_p values predicted by the Coulomb and Log Spiral theories are essentially the same. Once the wall friction angle increases past 0.4ϕ, the Coulomb theory begins to predict much higher values of K_p than the Log Spiral theory. Table 2-2 from Duncan and Mokwa (2001) shows the calculated K_p values for the Rankine, Coulomb, and Log Spiral theories for different magnitudes of wall friction.

Table 2-2. Comparison of K_p Values Computed by the Rankine, Coulomb, and Log Spiral Theories for Level Ground Surface with $\phi = 40°$ (Reproduced from Duncan and Mokwa 2001)

Wall Friction (δ/φ)	Rankine Theory (K_P)	Coulomb Theory (K_P)	Log Spiral Theory (K_P)
0	4.6	4.6	4.6
0.2	NA	6.3	6.6
0.4	NA	9.4	9.0
0.6	NA	15.3	11.9
0.8	NA	30.4	15.5
1	NA	92.6	17.5
Note: NA=Not Applicable			

As the data show, all the results are the same for the case with no wall friction. As δ increases, the Rankine theory becomes invalid, and the Coulomb theory over-predicts K_p by a large margin. The effects on the predicted failure surfaces are displayed in Figure 2-6 from Marsh (2013).

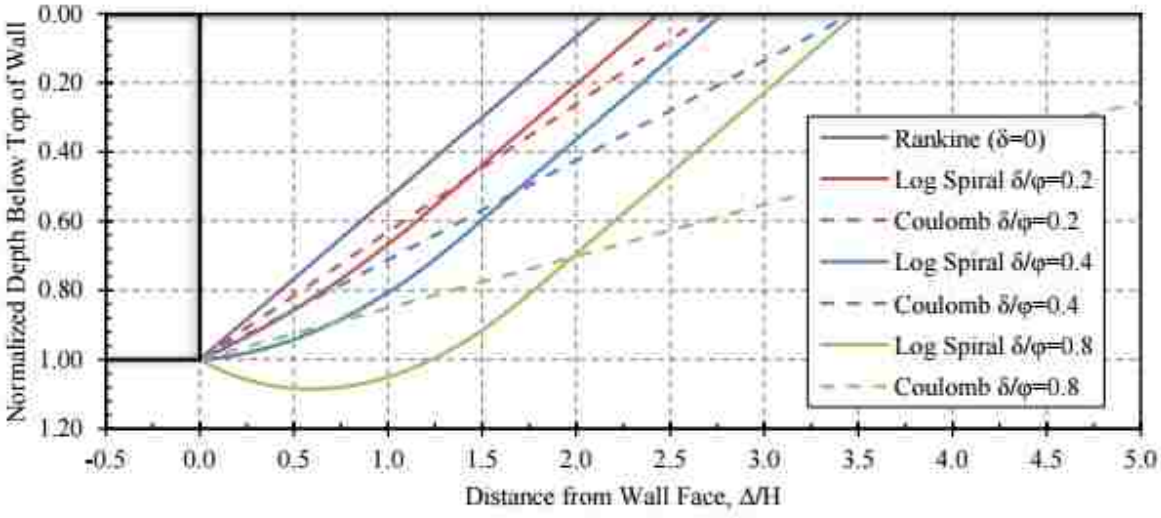

Figure 2-6. Failure surface geometries predicted by the Rankine, Coulomb, and Log Spiral theories (Marsh 2013).

2.2.3 Factors Governing Passive Earth Pressures

Passive earth pressures are generated in the backfill zone of a bridge abutment when the abutment backwall is forced laterally into the backfill. The magnitude, direction, and distribution of the passive pressure within the abutment-backfill system are dependent upon many different soil and structure parameters. According to Duncan and Mokwa (2001), the four principal parameters are as follows: (1) magnitude and direction of structural movement, (2) strength and stiffness of the soil, (3) friction and/or cohesion between the structure and the soil, and (4) shape of the structure. The following subsections discuss these four factors in greater detail.

2.1.3.1 Amount and Direction of Movement

In passive earth pressure conditions, the structure is typically moved horizontally into the resisting soil. If the structure movement is enough to cause failure of the material resisting its motion, a failure plane develops. When the resisting material fails, the failed wedge moves along its failure plane, which contains both a vertical and a horizontal component. The upward movement of the soil with respect to the structure creates a vertical shear force at the soil-structure interface. Duncan and Mokwa (2001) stated that, because there is both a horizontal and vertical force generated by the structural and soil movement, the resultant passive force, E_p, acts at an angle, δ_{mob}, to the soil-structure interface. The angle, δ_{mob}, at which the passive force, E_p, acts is known as the interface friction angle. If the structure is restrained either by its own weight or through a construction method, then the vertical forces on the soil-structure interface are able to fully mobilize, and the interface friction angle is maximized. If the structure is not sufficiently restrained, then the soil and the structure will move upward together, and the vertical force is not fully generated nor the interface friction angle fully mobilized. Figure 2-7 shows the structure

and soil movements, free-body diagram, and forces required for equilibrium in the case where the interface friction angle, δ_{mob}, is fully mobilized.

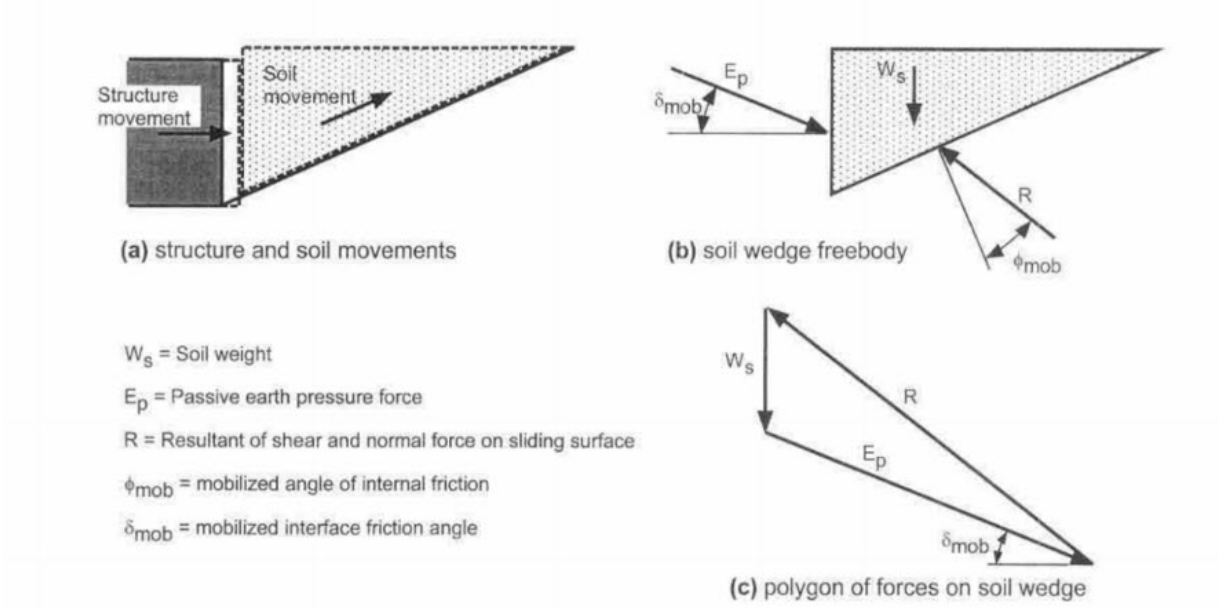

Figure 2-7. Movements, forces, and equilibrium requirements for passive pressure conditions (reproduced from Duncan and Mokwa 2001).

2.1.3.2 Strength and Stiffness of the Backfill

The development of passive force is dependent upon both the strength and the stiffness of the backfill. The passive force generated in the backfill is proportional to the strength of the material used. Higher backfill strength allows for the development of higher maximum passive earth pressures. Furthermore, higher backfill stiffness allows for higher passive force to be developed for a given amount of movement. For these reasons, it is important to properly consider these backfill parameters in design. Duncan and Mokwa (2001) provide tables with ranges for stiffness of sand and clay, but values for CLSM backfill are not generally available.

2.1.3.3 Soil-Structure Interface Friction and Adhesion

As previously mentioned, the resultant passive force acts at an angle inclined upward from normal to the soil-structure interface. This angle is called the interface friction angle, or δ. The resistance to vertical backfill movement relative to the structure is dependent on the magnitude of the interface friction angle. The development of δ is based on the nature or roughness of the interface material, the backfill material properties, and the amount of shear displacement across the interface.

The mobilized interface friction angle, δ_{mob}, is determined by both the roughness of the structural interface and the backfill material properties. Researchers have often expressed δ_{max} as a ratio of δ_{max}/ϕ, where ϕ is the angle of internal friction of the backfill material. Based on many studies, Potyondy (1961) created conservative tables of the δ_{max}/ϕ ratios for different types of structural and backfill materials. Those results are shown in Table 2-3.

Table 2-3. Minimum values for δ_{max}/ϕ (Potyondy 1961)

	Structural Material		
Soil Type	Steel (δ_{max}/ϕ)	Concrete (δ_{max}/ϕ)	Wood (δ_{max}/ϕ)
Sand	0.54	0.76	0.76
Silt and Clay	0.54	0.50	0.55

As the backfill material begins to move vertically relative to the structural interface, the interface friction, δ_{mob}, begins to mobilize. With continued movement, the interface friction development increases until a maximum friction angle, δ_{max}, is reached. Researchers agree that

the required amount of shear displacement at the soil-structure interface to fully mobilize the maximum interface friction, δ_{max}, is typically very small. Duncan and Mokwa (2001) suggest that displacements on the order of 0.1-0.25 in. (0.25-0.64 cm) fully mobilize the friction angle. If shear displacements are smaller than the required values, then the mobilized interface friction angle can safely be assumed to be less than or equal to the value of δ_{max}.

In addition to the friction between the structural and backfill materials, cohesive soils may also have an added amount of shear resistance due to adhesion. Duncan and Mokwa (2001) specify that the maximum amount of adhesion, c_a, is equal to the cohesion, c, of the backfill material. They also state that the adhesion can be characterized in terms of $\alpha = c_a/c$. The range of adhesion values varies from 0.5 for stiff soils to about 0.9 for soft soils (Duncan and Mokwa 2001). In the case of a cemented backfill material like CLSM, it is unclear whether the interaction between an abutment wall should be modeled using a wall friction factor or an adhesion factor or what appropriate values would be for each parameter.

2.1.3.4 Structure Shape

Conventional earth pressure theories are based on a two-dimensional cross section of the structure and soil. Inherent in these theories is the assumption that the passive pressure condition at each cross section is identical along the entire length of the structure. Various researchers have pointed out the fallacy of these assumptions and noted that the passive pressure conditions shift from two-dimensional at the wall center to three-dimensional at the ends of the wall (Ovesen 1964, Hansen 1966, Rollins and Cole 2006, Shamsabadi 2006) as shown in Figure 2-8. The three-dimensional effects at the ends of the structure can cause a large variance in the expected passive resistance (Duncan and Mokwa 2001). The difference in the passive pressure predicted

by the conventional methods and those actually measured is manifested particularly in structures of shorter length (Ovesen 1964, Duncan and Mokwa 2001). The failure surface illustrated in Figure 2-8 shows how the passive pressure conditions vary from two-dimensional to three-dimensional from the center to the boundary of the structure.

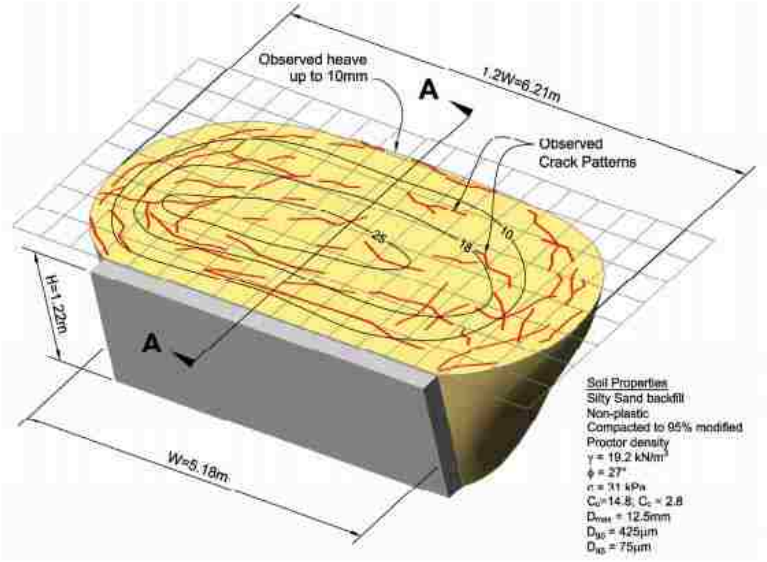

Figure 2-8. Three dimensional passive pressure failure surface [Shamsabadi, 2006 (after Rollins and Cole, 2006)].

Ovesen (1964) conducted a series of passive pressure tests, and from those results he concluded that the actual passive pressures for shorter structures is higher than those predicted by conventional theories. With reference to Figure 2-8, the volume of soil displaced per unit wall length is much greater on the ends than in the center. The extra width that adds to the resistance is known as the effective backwall width, b_e. The dimensions in Figure 2-8 show that, although the backwall width, w, is 5.18 m, the effective backwall width, b_e, is 1.2*w or 6.21 m. The additional, or effective width, causes passive resistance to be higher in structures of finite length than would be the case for a structure of infinite length. The three-dimensional end effects can be

accounted for in design by using an equation giving a shape correction factor developed by Hansen (1966) that ranges from 1.0 for a structure of infinite length to maximum of 2.0 for shorter structures (Rollins and Jessee 2012).

2.3 Passive Force-Displacement Tests for Non-Skewed Abutment Walls

Many researchers have studied the passive force-deflection relationship for laterally loaded pile caps or abutment backwalls. Their studies have included laboratory and large-scale field tests and finite element computer modeling in an effort to correctly predict the passive force-deflection relationship. This section summarizes the results found by Duncan and Mokwa (2001), Rollins and Sparks (2002), Rollins and Cole (2006), and Lemnitzer et al. (2009).

2.3.1 Duncan and Mokwa (2001)

The authors performed two passive pressure load tests on a reinforced concrete anchor block near Blacksburg, Virginia. They performed the tests on two different backfill materials. The first test was performed with the anchor block bearing against the natural ground material consisting of desiccated sandy silt (ML) and sandy clay (CL). The second was performed with the anchor block bearing against a mechanically compacted, well graded gravel backfill. A summary of the passive pressure calculated by the Rankine, Coulomb, Log Spiral with three-dimensional correction, and Log Spiral with no three-dimensional correction methods, compared to the measured passive pressure is shown in Table 2-4. Their findings state that the Log Spiral method with correction for three-dimensional effects most accurately modeled the measured values. Furthermore, they evaluated the results of the measured passive force-deflection curve compared with the curve calculated by their numerical analysis program, PYCAP. They found reasonable agreement between their numerical analyses and the measured results.

Table 2-4. Comparison of Computed and Measured Passive Resistances (kips) (Reproduced from Duncan and Mokwa 2001)

Method	Natural Soil			Gravel Backfill		
	High	Low	Average	High	Low	Average
Rankine	110	94.8	102	43.9	35.4	39.6
Coulomb	119	103	111	59	49.4	54.2
Log Spiral, without 3D correction	120	102	111	58	48.4	53.3
Log Spiral, with 3D correction	173	139	156	104	82.3	93.2
Measured	-----	-----	138	-----	-----	91.7

2.3.2 Rollins and Sparks (2002)

Rollins and Sparks completed a full-scale lateral load test on a 4.0 ft (1.22-m) high and 9.0 ft (2.74-m) square pile cap that encased a 3x3 pile group. The test was performed at the Salt Lake Airport with a soil profile consisting of low-plasticity silts and clays underlain by a sand layer. The test was performed by loading the pile cap into a sandy gravel backfill material. The authors concurred with Duncan and Mokwa (2001) that the log-spiral method yielded values nearest to the measured passive force. They stated that the Rankine method underestimated the peak passive force by a factor of 3.5 and that the Coulomb method overestimated the peak passive force by a factor of 2. The pile cap displacement required to mobilize the peak passive resistance was approximately 6% of the pile cap height. It was noted that this is on the high end of the typical estimate of displacement required to mobilize the peak resistance, and this was attributed to the soft clay layer beneath the backfill.

2.3.3 Rollins and Cole (2006)

Rollins and Cole performed several full-scale static and cyclic lateral load tests on a 4x3 pile group encased in a 3.67 ft (1.12 m) high, 17.0 ft (5.18 m) wide, and 10.0 ft (3.05 m) long pile cap. The tests consisted of the pile cap being laterally loaded into several backfill materials. The backfill materials were clean sand, fine gravel, coarse gravel, and silty sand. These materials had friction angles of 39, 27, 34, and 40°, respectively. The authors state that the Log Spiral method most correctly predicted the failure surface geometry and that the failure wedge increased in length with increasing friction angle. Finally, they observed that the peak passive force was mobilized at displacements of 3-5.2% of the backwall height.

2.3.4 Lemnitzer et al. (2009)

This research was conducted at the University of California, Los Angeles, and it consisted of the lateral loading of a full-scale model of a bridge abutment backwall that represented a typical California bridge design. The backwall model was 8.5 ft (2.6 m) high by 14.7 ft (4.5 m) wide by 3.0 ft (0.9 m) thick and was laterally loaded into a well-graded sand with silt (SW-SM) backfill material known in the construction industry as sand equivalent 30 (SE30). However, the backfill was only filled to a height of 5.5 ft (1.7 m) on the backwall face.

The test was set up in such a manner that both horizontal and vertical passive forces were monitored. Peak passive pressure was determined to have been reached at a horizontal displacement of approximately 3% of the backwall height. The authors concluded that the peak passive force was most accurately predicted by the log-spiral method and the method of slices developed by Shamsabadi (2007). The horizontal load-deflection curve was estimated using the

hyperbolic model based on the research of Duncan and Mokwa (2001) and was shown to be consistent with the general shape of the measured horizontal-load deflection curve.

2.3.5 Passive Force-Displacement Tests Summary

From these tests, several conclusions were drawn. First, the method that best estimated the passive force-deflection relationship was the Log Spiral method. It was best at predicting both the peak passive force and the failure surface geometry. Second, the displacements required to mobilize the peak passive force were found to be consistently 3-5%. However, no passive force-displacement tests have been conducted using CLSM as the backfill material. It remains to be seen whether its strength should be characterized as frictional or cohesive. Furthermore, the displacement required to mobilize the peak passive force in a CLSM backfill is unknown.

2.4 Movements and Forces for Skewed Bridges

The previous sections explain how the magnitude of the passive force acting on a structure and backfill are affected by the structural movement, backfill properties, backfill-structure interface conditions, and structure shape. This thesis is focused on the passive forces acting on an abutment backwall, and in these structures the passive force generation is also affected by the skew angle of the backwall (Rollins and Cole 2006, Shamsabadi 2006, Rollins and Jessee 2012, Marsh 2013). This section illustrates the forces generated at the interface between the bridge abutment and the backfill soil upon thermal expansion or seismic action. It also describes the required relationships to be satisfied for equilibrium and safe performance of the bridge.

Burke (1994) describes the forces that are present in a passive pressure condition at the bridge abutment backwall and backfill interface. All the forces that interact at the interface can

be expressed in terms of P_L, the total longitudinal force, and its components parallel and perpendicular to the abutment face. Figure 2-9 illustrates these forces.

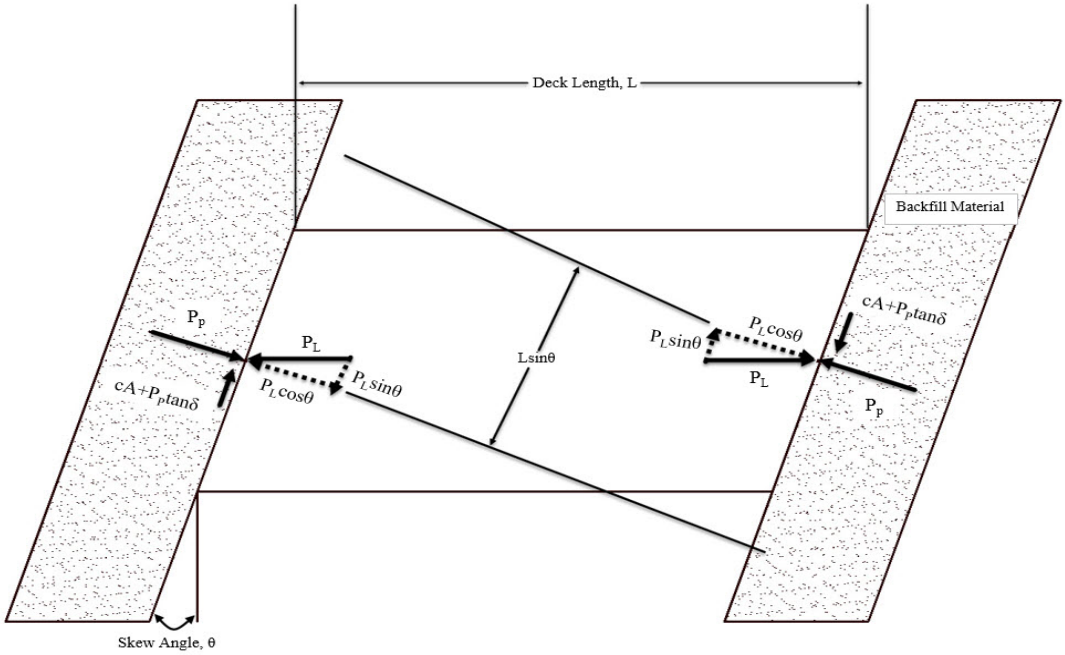

Figure 2-9. Typical interaction of forces on skewed bridges (Adapted from Burke, 1994).

The component of the longitudinal force normal to the interface has to be resisted by the passive earth force, P_p, given by Equation 2-5. The parallel, or shearing, component of P_L in Equation 2-6 is denoted as P_T. P_T has to be resisted by the shear resistance of the backwall-backfill adhesion and interface friction force, P_R. It is shown in Equation 2-7. The passive earth force applied on a skewed bridge resulting from a longitudinal load is calculated as

$$P_P = P_L \cos\theta \quad (2\text{-}5),$$

while the transverse shear is calculated as

$$P_T = P_L \sin\theta \quad (2\text{-}6)$$

where

$$\theta = skew\ angle\ of\ backwall.$$

The resistance to the transverse shear is given by

$$P_R = cA + P_P tan\delta \quad (2\text{-}7),$$

where

$$c = backfill\ cohesion,$$

$$A = backwall\ area, \text{ and}$$

$$\delta = backfill - backwall\ interface\ friction\ angle.$$

Summing the forces transverse to the interface, the inequality required to keep the backwall and backfill from moving relative to each other is derived in Equation 2-8 as

$$\frac{cA+P_P tan\delta}{F_S} \geq P_L \sin\theta \quad (2\text{-}8).$$

The bridge skew angle creates an offset for the passive forces, which results in a force couple. The couple causes the bridge to rotate about its vertical axis, so the moment exerted from the shear resistance forces must counteract the passive force moment. Equation 2-9 shows this inequality in terms of forces and lengths:

$$\frac{(cA+P_P tan\delta)L\cos\theta}{F_S} \geq P_P L \sin\theta \quad (2\text{-}9).$$

All of these forces and inequalities are based on the assumptions that the structure remains stable and that there is a linear pressure distribution on the backwall face (Burke 1994, Marsh 2013). If the bridge experiences movement or rotation, the described forces are no longer valid. Burke (1994) noticed that, if the cohesion of the backfill was ignored, then the inequality

governing the rotational restraint of the bridge structure would be independent of length and passive force. Burke (1994) also assumed a factor of safety of 1.5. This allowed the inequality for rotational potential to be simplified to Equation 2-10,

$$\theta \leq \tan^{-1}\left(\frac{tan\delta}{1.5}\right) \tag{2-10}$$

where

$\theta = skew\ angle\ of\ backwall$ and

$\delta = backfill - backwall\ interface\ friction\ angle.$

Based on a typical backfill-backwall interface friction angle of 22°, this no-cohesion assumption suggests that unstable conditions exist for bridges with skew angles greater than 15° (Burke 1994, Rollins and Jessee 2012, Marsh 2013). In reality, the critical skew angle depends on the interface friction angle mobilized in the structure.

2.5 Tests and Observations for Skewed Abutment Walls

Data from instrumented bridges, laboratory tests, and full-scale field tests have pointed out that skewed bridges do not perform as well as non-skewed bridges when subjected to lateral loads that can occur from seismic activity, thermal expansion, waves, wind, impacts, and other circumstances. In recent years, several tests have been performed with the intent of determining the passive force versus backwall deflection relationship for skewed bridge abutments.

This section discusses the results of laboratory and field results obtained from the research of Rollins and Jessee (2012), Marsh (2013), Franke (2013), and Rollins et al. (2015). It also describes the available numerical modeling from Shamsabadi (2007), discusses results obtained by Sandford and Elgaaly (1993) about the performance of skewed bridges they

instrumented, and provides observations of skewed bridge performance in an earthquake (Elnashi et al. 2010, Toro 2013).

2.5.1 Rollins and Jessee (2012) Laboratory Results

Rollins and Jessee (2012) performed a laboratory-scale passive force test on a 4.13 ft (1.26 m) wide and 2 ft (0.61 m) high concrete wall used to model a bridge abutment backwall. The concrete backwall was displaced into a dense sand backfill material just slightly wider than the backwall itself to induce a two-dimensional or plane-strain geometry. The backfill was a poorly graded washed concrete sand (SP) compacted to 98% of the maximum relative density. The test was repeated for backwall skew angles of 0, 15, 30, and 45° to evaluate the effect of the skew angle on the passive force-deflection relationship. As depicted in Figure 2-10, the peak passive force was found to be significantly reduced as the skew angle increased. However, the peak passive force still occurred at a longitudinal displacement between 3-5% of the wall height.

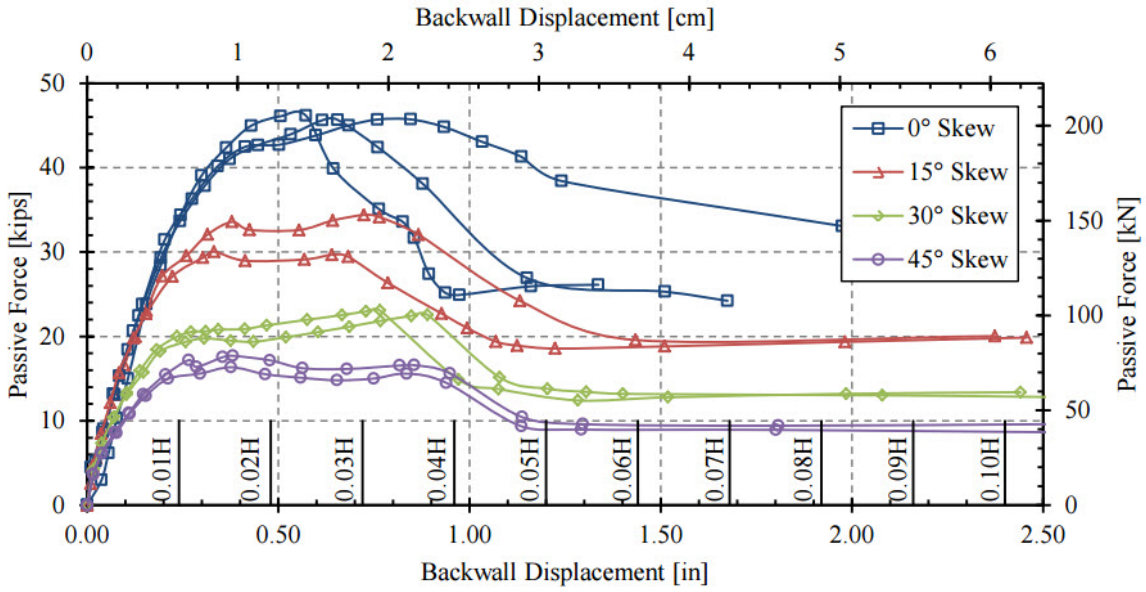

Figure 2-10. Laboratory test passive force-displacement results (Rollins and Jessee 2012).

From the data acquired from their tests, they proposed a correction factor, R_{skew}, for skewed bridge design. The correction factor, given by Equation 2-11, relates the passive force for a non-skewed bridge, $P_{p\text{-no skew}}$, and the passive force for a skewed bridge, $P_{p\text{-skew}}$, as a function of skew angle, θ. The authors' proposed reduction based on backwall skew angle is

$$R_{skew} = \frac{P_{p-skew}}{P_{p-no\ skew}} = 8.0 * 10^{-5}\theta^2 - 0.018\theta + 1 \quad (2\text{-}11).$$

Based on their reduction equation, a 30° skew angle produces a peak passive force that is approximately 53% of the peak passive force for a non-skewed bridge abutment.

Furthermore, Rollins and Jessee (2013) found that, even for the skewed tests, the peak passive force occurred at longitudinal displacements between 2.5 and 3.5%, which agrees with previous research done on non-skewed bridge abutments. However, the higher skew angle tests had passive force plateaus for longer displacements than the non-skew test. These force plateaus are presented in Figure 2-10.

2.5.2 Marsh (2013) Full-Scale Test Results

The author performed several large-scale, unconfined lateral load field tests at a test site near the Salt Lake City Airport. The abutment backwall was 11 ft (3.35 m) wide by 5.5 ft (1.68 m) high. Testing consisted of laterally loading the backwall into a backfill material consisting of dense compacted sand. Backwall skew angles of 0, 15, and 30° were tested, and the passive force-deflection relationships for each test were acquired. Marsh concurred with previous skewed abutment test results that as skew angle increased the peak passive force decreased significantly. The peak passive force for the 15° and 30° skew angle tests were reported to be

73% and 58%, respectively, of the peak passive force obtained for the 0° skew case. The passive force-deflection curves for the three skew angles are shown in Figure 2-11.

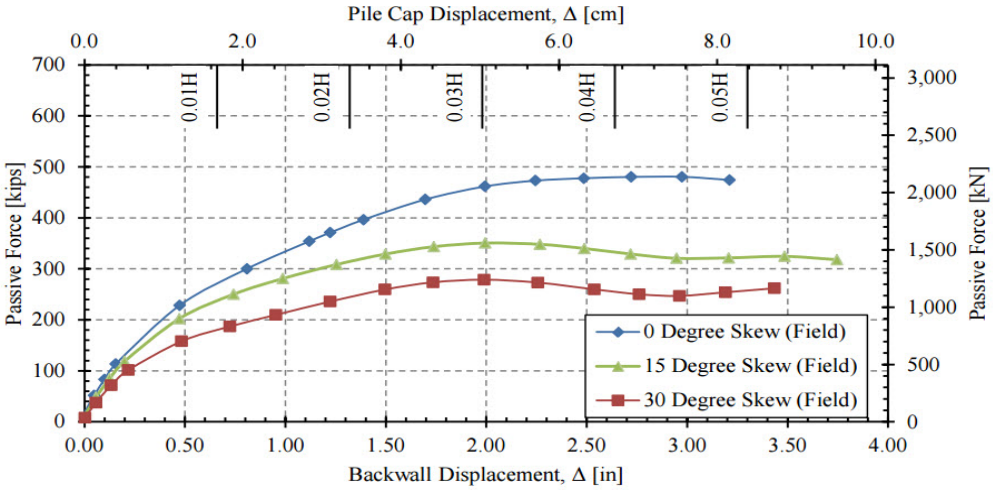

Figure 2-11. Passive force-deflection curves for the 0°, 15°, and 30° tests (Marsh 2013).

From these relationships, the author proposed that for a skew angle of 30° a peak passive force that is approximately 56% of the peak passive force for a non-skewed bridge abutment can be expected. This is very similar to the laboratory test results found by Rollins and Jessee (2012). This proposed reduction factor would allow bridge designers to estimate a peak passive force for a non-skewed bridge abutment and then use the R_{skew} factor and the skew angle, θ, to calculate the peak passive force for a skewed bridge abutment. The tests showed that, at low skew angles, the Log Spiral method most accurately estimated the peak passive force, the Coulomb method significantly overestimated it, and the Rankine method significantly underestimated it.

They also stated that the lateral displacement required to achieve the peak passive force is between approximately 3% and 5% of the backfill height. This displacement amount agrees with

previous research done on laterally loaded, skewed and non-skewed backwalls alike. Again, the Log Spiral method most accurately predicted the failure wedge geometry.

2.5.3 Franke (2013) Full-Scale Test Results

At the same test site and in conjunction with Marsh (2013), Franke (2013) performed several large-scale lateral load field tests on the same 11 ft (3.35 m) wide by 5.5 ft (1.68 m) high abutment backwall that was mentioned in the previous section. The difference between the two tests was the backfill set up. While Marsh used a dense, compacted sand backfill, Franke used mechanically stabilized earth (MSE) wingwalls in the backfill as shown in Figure 2-12. Similar to the tests performed by Marsh, lateral load tests were performed with backwall skew angles of 0, 15, and 30°.

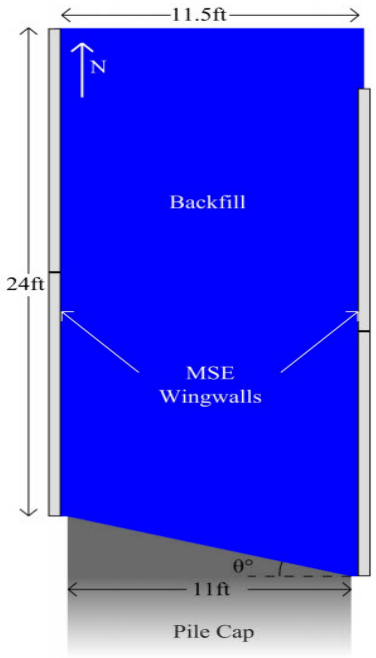

Figure 2-12. Diagram of MSE wingwall layout and configuration (Franke 2013).

Franke (2013) reported peak passive force reductions of 38% and 51% for skew angles of 15° and 30° respectively, as compared to the peak passive force generated by the 0° skew test. These values are comparable to the reductions due to skew angle found by previous researchers and fit the reduction curve proposed by Rollins and Jessee (2012) very well. Figure 2-13 shows the passive force-deflection curves for the lateral load tests with the MSE wingwalls installed.

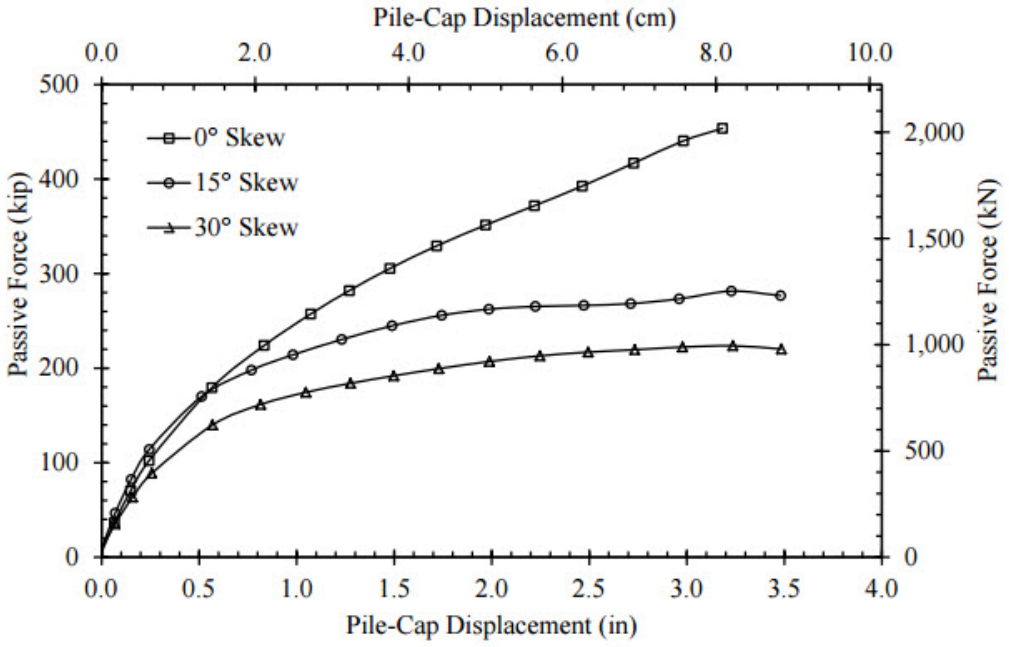

Figure 2-13. Passive force-deflection curves for all skew angles (Franke 2013).

For the non-skew test, the peak passive force was achieved at a displacement of approximately 5% of the wall height. In the skewed test, the peak passive force was mobilized at a displacement of approximately 3% of the wall height. Franke (2013) also noted that the skewed tests showed a substantial loss in the rate of strength gain after this deflection of approximately 3% of the backwall height. The hyperbolic methods for predicting the passive force-deflection

curve proposed by Duncan and Mokwa (2001) and Shamsabadi et al. (2007) most correctly modeled the measured passive force-deflection curve from Franke's tests.

2.5.4 Rollins et al. (2015) Full-Scale Test Results

The tests performed by Rollins and Jessee (2012), Marsh (2013), and Franke (2013) were all performed with abutment width-to-height ratios of about 2.0, but in typical construction practice this ratio is usually much higher. To evaluate the effect of the width-to-height ratio on laterally loaded, skewed abutments, Rollins et al. (2015) performed unconfined lateral load tests using the same 11 ft (3.35 m) wide by 5.5 ft (1.68 m) tall pile cap, but they used a backfill depth of 3 ft (0.9 m) instead of the full 5.5 ft (1.68 m). This nearly doubled the width-to-height ratio from 2.0 to 3.7. These authors performed the field tests on the same dense, compacted sand (SP) backfill with abutment skew angles of 0, 15, and 30°.

The findings from these tests provided similar results as the large and full-scale results obtained by the aforementioned researchers, with the confirmation that increased abutment skew angle dramatically decreases the peak passive force despite the increase in width-to-height ratio. Figure 2-14 shows the passive force-deflection curves resulting from these tests. The reductions in passive force due to skew angle were found to be closely approximated by Equation 2-11 given by Rollins and Jessee (2012). A peak passive force reduction of about 50% can be expected for a 30° skew angle according to their results.

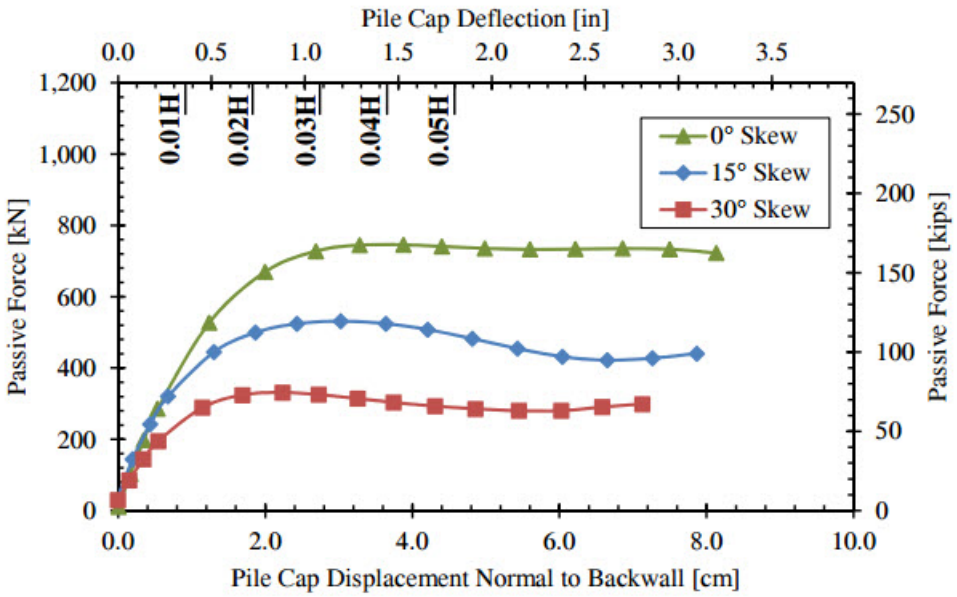

Figure 2-14. Passive force-deflection curves for 0, 15, and 30° skew angle (Rollins, Palmer, and Fredrickson 2015).

The authors stated that the peak passive force was achieved with displacements of 3.5% of the backfill height for the no-skew case and approximately 2.75% for the 15 and 30° skew cases. These results fell in the range that has been reported in the literature by almost all previous researchers. Though the peak passive force decreased with increasing skew angle, the initial stiffness was said to be unaffected by the skew.

2.5.5 Shamsabadi et al. (2006)-3D Numerical Modeling Results

Shamsabadi et al. (2006) created several three-dimensional, nonlinear finite-element models to estimate soil capacities behind non-skewed and skewed abutment backwalls as a function of wall displacement. Using Plaxis 3D (Brinkgreve 2004), the authors calibrated their

finite-element model using the backfill parameters and data obtained from the research done by Rollins and Cole (2006). The modeled backfill was a silty-sand typical of what is used for structural backfill in California. Table 2-5 summarizes the input parameters used in their Plaxis 3D finite-element model.

Table 2-5 Shamsabadi et al. (2006) Backfill Finite Element Model Parameters

Soil Type	γ kN/m^3 (lb/ft^3)	φ	c kPa (lb/ft^2)	δ	E_{50}^{ref} Mpa (kip/ft^2)	E_{ur}^{ref} Mpa (kip/ft^2)	ν
Silty Sand	18.8 (119.7)	34°	25 (54.4)	23°	100 (2,089)	200 (4,177)	0.35

The model that was created represented an actual bridge abutment backwall that was 75 ft (22.8 m) wide by 5.5 ft (1.68 m) tall. With a backwall width to height ratio of nearly 14, they assumed two-dimensional or plane strain conditions for the non-skew case. However, for the skewed cases, there are three dimensional effects involving bridge rotation during dynamic loading. They used their models to compare the passive force-deflection relationship on backwall skew angles of 0, 30, 45, and 60°, and the resulting passive force-deflection curves, shown in Figure 2-15, were obtained. The results indicated that the passive soil capacity decreased with increasing skew angle.

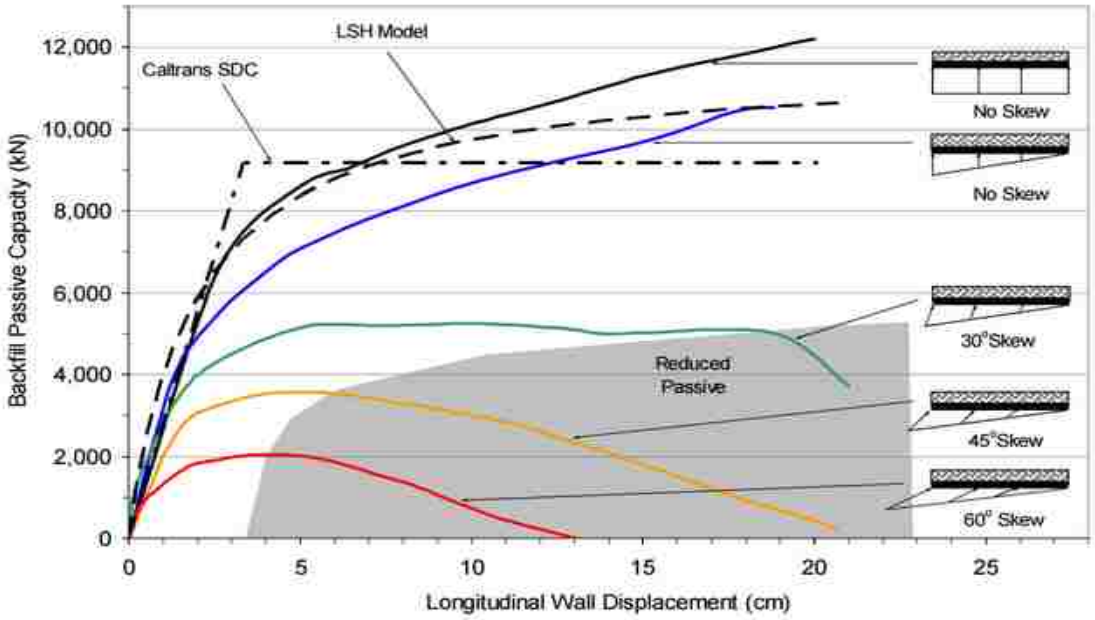

Figure 2-15. Passive force-deflection curves for 0, 30, 45, and 60° skew angles (Shamsabadi et al. 2006).

On the right side of Figure 2-15, the pressure distribution that was assumed to be acting on the backwall for each skew angle is shown. The pressure was assumed to be acting at an angle equal to the backwall skew angle with the maximum pressure acting on the obtuse corner of the backwall and decreasing linearly to zero pressure at the acute corner. The finite-element model results of the failure wedge due to a 45° skew angle are shown in Figure 2-16. Because of the asymmetric pressure distribution, the superstructure tends to rotate about a vertical axis in the center of the deck. This rotation of the superstructure forces primarily the obtuse corners of the deck into the backfill and forms an asymmetrical passive wedge. The finite element analysis of the passive wedge is shown in Figure 2-16.

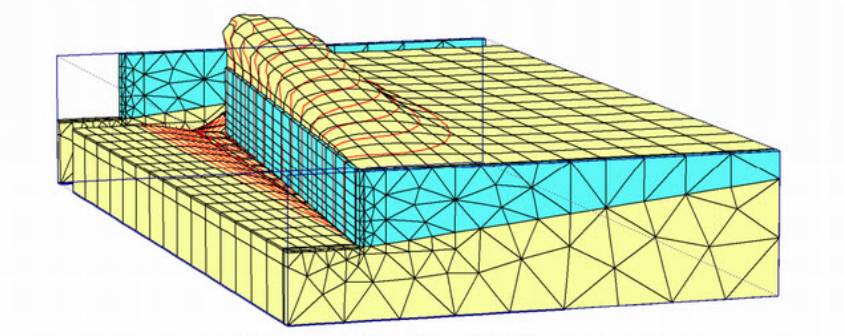

(a) Deformed mesh and displacement contours.

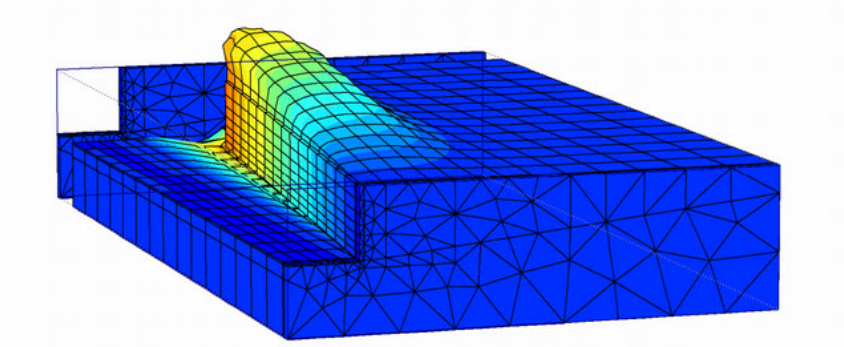

(b) Total displacement contours.

Figure 2-16. Passive soil wedge behind a 45° skew backwall (Shamsabadi et al. 2006).

To further model the interaction of a skewed bridge deck with a skewed abutment, the authors created a global three-dimensional nonlinear dynamic model of a 45° skewed, two-span, pre-stressed concrete box-girder bridge. The results of this global model confirmed that the pressure distribution on the face of the abutment backwall truly was nonlinear with the maximum pressures occurring at the obtuse corner of the bridge deck and that the superstructure underwent a significant rotation about a vertical axis shown in Figure 2-17. As previously mentioned, this bridge deck rotation causes an asymmetrical passive wedge behind the abutment. The authors concluded that the asymmetrical passive soil wedge results in a reduced mobilized soil capacity as compared to ordinary non-skewed abutments.

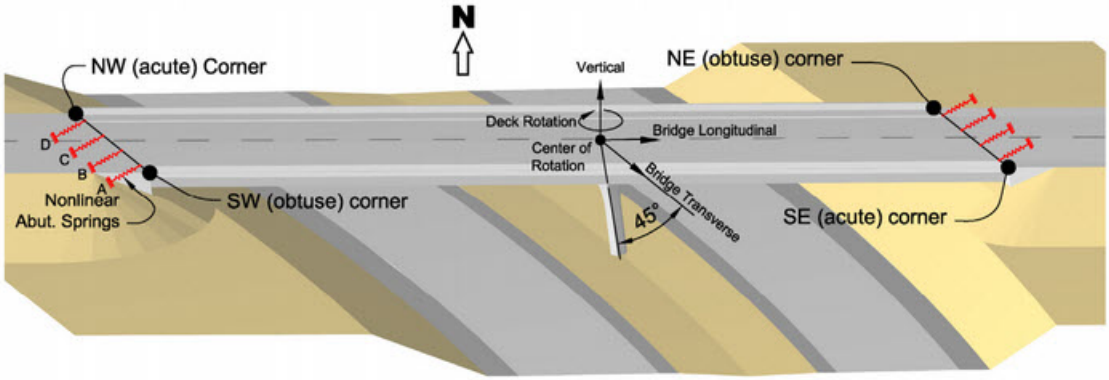

Figure 2-17. Skewed box-girder bridge used in global bridge analysis (Shamsabadi et al. 2006).

2.5.6 Sandford and Elgaaly (1993)-Skew Effects on Backfill Pressures at Frame Bridge Abutments

These authors installed total pressure cells and temperature indicators on a previously constructed bridge in Maine for a period of 33 months. Their objective was to monitor the effects of skew angle and temperature on the backfill pressures. The bridge had a skew angle of 20°, and the soil pressure and temperature data were monitored four times per day on both the obtuse and the acute sides of the bridge abutment. When warmer temperatures caused the bridge to expand into the backfill, the pressures measured on the obtuse side reached nearly three times the pressures on the acute side. These pressures were then relieved when the weather cooled and the bridge superstructure contracted.

However, the authors stated that the effects of skew angle diminished over time and claimed that the skew angle effects diminished because of greater permanent deformation of the backfill on the obtuse side than the acute side. The cause of this permanent deformation was the

rotation of the superstructure into the backfill. Sandford and Elgaaly concluded that the obtuse side of the bridge was forced into the backfill significantly more than the acute side.

Finally, they commented that the lateral variation of pressure due to thermal expansion was higher than the vertical variation of pressure due to thermal expansion. As a cause of this, they proposed a new horizontal soil envelope to be considered when designing a skewed bridge. As shown in Figure 2-18, the envelope used the Rankine active pressure on the acute side and the Rankine passive pressure on the obtuse side.

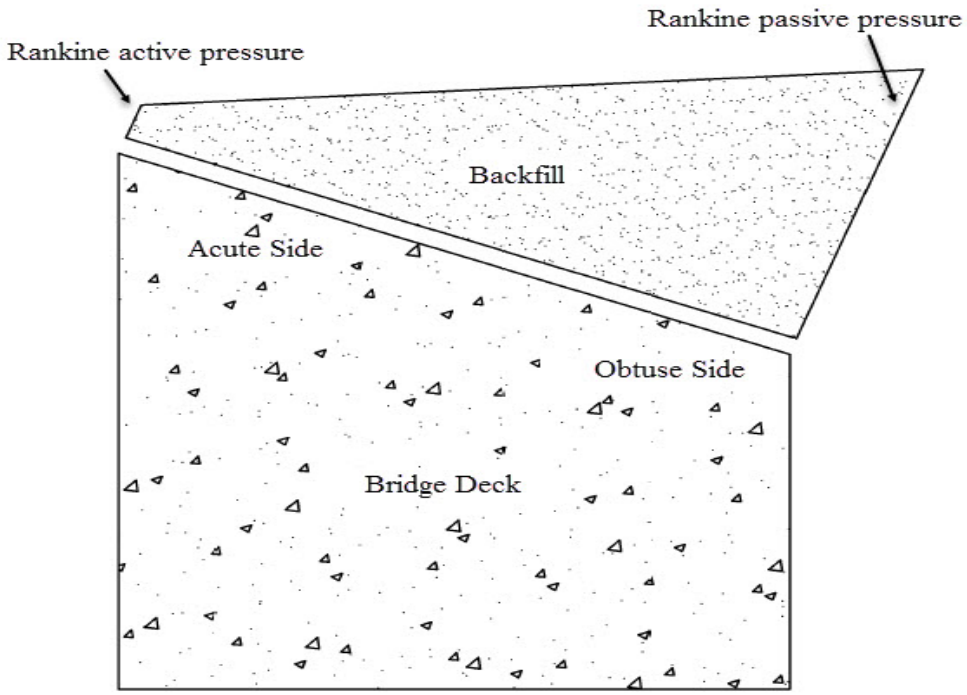

Figure 2-18. Proposed design soil pressure envelope (Sandford and Elgaaly 1993).

2.5.7 Steinberg et al. (2004)- Forces in Wingwalls of Skewed Semi-Integral Bridges

Steinberg et al. studied the forces developed in abutment wingwalls due to thermal expansion and consequent rotation of the superstructure of two skewed semi-integral bridges. The first bridge had a span of 87.0 ft (26.5 m) and was 32 ft (9.8 m) wide with a skew angle of 65°. The second was a four-span semi-integral bridge with outer spans of 70.0 ft (21.3 m) and inner spans of 87.0 ft (26.5 m) and was 40.0 ft (12.2 m) wide with a skew angle of 25°. Load cells and thermocouples were installed to monitor the forces and temperature changes.

In addition to the field tests done on these two bridges, the authors used a finite element computer program called *SAP 2000* to analyze the bridges. They also analyzed fictitious bridges with skew angles of 25, 35, and 45° and spans of 100, 200, and 400 ft (30.5, 61, and 122 m) with this software. Their findings were that the monitored bridges experienced significant forces in the wingwalls due to backwall displacements and bridge rotation, and they cautioned that bridge designers should be aware of these forces in skewed bridges. Furthermore, their numerical analysis showed that lower skews and lower backfill stiffness values generated lower magnitudes of force in the wingwalls compared to higher skew angles and stiffer backfill.

2.5.8 Elnashi et al. (2010a)- The Maule (Chile) Earthquake of February 27, 2010

Elnashi et al. (2010) were part of a team sent to assess the damage produced by the M_w 8.8 2010 earthquake in Chile. Among other structural failures, they examined the damage done to bridges. The authors state that the most commonly observed bridge damage was due to unseating or displacement of the superstructure. This damage was especially prevalent in skewed bridges. Elnashi commented that the skewed bridges tended to rotate about a vertical axis, which resulted in the unseating of the bridge girder or failure of the shear keys. This rotation can be seen in

Figure 2-19. Furthermore, the newer bridges performed worse than the older bridges because of new bridge design code modifications that permitted smaller shear keys and transverse lateral restraint systems that were thought to simplify design and construction procedures.

Figure 2-19. Bridge superstructure translation (Elnashi et al. 2010).

2.5.9 Toro et al. (2013) Bridge Damage Analysis from 2010 Maule, Chile Earthquake

These researchers analyzed the performance of 88 overpasses in the M_w 8.8 Maule, Chile earthquake in 2010. They aimed to find a correlation between bridge characteristics and the damage level resulting from the earthquake. Their findings were that the damage level and collapse rate for skewed bridges were much higher than for non-skewed bridges. They concluded

that the skew angle facilitated the bridge deck rotation and displacement. Finally, they stated that the percentage of the initial total construction cost to repair the skewed bridges was an average of 26% and only 7% for the non-skewed bridges.

2.5.10 Summary of Skewed Bridge Tests and Observations

The results of the studies and observations done on skewed bridges indicate that the performance of skewed bridges is worse than that of non-skewed bridges. Passive resistance is reduced significantly as skew angle increases, but the displacement required to reach the peak passive resistance is still found to be 3-5%. Furthermore, the skew angle causes the bridge deck to rotate about a vertical axis. This rotation causes additional forces to be exerted on bridge shear keys and wingwalls compared to a non-skewed bridge.

2.6 Literature Review Summary

There has been a large amount of time spent and research performed to determine the effect of skew angle on the passive force-displacement relationship for laterally loaded bridge abutment backwalls. As explained in Section 2.4.8, the improper design of skewed bridges can have very costly impacts on their performance when loaded in an earthquake, thermally, etc. The research that has been done can be implemented to safely and efficiently design skewed bridges to withstand rotation and the forces exerted on the structure that result from their displacement. Previous work has been performed exclusively with conventional backfill materials typically used on a bridge abutment construction site.

Using CLSM as an alternative backfill material has its merits, but it also has uncertainties. The uncertainties relating to the passive force-deflection relationship for an abutment backwall displaced into CLSM backfill include the following topics:

- Strength characterization of CLSM in computing passive force
- Displacement required to develop ultimate passive resistance in CLSM
- The effect of backwall skew angle
- CLSM backfill failure plane geometry compared to conventional backfill materials
- Shape of the passive force-deflection relationship

All of these uncertainties are addressed in the following chapters.

3 LABORATORY TEST LAYOUT AND CLSM BACKFILL PROPERTIES

3.1 Test Layout

Figure 3-1 shows the plan view layout of the passive force-deflection tests, and Figure 3-2 shows an elevation view of the cross section through the middle of the wall. The two tests were performed with backwall skew angles of 0 and 30°. The simulated abutment backwalls were two reinforced concrete blocks with one square face to connect to the actuator, and the opposite face, which was to be forced into the backfill, was skewed to either 0 or 30°. The blocks were 49.5 in. (1.26 m) wide and 24 in. (0.61 m) tall. They were placed on top of a 12 in. (0.30 m) tall support block that consisted of an 11 in. (0.28 m) tall wooden support block with 1 in. (2.54 cm) diameter steel rollers placed on top to reduce the friction between the abutment backwall and the wooden support.

Behind the backwalls, the backfill was comprised of CLSM. It was mixed and delivered in a ready mix truck and poured into the form with a concrete bucket hoisted from an overhead crane. The backfill zone was made just wider than the backwall to create a two-dimensional or plane strain condition. In other words, the configuration was designed to eliminate the three-dimensional or end effects described in Section 2.1.3.4. In total, the backfill was 51 in. (1.29 m) wide, 96 in. (2.44 m) long, and 36 in. (0.91 m) deep. Double sheeted plastic liners with lubricant between them lined the inside of the form walls to allow the CLSM to displace with minimal friction on the floor and form walls.

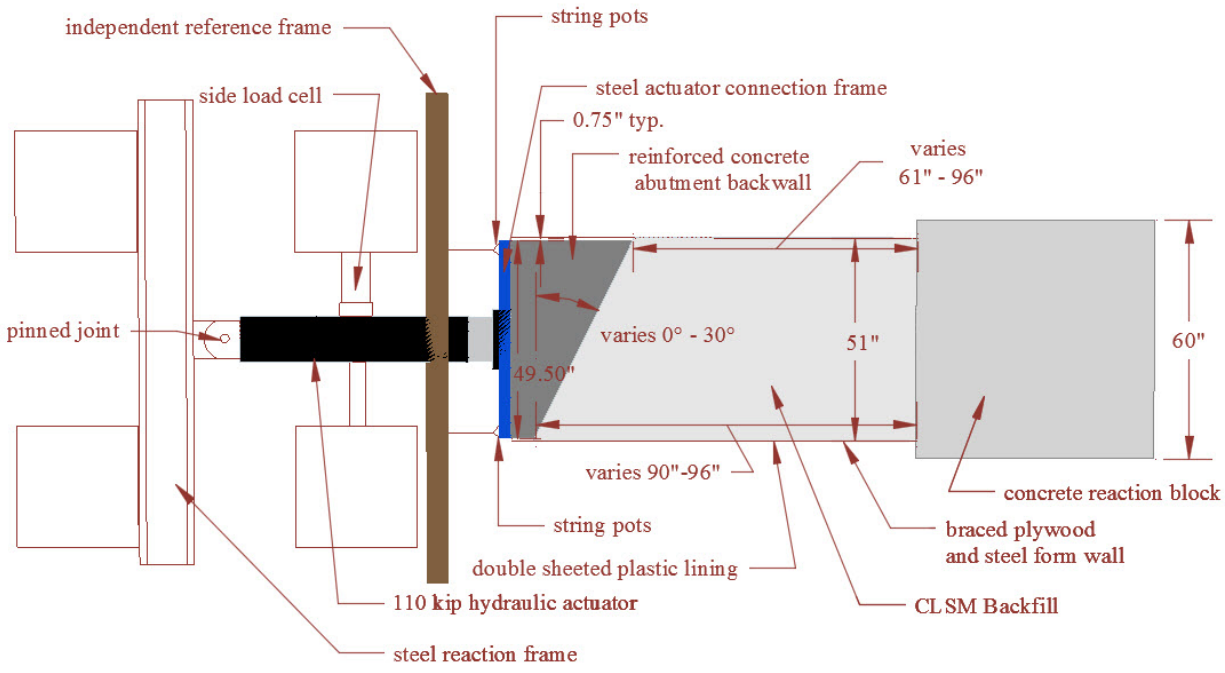

Figure 3-1. Plan view of test layout.

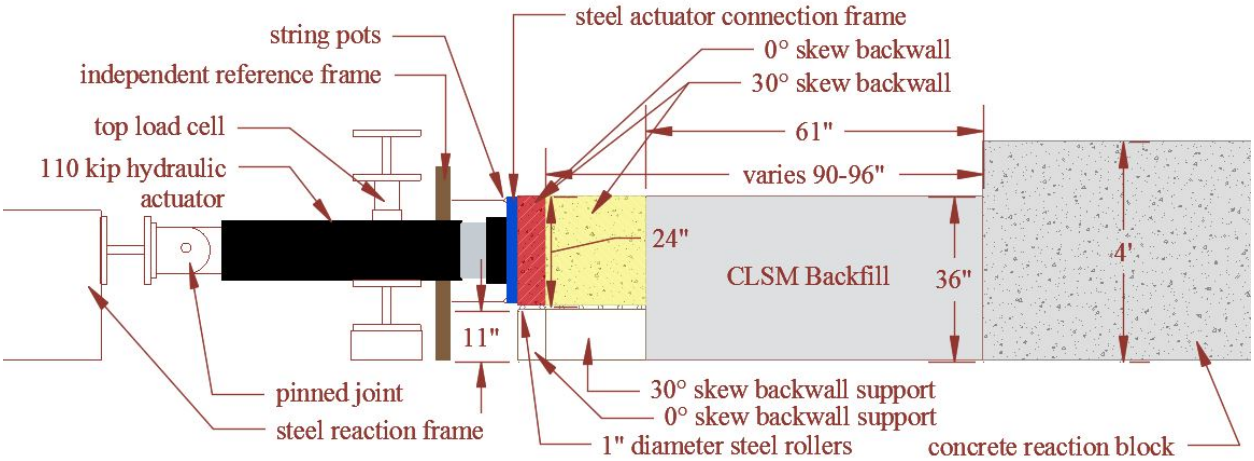

Figure 3-2. Elevation view of test layout.

The CLSM was poured to the level of the top of the backwall and it extended 12 in. (0.30 m) below the backwall base to allow for failure plane development below the backwall as would be expected with the Log Spiral failure theory. The reaction for the backfill was provided by a 5 ft (1.52 m) square, 4 ft (1.22 m) tall concrete block bolted to the floor. Three-dimensional models of the 0 and 30° test setup are shown in Figures 3-3 and 3-4.

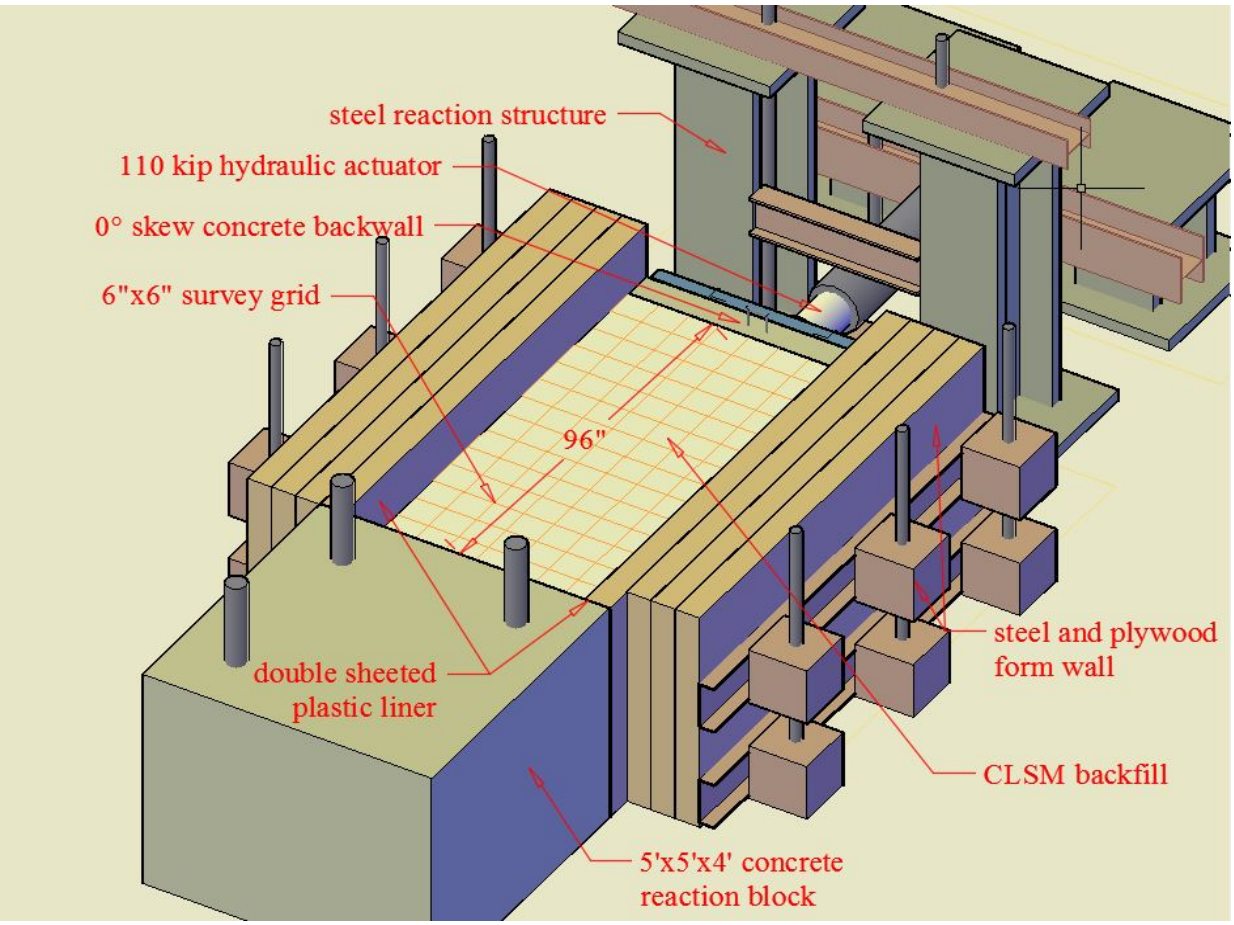

Figure 3-3. Three dimensional 0° skew test setup model.

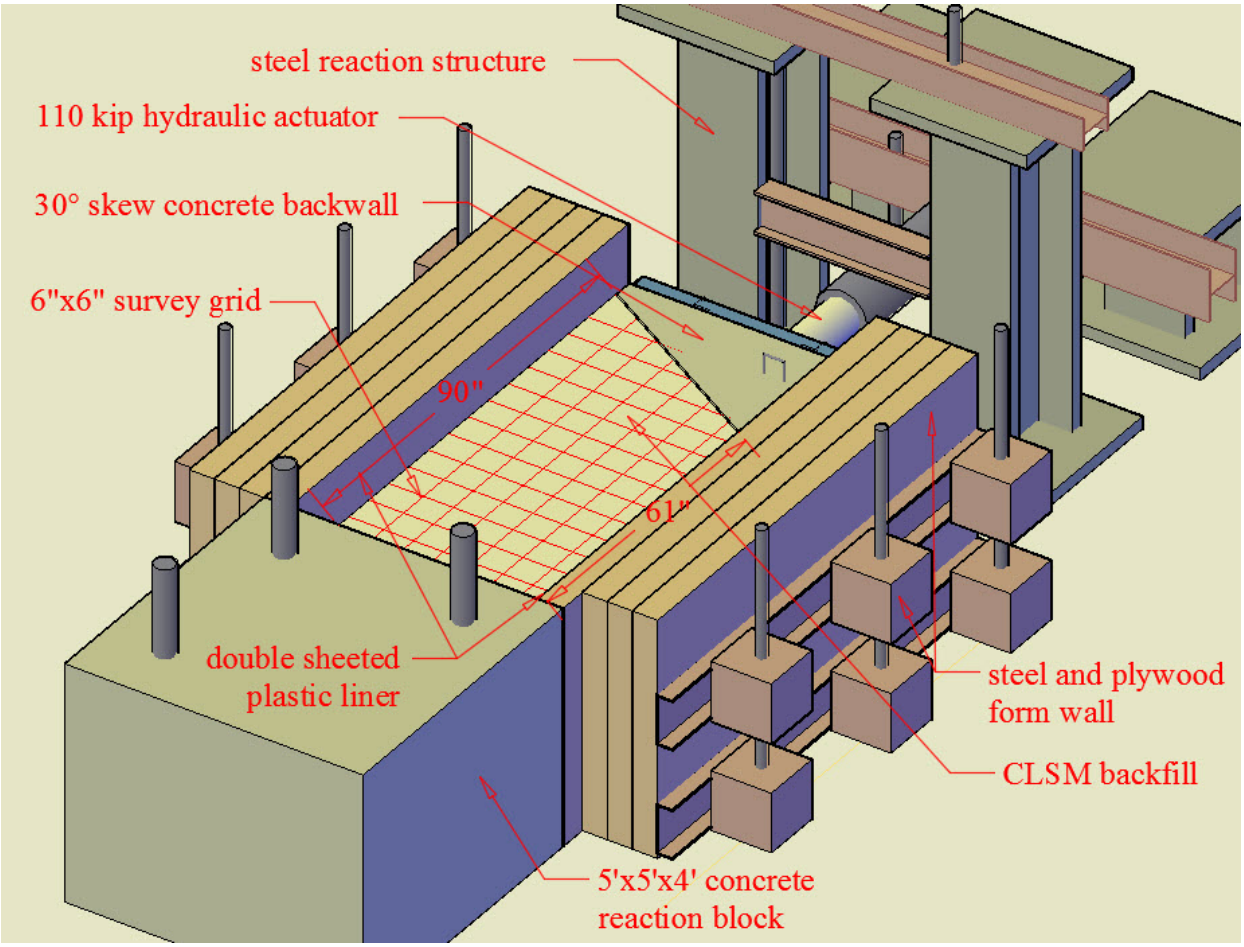

Figure 3-4. Three dimensional 30° skew test setup model.

3.2 Instrumentation

The load test was instrumented to measure the following parameters: longitudinal load, longitudinal backwall displacement, transverse backwall displacement, backfill longitudinal compressive strain, backfill surface heave, and CLSM backfill thermocouple data as described in the following sections.

3.2.1 Longitudinal Load Instrumentation

The longitudinal load was measured by pressure transducers installed by the manufacturer within the MTS actuator. With the actuator attached to the backwall, these pressure transducers measured the longitudinal load applied on the backwall, and this load was used to calculate the passive earth pressure generated within the CLSM backfill. As the tests were conducted, this load was recorded four times each second and saved into a text file.

3.2.2 Longitudinal Displacement Instrumentation

Four string potentiometers were installed on each of the corners of the backwall to measure the longitudinal displacement. As shown in the simplified Figure 3-5, the string pots were attached to an independent reference frame that ensured a measurement of strictly backwall movement. This system could also be used to determine rotations of the wall about a vertical or horizontal axis through the wall.

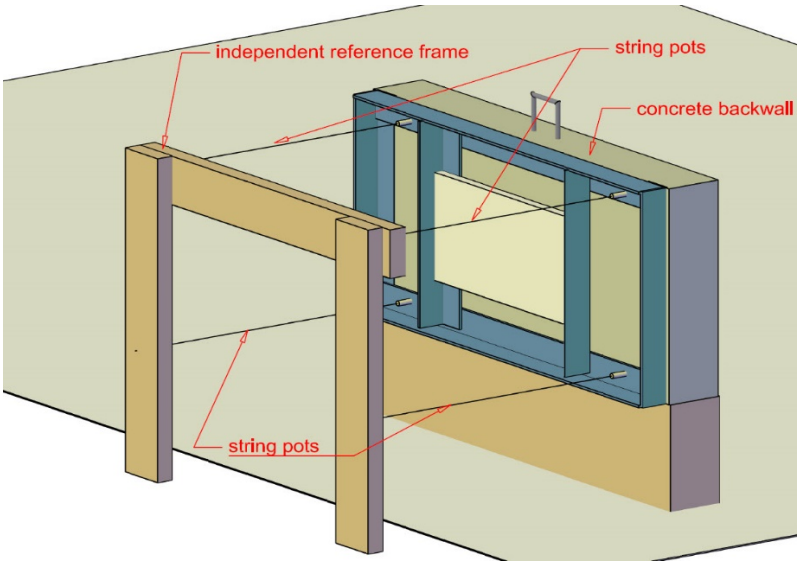

Figure 3-5. Longitudinal displacement instrumentation.

3.2.3 Transverse Displacement Instrumentation

Along with the longitudinal string potentiometers, two transverse string potentiometers were connected to the top and bottom of one side of the backwall. They provided information on the transverse displacement of the backwall as a test progressed.

3.2.4 Compressive Strain Instrumentation

Seven more longitudinal string potentiometers were installed near the center of the independent reference frame. Figure 3-6 shows how each one was connected to the backfill surface using the head of a screw that was inserted into the CLSM backfill at intervals of 1 ft (0.3 m). This allowed data to be recorded that showed the ground surface displacement at different distances from the backwall face, and thus the longitudinal compressive strain at these locations could be computed.

Figure 3-6. Compressive strain instrumentation.

3.2.5 Backfill Surface Heave Measurement

A 6 in. by 6 in. (0.15 m by 0.15 m) square grid was painted on the surface of the CLSM backfill using marking spray paint. A survey level was set up alongside the CLSM form, and the intersection points of each gridline row and column were surveyed before and after the tests. These data allowed for the calculation of the change in elevation, or heave, at each grid point.

3.2.6 Thermocouple Instrumentation

A four-channel thermocouple data recording device was used to record the temperature and CLSM aging data at four different locations. The first thermocouple lead wire was placed in a 4 in. (0.10 m) diameter by 8 in. (0.2 m) tall CLSM cylinder placed on the concrete reaction block at the rear of the backfill zone. The other three lead wires were placed directly into the CLSM as it was being poured at depths of 6 in. (0.15 m), 18 in. (0.45 m), and 27 in. (0.69 m) from the surface. This was done to monitor the CLSM curing process at different depths in the backfill zone.

3.3 Load Test Procedure

The tests were conducted by bolting a 110 kip (490 kN) capacity hydraulic actuator to the concrete backwalls and displacing them longitudinally into the CLSM backfill. The previously mentioned plastic sheeting prevented the form wall and laboratory floor from providing friction that could alter the results. The actuator was set to a displacement rate of 0.1 in/min (0.25 mm/min), and the tests were continued until clear failure planes had been developed and longitudinal displacements were near 3 in. (76.2 mm). Between the actuator and the steel reaction frame, load cells were installed, as shown in Figures 3-1 and 3-2, to measure the top and side loads on the actuator as the displacement of the backwall progressed.

3.4 CLSM Engineering Properties

This section addresses the measurement of the following CLSM properties: unit weight, UCS, shear strength, interface shear strength, and curing rate. Each test was performed on the CLSM used in both the 0 and 30° skew tests. Figure 3-7 shows the mix design that was used in the two tests.

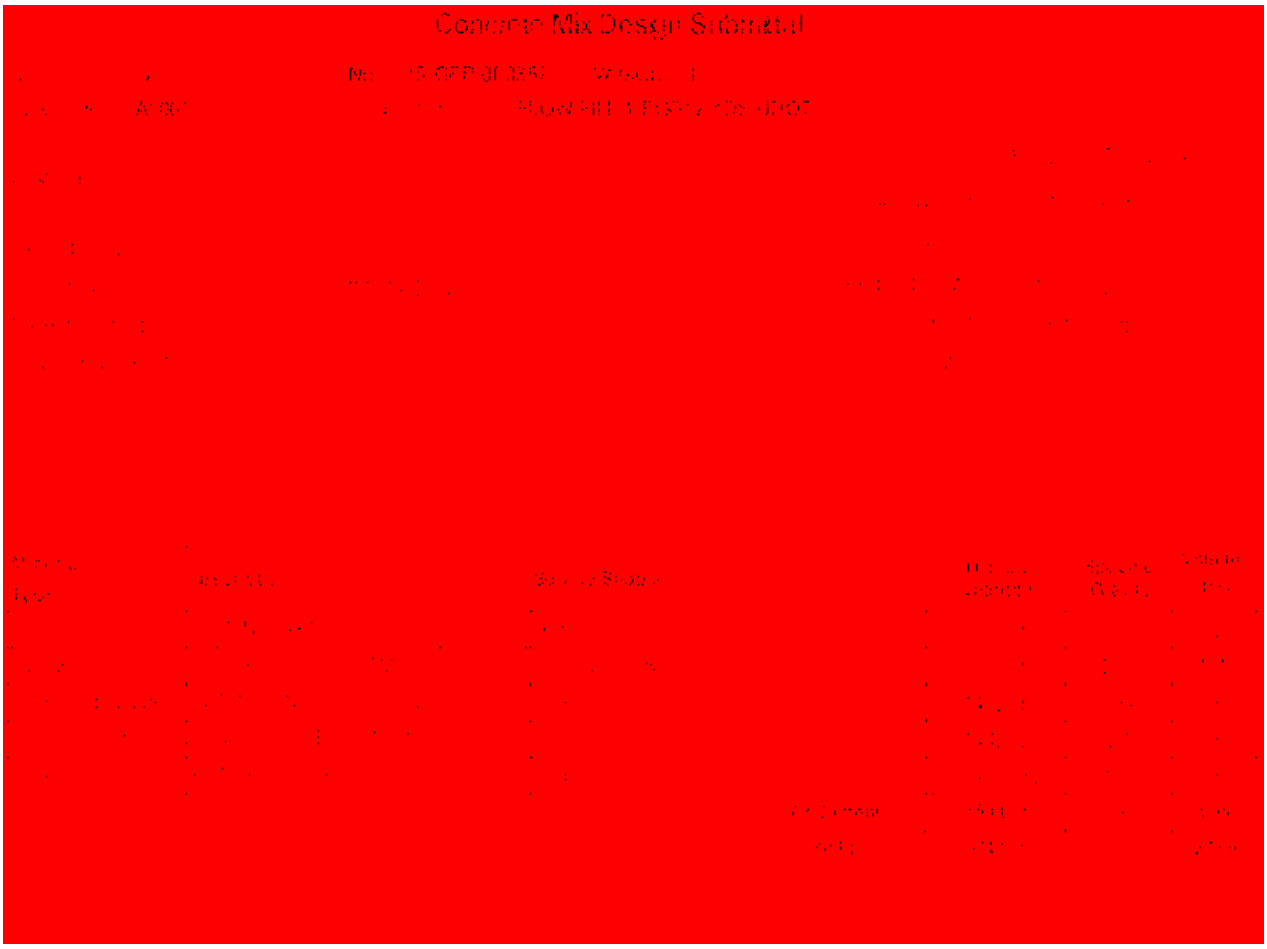

Figure 3-7. CLSM mix design

The CLSM used for these tests was taken from the middle of the truck unloading process to get an accurate representation of the material. The slump and flow cone diameter were measured according to ASTM C143 and ASTM D6103 standards (mentioned in Section 2.1.1), respectively. In both batches, the diameter for the flow cone did not reach the FHWA specified minimum for flowability of 8 in. The lower flow diameters were determined to be acceptable because the slump was already in the desired range and the addition of excess water was avoided to prevent negatively affecting the cementitious properties of the CLSM. The slump and flow diameter for the 0 and 30° skew test batches are shown in Table 3-1.

Table 3-1. Slump and Flow Cone Measurements for CLSM

CLSM Batch	ASTM C143	ASTM D6103
	Slump (in.)	Flow Diameter (in.)
0° Skew Test	7.0	7.25
30° Skew Test	8.0	6.00

3.4.1 Unit Weight

On the same 7-day intervals at which the cylinders were to be tested for their UCS, their unit weights were also measured. This was accomplished by weighing each cylinder on a scale and then measuring the height of the cylinder on opposite sides using a set of digital calipers. The diameter of each cylinder always remained at 4 in. (0.10 m). Based on the average of the two height measurements and the constant diameter, the volume of the cylinder was calculated, and the wet unit weight was determined using the Equation 3-1

$$\gamma_m = \frac{\text{Weight}_{\text{cylinder}}}{\text{Volume}_{\text{cylinder}}} \quad \text{3-1.}$$

After the cylinders had been tested in compression for their UCS, a large portion of each cylinder was weighed and then placed in an oven to dry. After thoroughly drying, the cylinder was weighed again, and the water content, in percent, was found using Equation 3-2

$$\mathrm{w} = \frac{\text{wet cylinder weight} - \text{dry cylinder weight}}{\text{dry cylinder weight}} (100\%) \qquad 3\text{-}2.$$

With the two different curing methods, the water contents were expected to be significantly different for the open-air cured cylinders and the fog room cured cylinders. Using the moisture content, the dry unit weight was obtained to make a comparison between the cylinders that was more representative. The dry unit weight in Equation 3-3 was calculated as

$$\gamma_{\mathrm{d}} = \frac{\gamma_{\mathrm{m}}}{1+\mathrm{w}} \qquad 3\text{-}3$$

where

$\gamma_{\mathrm{d}} = dry\ unit\ weight,$

$\gamma_m = wet\ unit\ weight$, and

$w = water\ content.$

The water content of the specimens cured in open air averaged approximately 1%, while the specimens cured in the fog room typically had a water content closer to 10%. Tables 3-2 and 3-3 show the average moist unit weight, the average moisture content, and the average dry unit weight for the cylinders tested in each of the 7-day, 14-day, 21-day, and 28-day unconfined compression tests for the 0 and 30° skew test cylinders. Table 3-2 shows the fog room cured and open-air cured data side by side. It was noted in the first passive force-displacement test that the strength of the CLSM in the load test was better represented by the open-air cured cylinders.

Thus, the second set of cylinders that were cast only contained open-air-cured cylinders as shown in Table 3-3.

Table 3-2. Unit Weight and Moisture Content Data for 0° Skew Test Cylinders

		Open-Air Cured	Fog Room Cured
7-Day Cure	γ_m (lb/ft^3)	124.2	135.9
	w (%)	2.76%	11.59%
	γ_d (lb/ft^3)	120.8	121.8
14-Day Cure	γ_m (lb/ft^3)	121.4	136.1
	w (%)	1.16%	10.84%
	γ_d (lb/ft^3)	120.0	122.8
21-Day Cure	γ_m (lb/ft^3)	121.9	135.3
	w (%)	0.89%	10.75%
	γ_d (lb/ft^3)	120.8	122.2
28-Day Cure	γ_m (lb/ft^3)	120.5	135.9
	w(%)	0.70%	9.78%
	γ_d (lb/ft^3)	119.6	123.8

The average open-air cured moist unit weight for the 30° skew test CLSM was 112.5 lb/ft^3 (17.7 kN/m^3). This is nearly 10 lb/ft^3 (1.5 kN/m^3) lower than the open-air cured average moist unit weight of 122 lb/ft^3 (19.17 kN/m^3) for the CLSM used in the 0° skew test. The same mix design was ordered from the same ready mix supplier for both tests, and the rodding and casting of the cylinders were done by the author in the same manner for both tests according to ASTM D4832 standards. It is unclear what the determining factor was for the difference in unit weights of the two batches.

Table 3-3. Unit Weight and Moisture Content Data for 30° Skew Test Cylinders

All Cylinders Open-Air Cured

7-Day Cure	γ_m **(lb/ft^3)**	113.4
	w (%)	2.03%
	γ_d **(lb/ft^3)**	111.2
14-Day Cure	γ_m **(lb/ft^3)**	111.9
	w (%)	1.33%
	γ_d **(lb/ft^3)**	110.4
21-Day Cure	γ_m **(lb/ft^3)**	113.2
	w (%)	0.84%
	γ_d **(lb/ft^3)**	112.2
28-Day Cure	γ_m **(lb/ft^3)**	111.5
	w (%)	0.70%
	γ_d **(lb/ft^3)**	110.8

3.4.2 Unconfined Compressive Strength

To measure the UCS, several CLSM cylinders were cast every time a passive force-displacement test was prepared. Unconfined compression testing was performed in general agreement with ASTM D4832. The cylinders were cast in greased plastic molds that measured 4 in. (0.10 m) in diameter and 8 in. (0.20 m) in height. They were left in the plastic molds for three days with the lids on. After the initial three day curing period, they were removed from their plastic molds using a compressed air nozzle inserted over a hole pre-drilled into the bottom of each mold. Once removed, the curing methods differed. The cylinders were either cured in a fog room environment or in the ambient laboratory environment with exposure to air from all sides. This was done in order to see what strength difference could be expected for the cylinders cured

in the fog room versus the cylinders cured in the ambient laboratory environment because the CLSM backfill that was used in the passive force-displacement tests was also simply cured in the ambient laboratory conditions.

On the day of the CLSM pour for the 0° skew test, a total of 25 cylinders were cast. Twelve were cured in the fog room, 12 in the laboratory, and one was left in its mold next to the CLSM backfill form with a lead wire inserted to obtain thermocouple data. Each week, the cylinders were tested following the ASTM D4823 specification. The tests were performed in an unconfined compression test machine with the strain rate set to 0.04 in/min. The cylinders were capped using gypsum cement as per the ASTM specification. A test cylinder just after testing is shown in Figure 3-8. The unconfined compression test results for the CLSM used in the 0° skew test are shown in Table 3-4.

Table 3-4. Average Unconfined Compressive Strength (*Note that the bold row indicates passive force–deflection test day)

0° Skew Test

Curing Time (days)	Curing Environment	
	Open-Air	Fog Room
	Avg Comp. Strength (psi)	
7	32.36	40.58
14	**45.23**	**84.62**
21	41.51	114.46
28	36.47	136.61

The difference in UCS was very significant for the two different curing methods. The measured strength of the CLSM backfill for the 0° skew test was better represented by the UCS of the open-air-cured cylinders. For this reason, when the CLSM backfill for the 30° skew test

was poured, all the test cylinders were cured in ambient laboratory conditions. Table 3-5 shows the UCS test results for the CLSM used in the 30° skew test.

Figure 3-8. Gypsum Cement capped CLSM cylinder after failure.

Table 3-5. Average Unconfined Compressive Strength (Note* bold row indicates passive force-deflection test day)

30° Skew Test

All Cylinders Open-Air Cured	
Curing Time (days)	**Strength (psi)**
7	53.81
8	**58.75**
14	69.23
21	78.98
28	67.84

Tables 3-4 and 3-5 show that the CLSM used for the 30° skew test gained strength much faster than the open-air-cured cylinders of the CLSM used in the 0° skew test. The average open-air-cured UCS on test day for each of the 0 and 30° skew tests were 45.2 psi (311.8 kPa) and 58.7 psi (405.1 kPa), respectively. In a material like CLSM with a very low cement content, even tiny differences in the amount of cement in the mix can make a significant difference in the UCS. Though the mix design for the two tests was the same, there was likely some slight variation that caused the difference.

Figure 3-9 provides a plot of the CLSM UCS versus time for the different tests and curing methods. The shape of the strength gain curves for the samples cured in the laboratory are quite similar and show a peak in strength after 14 to 21 days. However, the cylinders cured in the fog room continued to gain strength with time up to 28 days and the trend was still upward at that point. Furthermore, the strength of the laboratory cured cylinders was significantly less

than the strength obtained by curing the same CLSM in the fog room. Figure 3-10 shows the UCS values normalized by the 28-day fog room-cured UCS. It is notable that the UCS values for the laboratory-cured specimens achieved strengths of only approximately 35% and 58% of the 28-day strength of the cylinders cured in the fog room for the 0 and 30° skew test CLSM batches, respectively.

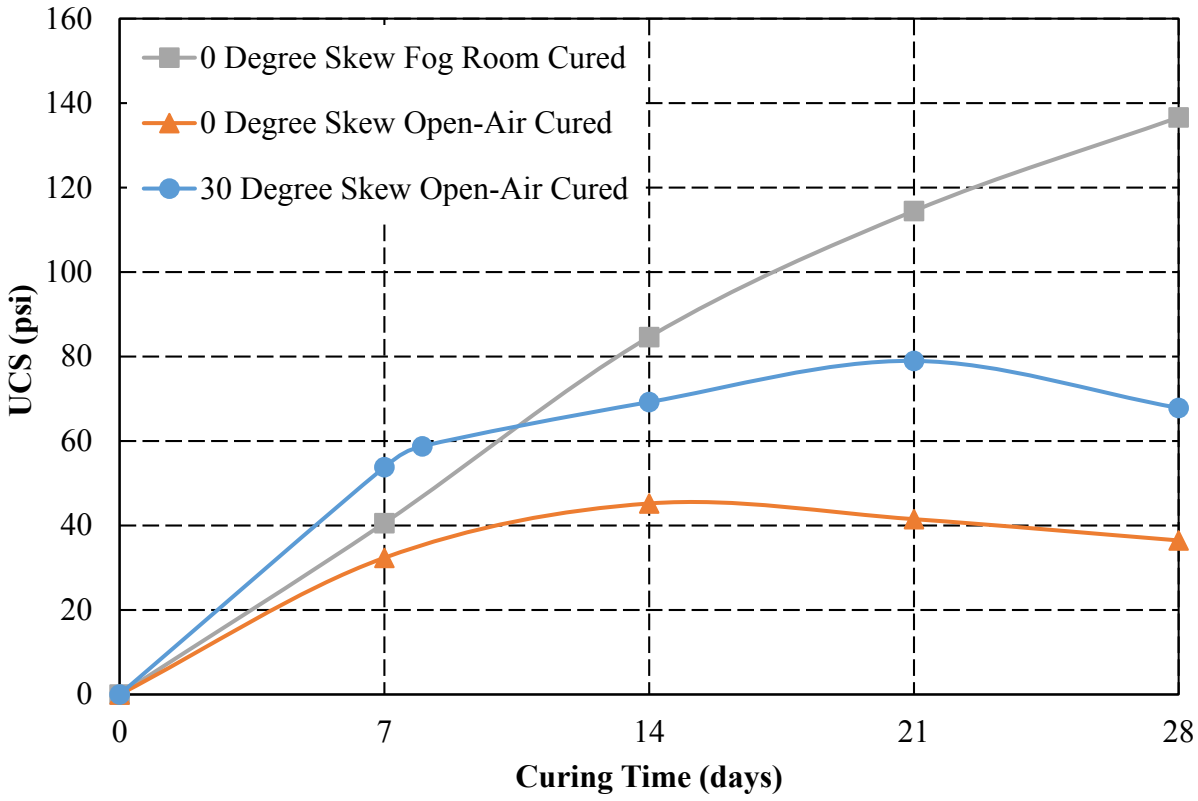

Figure 3-9. Unconfined compressive strength vs. time.

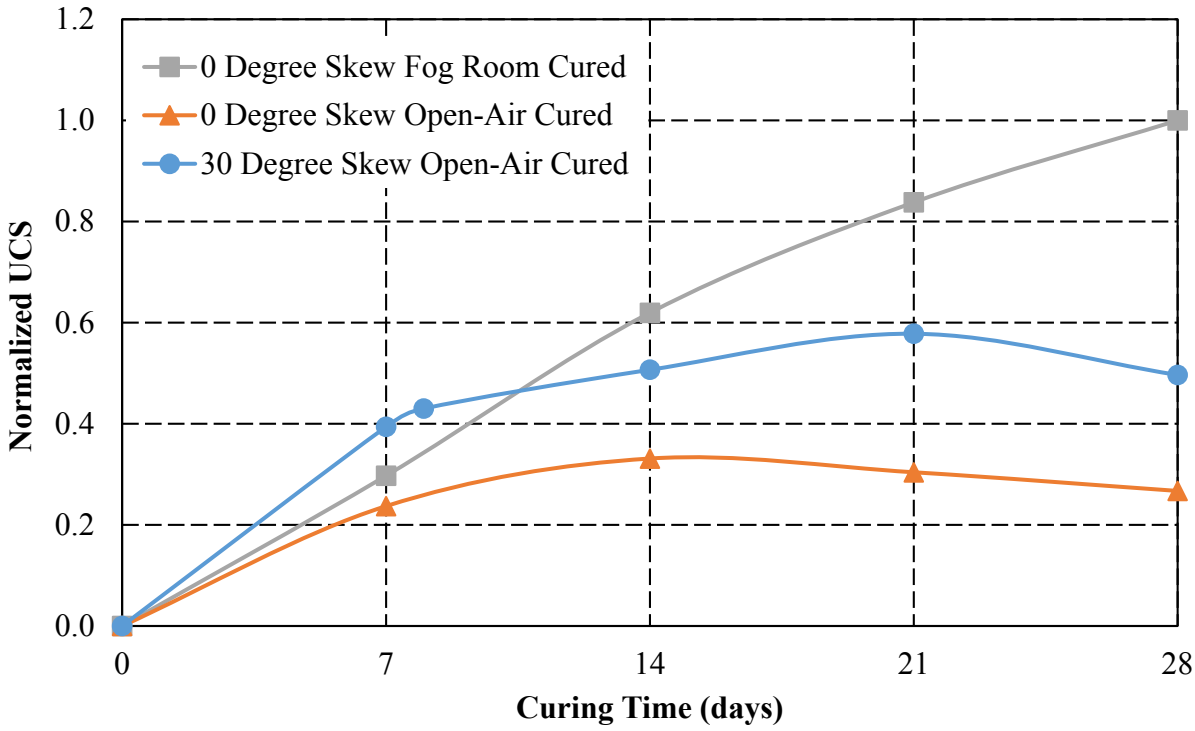

Figure 3-10. Normalized UCS vs. time.

3.4.3 Shear Strength

Both times that the CLSM backfill was poured for the passive force-deflection tests, direct shear test specimens were also poured. There were a total of eight direct shear box tests. Two were used to determine the wall or interface shear strength and six were used to evaluate potential relationships between shear strength and effective normal stress. For each skew angle test, three direct shear tests were performed at different normal stresses. These results are discussed in Section 3.3.4.

The six direct shear boxes that were used to determine the shear strength and interface shear strength of the CLSM were 12 in. x 12 in. x 8 in. (0.30 m x 0.30 m x 0.20 m) steel boxes without tops or bottoms. The boxes were stacked in pairs and tack welded together to hold them

in place when the CLSM was poured. Figures 3-11 and 3-12 show the described pour set-up and Figure 3-13 illustrates the loading set up for the direct shear test.

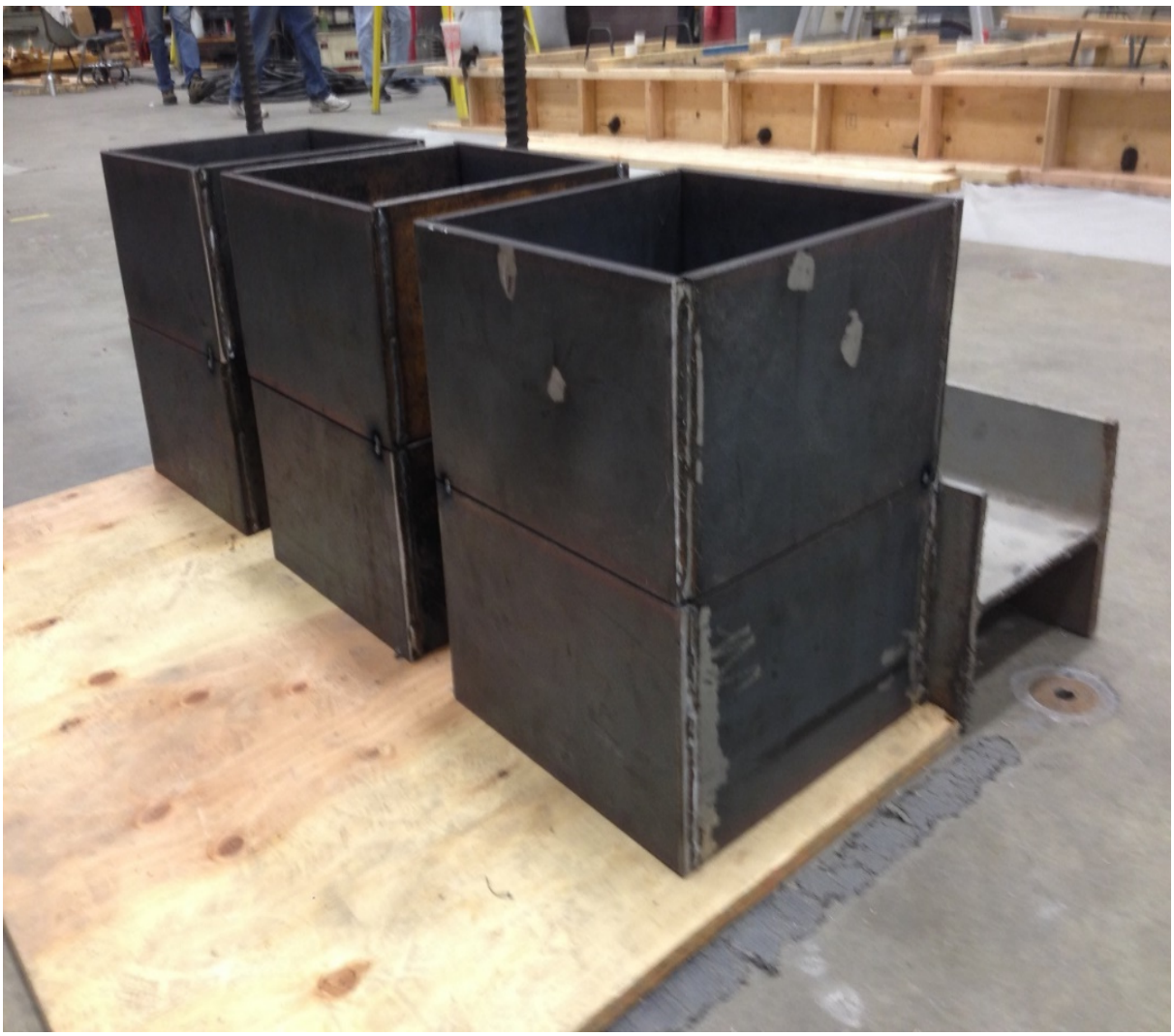

Figure 3-11. Photograph of CLSM direct shear boxes.

Figure 3-12. CLSM being poured into direct shear boxes.

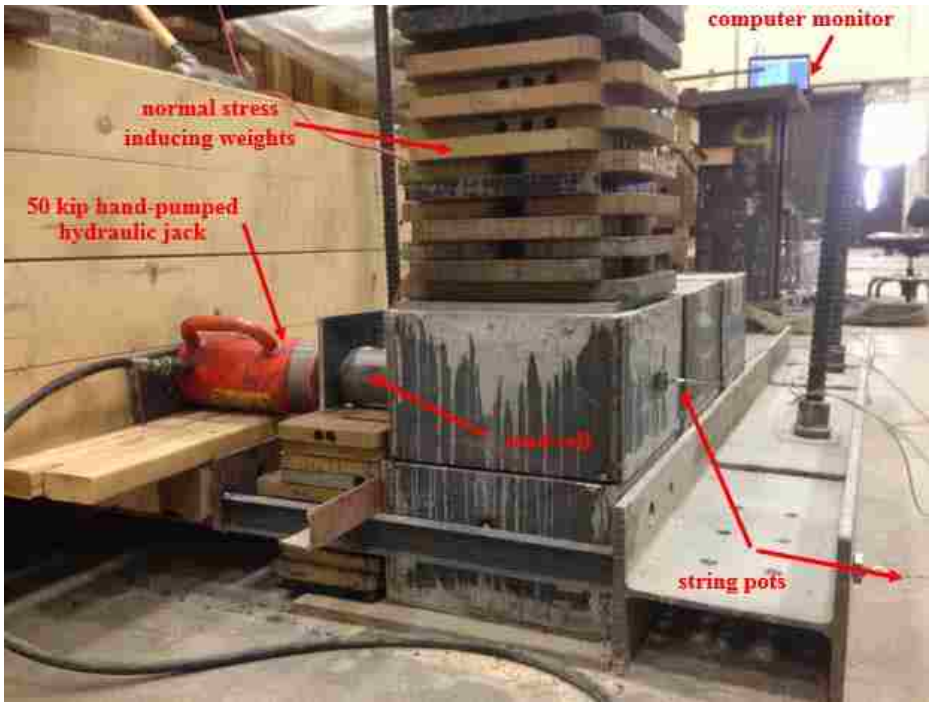

Figure 3-13. Direct shear test set-up.

On the day of the passive force-displacement tests, the tack welds holding the pairs of steel boxes together were ground off. On top of each direct shear box, a 0.50 in. (1.27 cm) thick steel plate was placed to spread the normal stress evenly over the entire surface of the direct shear box. The plate was cut just smaller than the inside dimensions of the box so that the load inducing the normal stress would rest entirely on the CLSM and not on the edge of the steel box. As shown in Figure 3-13, numerous steel weights were then loaded onto the plate until the desired load was achieved. Loads of differing magnitude were used for each of the three direct shear boxes. The first box was placed under a normal load of 866 lbs (393 kg). The second and third boxes were scaled to have two thirds and one third of the first test's load. The corresponding normal stresses for each of the tests were 6.02 psi (41.5 kPa), 4.06 psi (28.0 kPa), and 2.10 psi (14.5 kPa).

A load cell was placed between a hand-pumped hydraulic jack and the direct shear boxes to measure the load applied to the structure. Furthermore, a string potentiometer was attached to the back of the boxes and to the reaction block in order to measure the displacement of the direct shear box as well as the global displacement of the entire support structure. A stop watch and a computer screen displaying the load and displacement were used to monitor the strain rate of the direct shear tests. With the aid of a stopwatch, the operator of the hand-pumped hydraulic jack adjusted the loading rate to keep the strain rate at approximately 0.1 in/min.

The direct shear test process was performed on the CLSM used for both the 0 and 30° skew tests. The process, set-up, normal loads, normal stresses, and displacement rates were the same for both tests. The only variation was that the UCS of the CLSM used in the 30° skew test was higher than for the 0° skew test. The results of the direct shear tests are summarized in Table 3-6. The three different normal stresses, σ, are listed in the left column, and the shear stresses at

failure, τ_f, for both tests are listed in the right two columns. Figure 3-14 is a plot of shear stress at failure versus normal stress for both the 0 and 30° skew CLSM batches.

Table 3-6. Normal Stresses vs. Shear Stresses at Failure

			0° Skew Test	30° Skew Test
U.C. Strength (psi)			**45.23**	**58.75**
σ_{max} (psi)	6.02	**$\tau_{f\,max}$ (psi)**	18.01	17.38
$\sigma_{2/3}$ (psi)	4.06	**$\tau_{f\,2/3}$ (psi)**	18.17	21.63
$\sigma_{1/3}$ (psi)	2.10	**$\tau_{f\,1/3}$ (psi)**	16.48	15.83

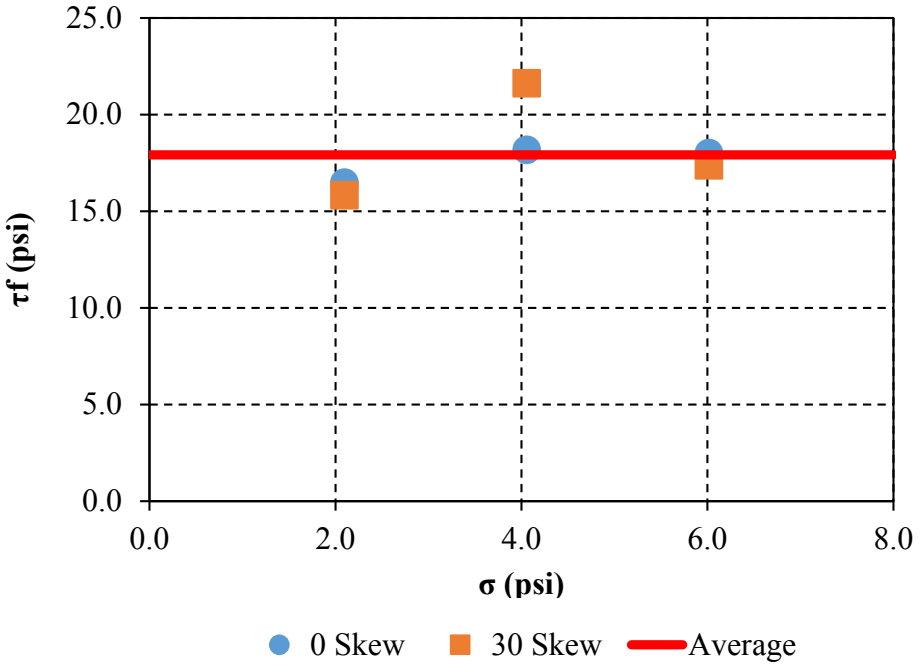

Figure 3-14. Plot of normal stress vs. peak shear stress.

Figure 3-14 shows that the shear strength of the CLSM was relatively unaffected by normal stress. This is in agreement with previous research done on soil-cement mixtures (Filz et al. 2015, Kitazume and Terashi 2013) and the 0° friction angle assumption. Based on this assumption the shear strength would be equal to the cohesion or the UCS divided by two. Figure 3-15 shows the normal stress versus shear stress normalized by the UCS for each test.

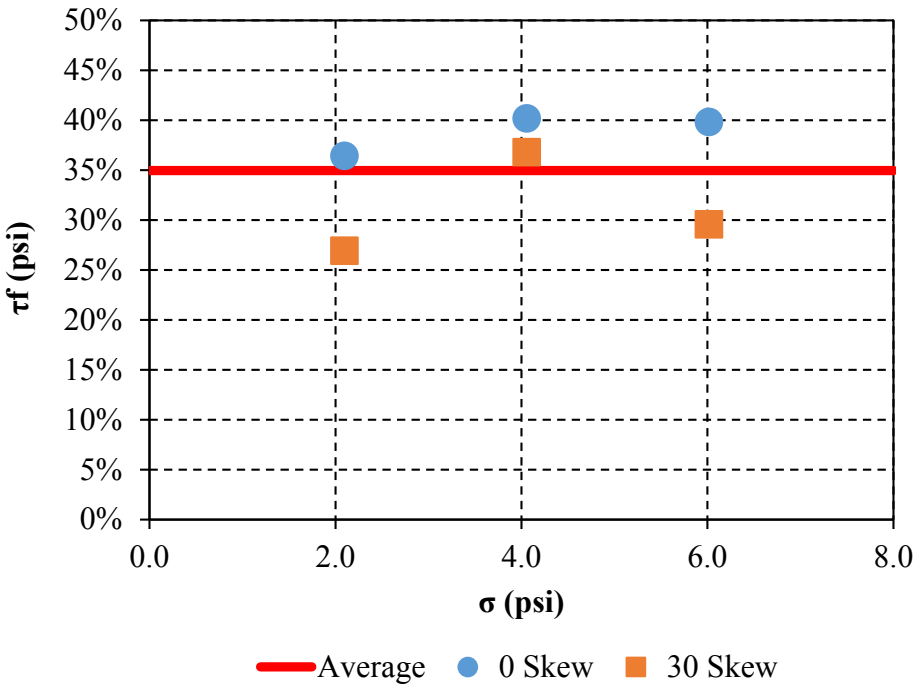

Figure 3-15. Plot of normal stress vs. normalized peak shear stress.

The average shear strength for the 0 and 30° skew CLSM batches was 17.9 psi (120.7 kPa). The normalized average shear strength for the 0 and 30° skew CLSM batches were 38.8% and 31.1% of their respective UCSs. Overall, the average shear strength of the CLSM was 35% of its UCS. The shear strength, or cohesion, was anticipated to be 50% of the UCS. The lower

strengths are likely attributable to the fact that the direct shear boxes were not able to be constrained to be loaded perfectly in shear. This caused a moment to be applied to the direct shear boxes, which compelled them to rotate, and the applied moment at the CLSM interface aided in the initial cracking of the CLSM and likely lowered the measured shear strengths. This occurred much more visibly during the tests with lower normal stresses, because they had less weight resisting the rotation of the box. Figure 3-16 illustrates the applied moment causing the apparent reduction in shear strength.

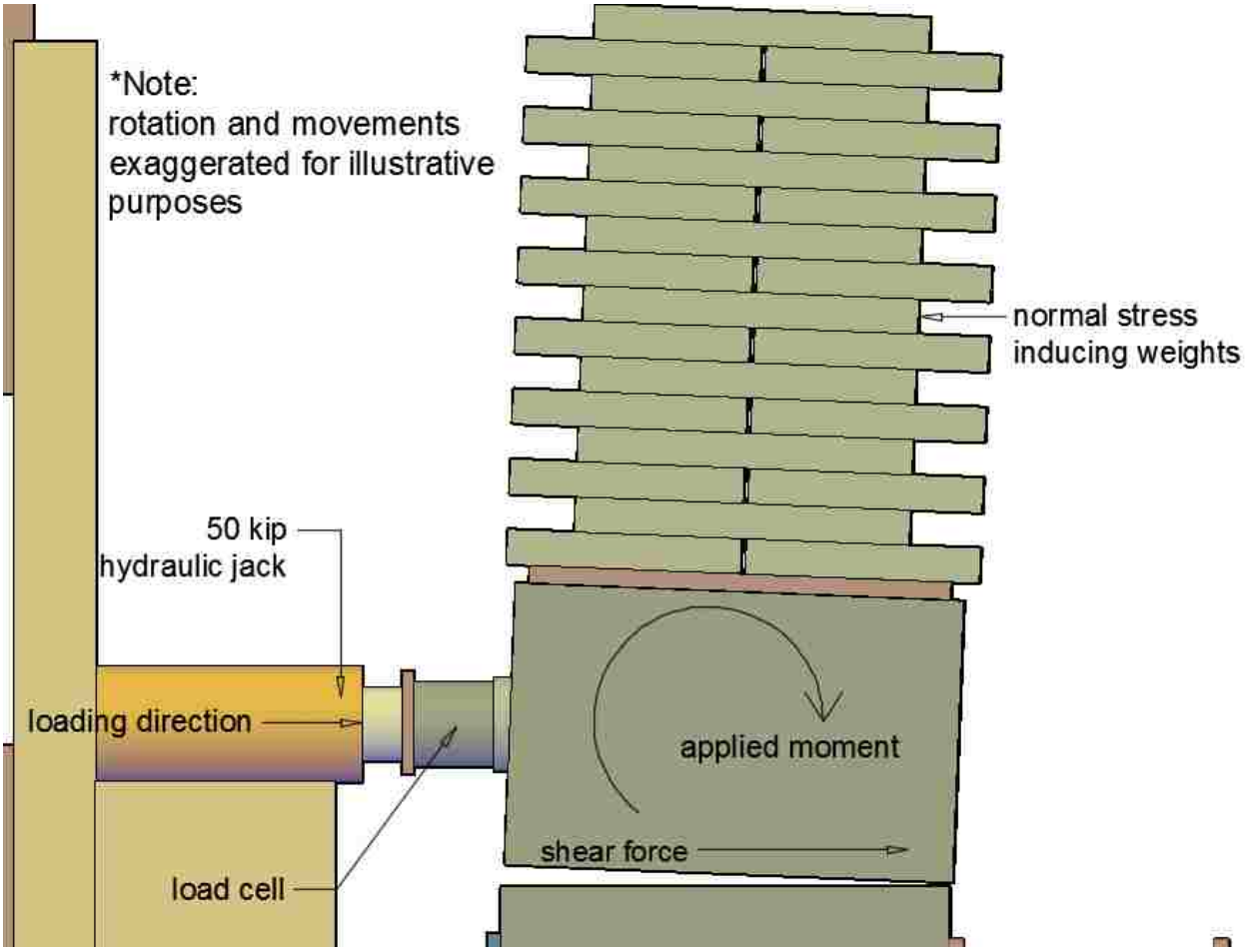

Figure 3-16. Moment application on the direct shear test set up (rotation exaggerated for illustration).

3.4.4 Interface Shear Strength

For each of the passive force-displacement tests, two direct shear tests were performed in an effort to evaluate the interface shear strength between formed concrete (the concrete reaction block) and the CLSM. The CLSM was poured into two 18 in. (0.46 m) square, 8 in. (0.20 m) tall direct shear boxes that sat on top of the concrete reaction block as shown in Figure 3-17. In contrast to the previous direct shear tests where shear occurred within the CLSM, the shear surface in these tests was constrained to occur at the interface between the concrete and the CLSM at the base of the box.

Figure 3-17. Interface shear boxes being filled with CLSM.

The testing procedures and equipment used were identical to those used in the direct shear tests mentioned in the previous section. However, the interface shear strength shear boxes were larger and had to be loaded with more weight to achieve the desired normal stresses. The first box was placed under a normal load of 1958 lbs (888 kg). The second shear box was scaled to have two thirds of the first test's load. The corresponding normal stresses for each of the tests were 6.04 psi (41.5 kPa) and 4.03 psi (28.0 kPa). This set up was repeated for the 0 and 30° skew CLSM batches. Figure 3-18 shows one of the interface shear strength tests ready to be performed.

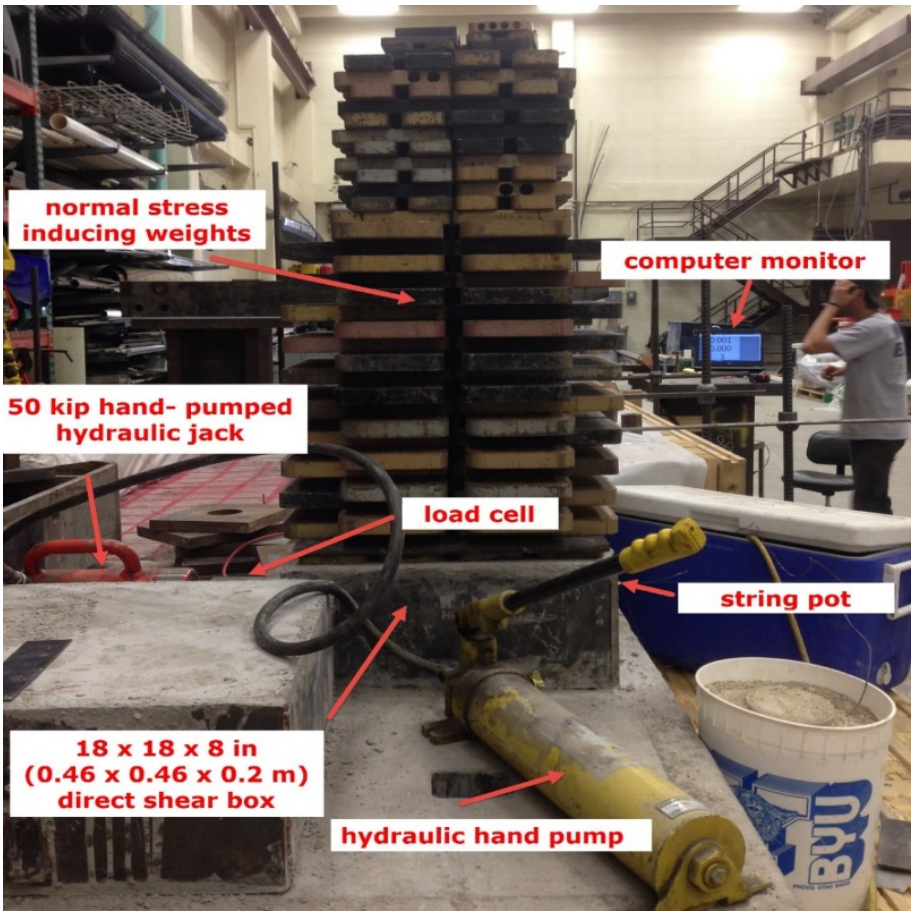

Figure 3-18. Interface shear strength test set up.

The results for the interface shear strength tests were also lower than the anticipated 50% of the UCS. Table 3-7 shows the interface shear strength results for the two tests performed for each of the CLSM batches. Figure 3-19 plots the interface shear strength versus normal stress and Figure 3-20 is a plot of the interface shear strength normalized by its corresponding UCS versus normal stress.

Table 3-7. Normal Stresses vs. Shear Stresses at Failure

			0° Skew Test	30° Skew Test
U.C. Strength (psi)			**45.23**	**58.75**
σ_{max} (psi)	6.04	**$\tau_{f\,max}$ (psi)**	15.35	12.35
$\sigma_{2/3}$ (psi)	4.03	**$\tau_{f\,2/3}$ (psi)**	14.61	10.54

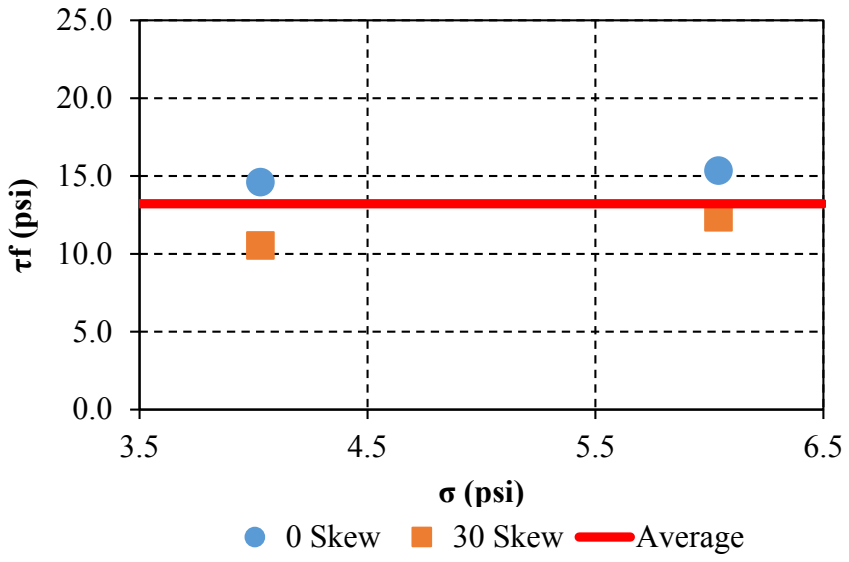

Figure 3-19. Plot of normal stress vs. peak interface shear stress.

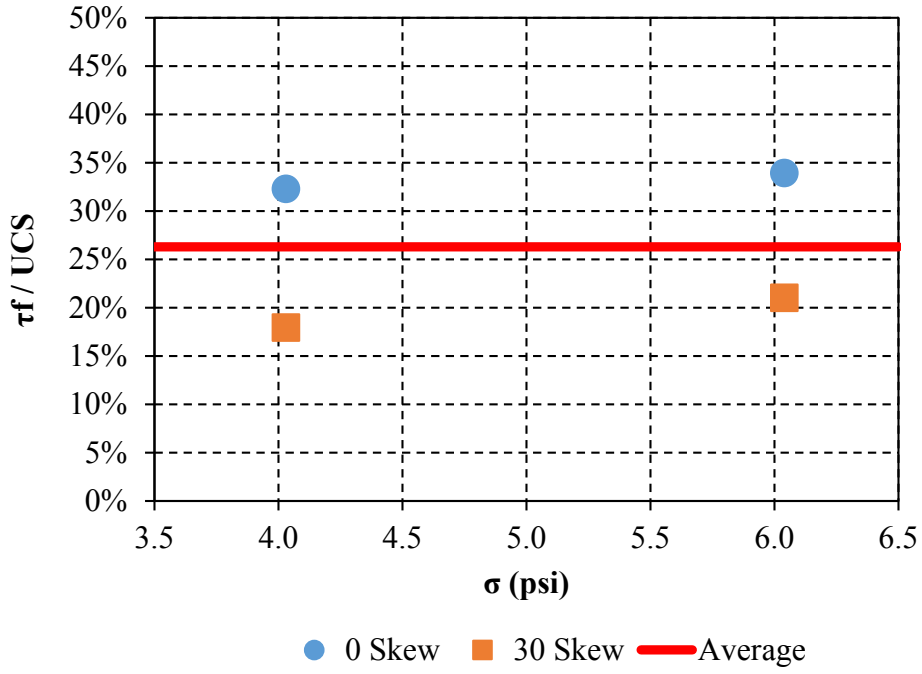

Figure 3-20. Plot of normal stress vs. normalized peak interface shear stress.

The average interface shear strength was 15.0 psi (103.4 kPa) for the 0° skew CLSM batch and 11.5 psi (79.3 kPa) for the 30° skew CLSM batch. As a percentage of the UCS, this translates to 33.1% and 19.5% for the 0 and 30° CLSM batches, respectively. The overall average interface shear strength for the two tests was 26.3% of the CLSM's UCS.

It is notable that the interface shear strength was much lower than the anticipated 50% of the UCS. These lower strengths are likely because of the applied moment discussed in the previous section, and also because the fresh CLSM poured on top of the concrete reaction block formed a cold joint in which the bonding between the CLSM and concrete block could not be fully developed. This can be attributed to a phenomenon like the interfacial transition zone (ITZ) familiar to the concrete industry. The ITZ is a microscopic zone that occurs within cemented-materials. It is a zone of weakness around individual aggregate particles where cracking and

fractures tend to occur. Mindess (2003) states that the structure of the ITZ is different from the bulk of the cement paste in that it has less unhydrated cement, higher porosity, lower density, and less calcium-silicate-hydrate (primary cementing product). In this research, the occurrence of a weak zone along the interface failure plane likely affected the interface shear strength detrimentally. It should also be noted that the reaction blocks were swept clean of dust and debris prior to CLSM placement, but the cleaning process may not have removed the finer dust or any grease that may have been present on the surface. This may have also reduced the adhesion of the CLSM to the concrete reaction block. All of these factors contributed to the lower-than-expected interface shear strength.

The shear strength envelope referred to in Figure 2-2 for soil-cement materials was plotted and then the results from these direct and interface shear tests were imposed on top of it to examine the correlation between the two. Figure 3-21 shows the results of these tests placed on the shear strength envelope proposed by Filz et al. (2015). It can be seen that the results from the shear tests done on CLSM compare very well with the proposed lower-bound shear envelope for soil-mixed material, though the direct shear strength of CLSM plotted slightly higher than the soil-cement, and the interface shear tests plot slightly lower for the reasons explained in the previous paragraph. As mentioned previously, the assumed cohesion for soil-cement material is generally assumed to be 0.7 * 50% of the UCS. Filz et al. (2015) stated that the 50% was to account for the shear strength of the material, and that the 0.7 was to account for the mass strength in terms of the small-sample strength. The assumed cohesion was not corrected by the 0.7 factor for the passive force displacement tests that are outlined in Chapter 4. The cohesion was assumed to simply be 50% of the UCS of the CLSM. This was done because CLSM is mixed thoroughly in a truck or at a batch plant, and should theoretically have no mass effects like

soil-mixed cement. This assumption gave much more accurate predictions of the passive force than when corrected by the 0.7 factor.

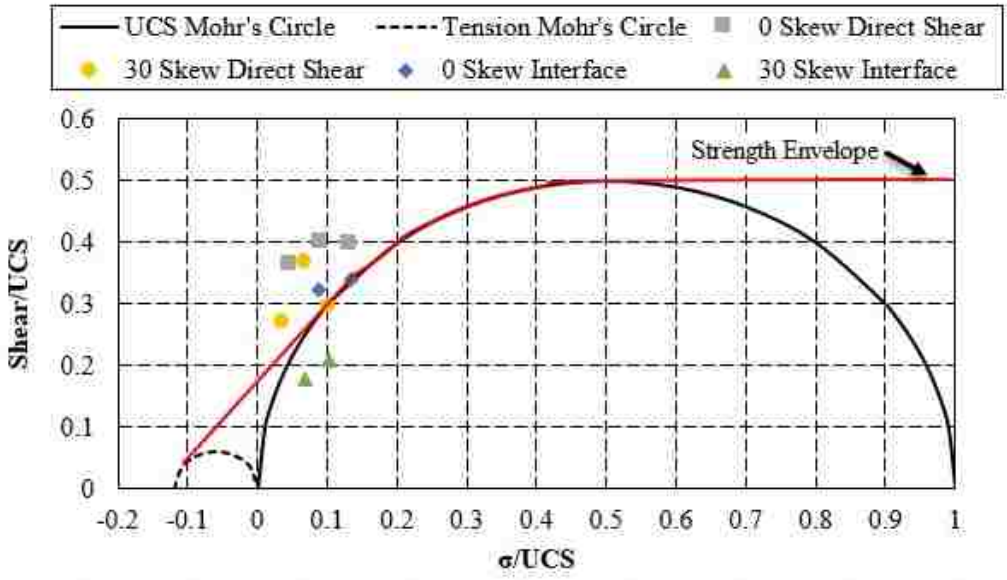

Figure 3-21. Direct and interface shear strengths compared to soil-cement shear strength envelope proposed by Filz et al. (2015).

3.4.5 Curing Rate

Thermocouple data were collected for the CLSM used in both tests with a four-channel thermocouple data recording device. As mentioned in Section 3.2.6, the thermocouple lead wires were installed into four locations: a test cylinder still in its plastic mold, the upper third of the CLSM backfill, the middle third of the backfill, and the lower third of the backfill. The data-recording device measured the internal temperature of the CLSM and also calculated the maturity. These measurements give information about the curing process within the backfill and any differences in the curing process at the various depths. Figure 3-22 shows a plot of the maturity versus time for the 0° skew test CLSM batch, and Figure 3-23 is the same plot for the

30° skew test batch. The maturity is simply the area under the time versus temperature curve, and the baseline for the curve is -10°C, which is the lower limit for cement hydration to occur. So, maturity is the temperature above -10°C multiplied by the time interval to obtain a maturity value with units of °C-hr. It should be noted that recording of the thermocouple data was concluded for the 30° skew test much earlier than for the 0° skew test. This was done because the 30° skew test was performed after just 8 days rather than 14 as with the 0° test. The CLSM used in the 30° skew test reached the anticipated test strength much faster than that used for the 0° skew test, so it was tested sooner, and the thermocouple data recording was terminated sooner as well. To keep the graphs comparable, the data for the 0° skew test is cut off at 300 hours.

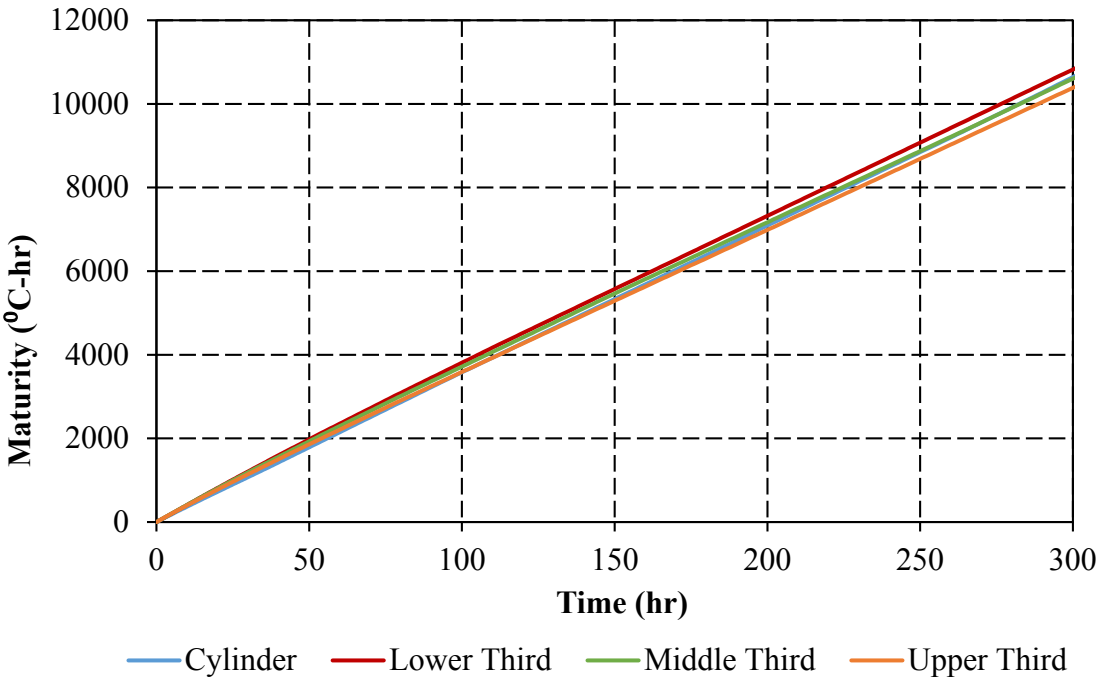

Figure 3-22. Maturity vs. time for the 0° skew test CLSM.

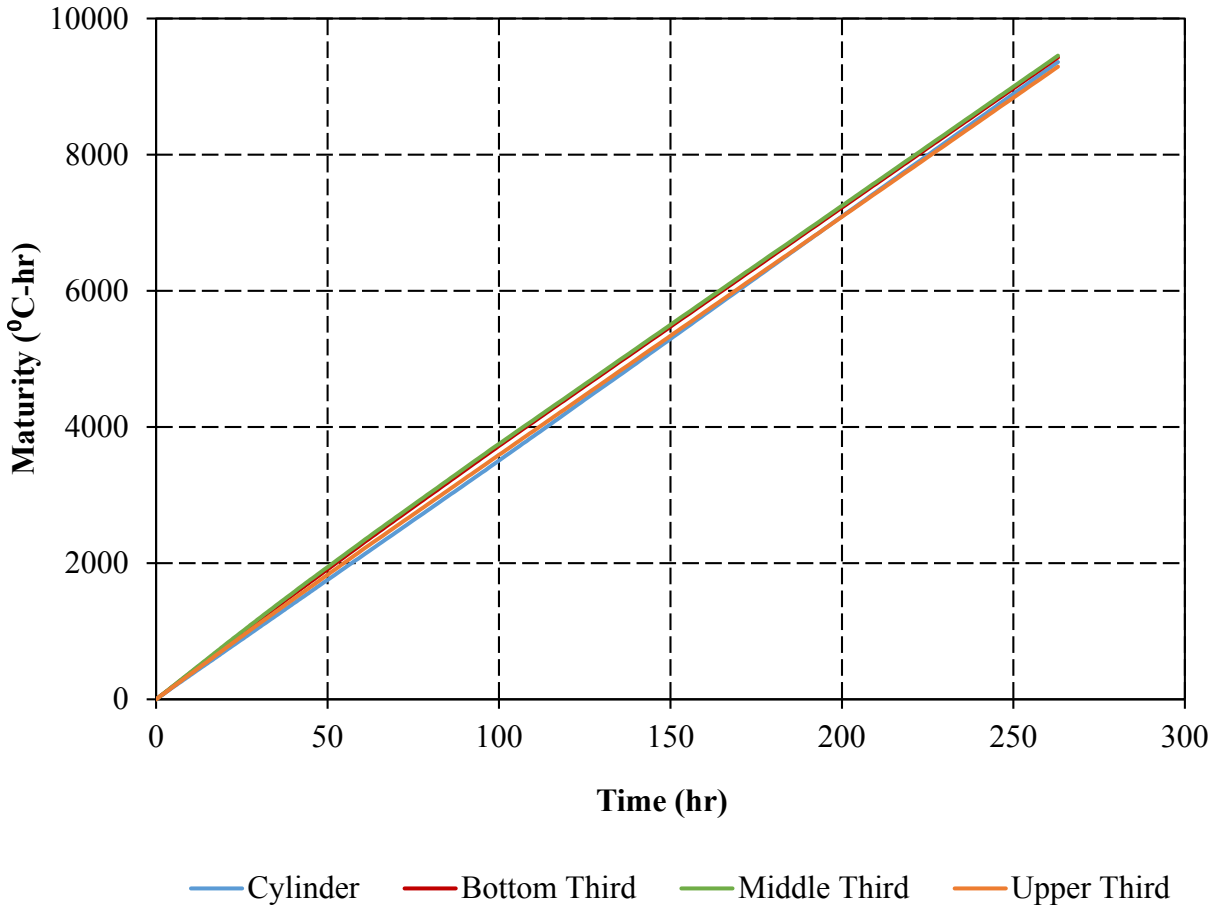

Figure 3-23. Maturity vs. time for the 30° skew test CLSM.

Figures 3-22 and 3-23 show that the maturity over time at the four different locations were all very similar. This indicates a very uniform curing process throughout the CLSM backfill. The depth into the backfill had little effect on the maturity of the CLSM as it cured.

Also of interest was the temperature gradient within the CLSM backfill as the curing continued. Portland cement hydration reactions are exothermic, so the cement hydration causes higher temperatures that lead to faster curing concrete or CLSM. The temperature at various

times is plotted at the three depths within the CLSM backfill for both the 0° and 30° skew tests in Figures 3-24 and 3-25, respectively.

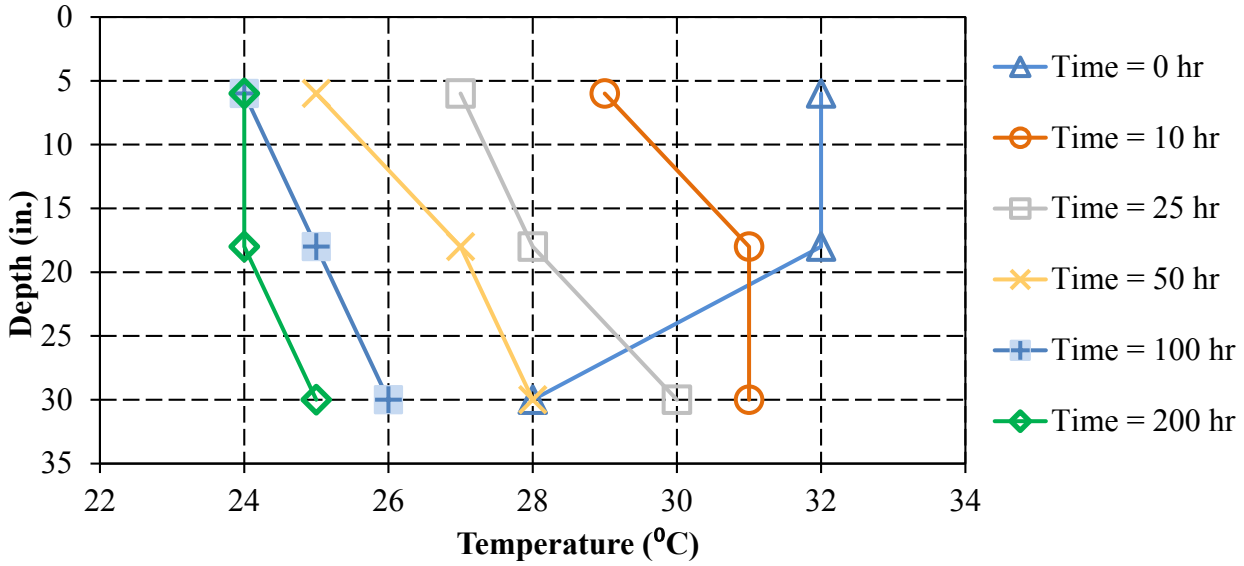

Figure 3-24. Temperature vs. depth at varying times for 0° skew test CLSM backfill.

The temperature gradient, or difference in temperature, was usually largest in the first few hours because the rate of cement hydration reactions decreases with time. In the 0° skew test, the bottom of the CLSM backfill mass was generally the highest temperature, but only by a few degrees. The maximum temperature difference was 3°C (5.4°F), and the mass uniformly cooled to the ambient laboratory temperatures of 25-26°C (77-79°F) after approximately 200 hours. In the 30° skew test, it was typically the middle of the backfill that had the highest temperatures. This is evident in Figure 3-25. It is reasonable to suggest that the heat from the bottom and upper sections of the backfill was being absorbed by the floor and the air in the

laboratory, and that the middle section was insulated and kept the warmest. This CLSM also cooled uniformly to ambient temperatures of 25-26°C (77-79°F) after approximately 200 hours.

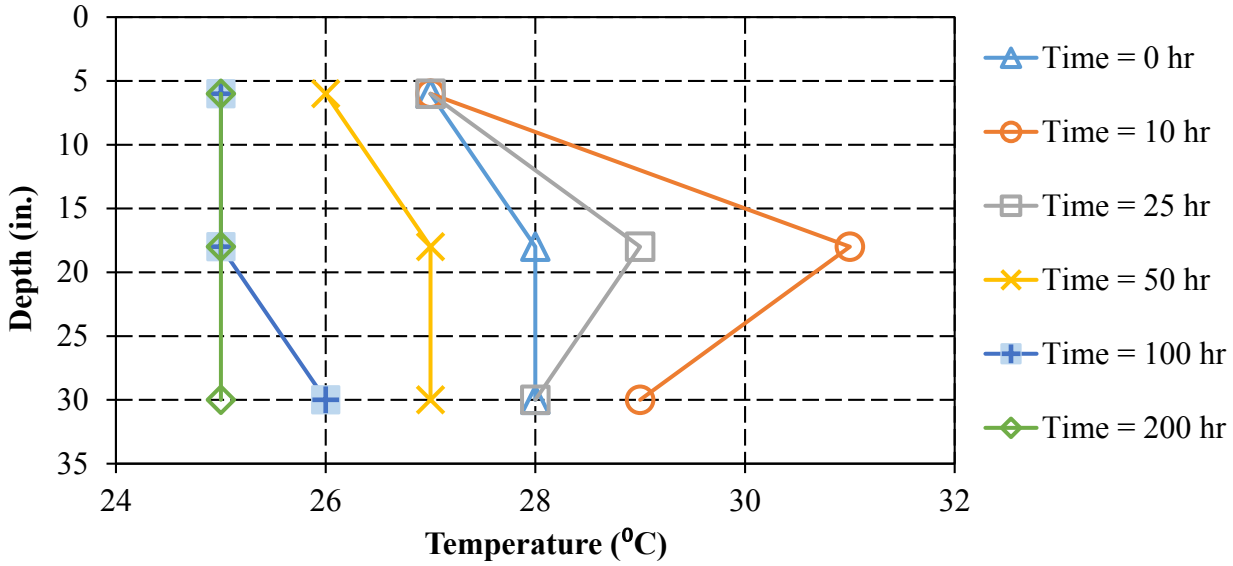

Figure 3-25. Temperature vs. depth at varying times for 30° skew test CLSM backfill.

The data show that though a thermal gradient was apparent at differing depths, the gradient was small. With a virtually uniform temperature gradient at the three different depths, this further suggests that the CLSM cured fairly uniformly.

Thermocouple data were also monitored and recorded in conjunction with the unconfined compression tests in an attempt to relate maturity to UCS. The thermocouple data were only monitored for approximately two weeks because of the negligible changes in temperature in the CLSM backfill after 100-200 hours. For the 0° skew test CLSM, the maturity data were recorded

at the same time as the 7-day and 14-day UCS values were obtained. However, because the 30° skew test was performed after only 8 days of curing, the maturity data were only recorded at the time of the 7-day UCS tests. However, after 8-10 days the temperature, and thus the additional maturity per hour, remained constant. So, the maturity data were extrapolated for the 21-day and 28-day UCS tests using Equation 3-4.

$$Maturity = m_f + t * 36 \quad (3\text{-}4),$$

where

$$m_f = final\ maturity\ reading\ from\ thermocouple\ recording\ device,$$

and

$$t = number\ of\ hours\ from\ time\ of\ final\ reading\ to\ 14, 21, or\ 28\ days.$$

The number of hours from the final reading to the specific curing time is multiplied by 36 because the ambient temperature to which the measurement normalized for the instrumented cylinder was 26°C for both tests, so the height from the baseline of -10°C was a constant of 36°C. Thus, every hour, the maturity increased by 36°C-hr. The results of the maturity and extrapolated maturity versus strength data are tabulated in Table 3-8. To generate a maturity versus UCS curve, the averages of the maturity and UCS for the two CLSM batches at the 7-day, 14-day, 21-day, and 28-day curing times were calculated. The resulting plot is shown in Figure 3-26.

Table 3-8. Maturity versus UCS Data

Curing Time (days)	Curing Time (hrs)	0° Skew Test CLSM		30° Skew Test CLSM	
		Maturity	UCS	Maturity	UCS
7	167	5927	32.36	5906	53.81
14	336	11949	45.23	11990	69.23
21	504	17997	41.51	18038	78.98
28	672	24045	36.47	24086	67.84

*note: $mf_{0\ skew}$ taken at t=397 hr

$mf_{30\ skew}$ taken at t=263 hr

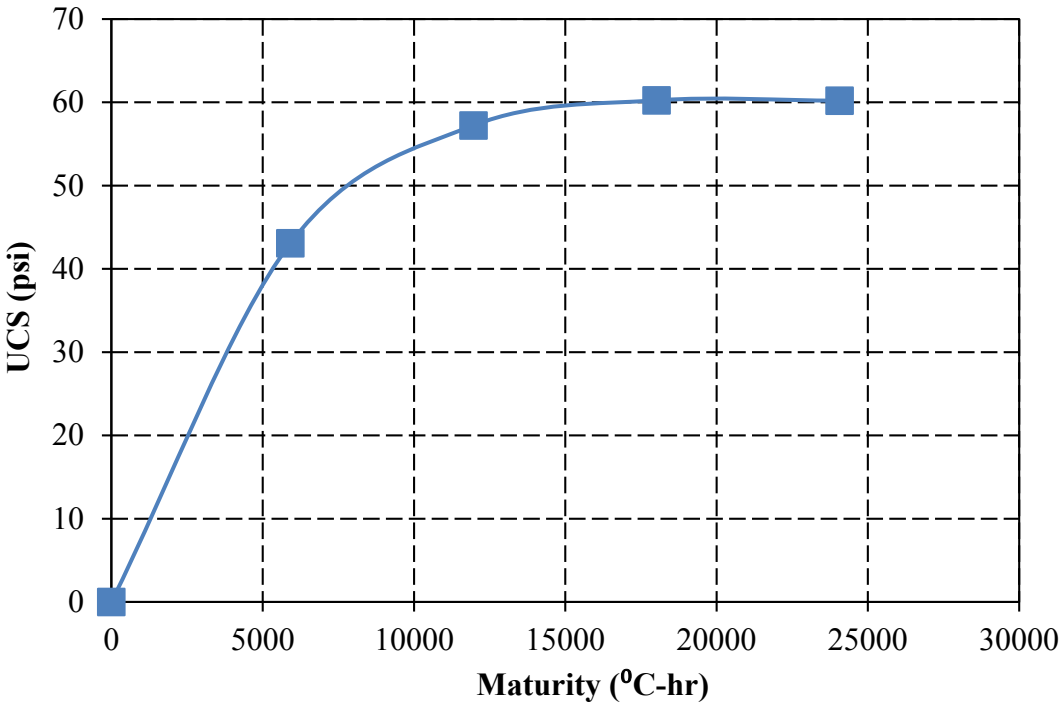

Figure 3-26. Maturity vs. UCS curve.

This curve is very crude because of the few available data points and the extrapolation of the data, but for the same type of CLSM cured in ambient conditions Figure 3-26 could provide an estimate of the CLSM UCS based on maturity data only. Including more data points would give greater definition to the curve and then it could be used to determine when a specified strength is achieved without having to break cylinders so often. Instead, the maturity data from the thermocouple device would give an estimate of when the designated strength is reached, and then cylinders could be tested to verify the estimate. However, the sample size of the data in this thesis did not provide for a curve with such high resolution.

In summary, the thermocouple data gave valuable information regarding the curing of the CLSM backfill as a whole. The data suggest that the mass of CLSM cured relatively uniformly with depth, and that the temperature gradient was never excessive through the backfill. Finally, the data also allow for a crude estimation of the UCS based on the maturity reading from a thermocouple device.

4 PASSIVE FORCE TEST RESULTS

4.1 Passive Force-Deflection Curves

The passive force-deflection curves were created from the actuator longitudinal load and string pot longitudinal displacement data collected during each test. The passive force, P_P, acting on the abutment backwall was computed using the actuator longitudinal load data and Equation 2-5. Longitudinal displacement, Δ, was taken as the average of all four longitudinal string pot measurements. Figure 4-1 shows the longitudinal force plotted against deflection for the two tests, and Figure 4-2 is a plot of the longitudinal force versus displacement, Δ, normalized by the wall height, H, of 24 in. (0.61 m).

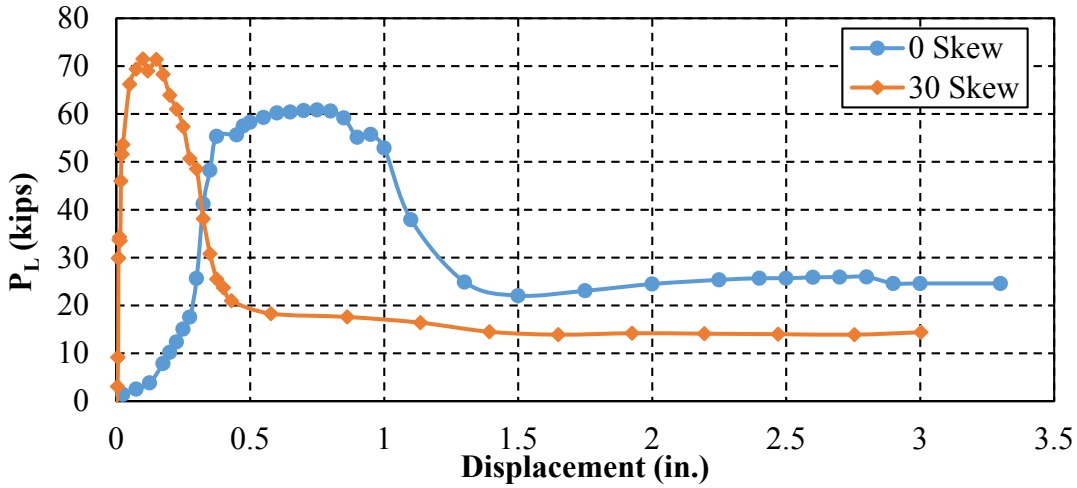

Figure 4-1. Longitudinal load versus displacement curves.

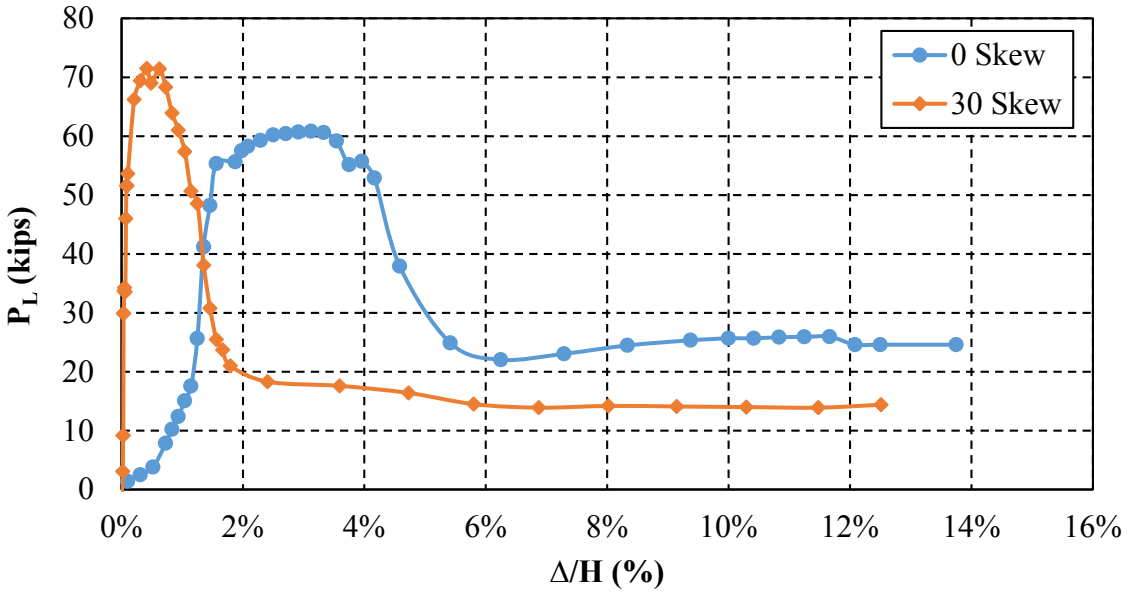

Figure 4-2. Longitudinal load versus normalized displacement.

As can be seen Figures 4-1 and 4-2, the longitudinal load versus displacement relationship for the 0° skew case was concave up at the beginning of the test. This was assumed to be due to the actuator loading the entire reaction structure and closing any gaps that were present in the system. In the first test (the 0° skew test), the backwall was put in place and then the CLSM was poured with only a temporary bracing on the backwall. However, the reaction frame was yet to be built and the backwall still had not been connected to the actuator. Likely, the backwall for the 0° skew test was not flush against the CLSM backfill to begin the test. In contrast, the reaction structure and actuator were already in place to restrain the backwall from moving away from the backfill for the 30° skew test. Excluding the concave up section in the 0° skew test, both curves display a hyperbolic longitudinal force-displacement relationship.

Equation 2-5 was used to calculate the passive force, P_P, from the longitudinal load data, and Figure 4-3 shows the plot of passive force versus displacement for the two tests. The concave up portion of the 0° skew test was shifted towards the origin and the plot begins at the linear-elastic portion of the curve. In Figure 4-4, the passive force-displacement curve has its displacement, Δ, normalized by the wall height, H, of 24 in. (0.61 m).

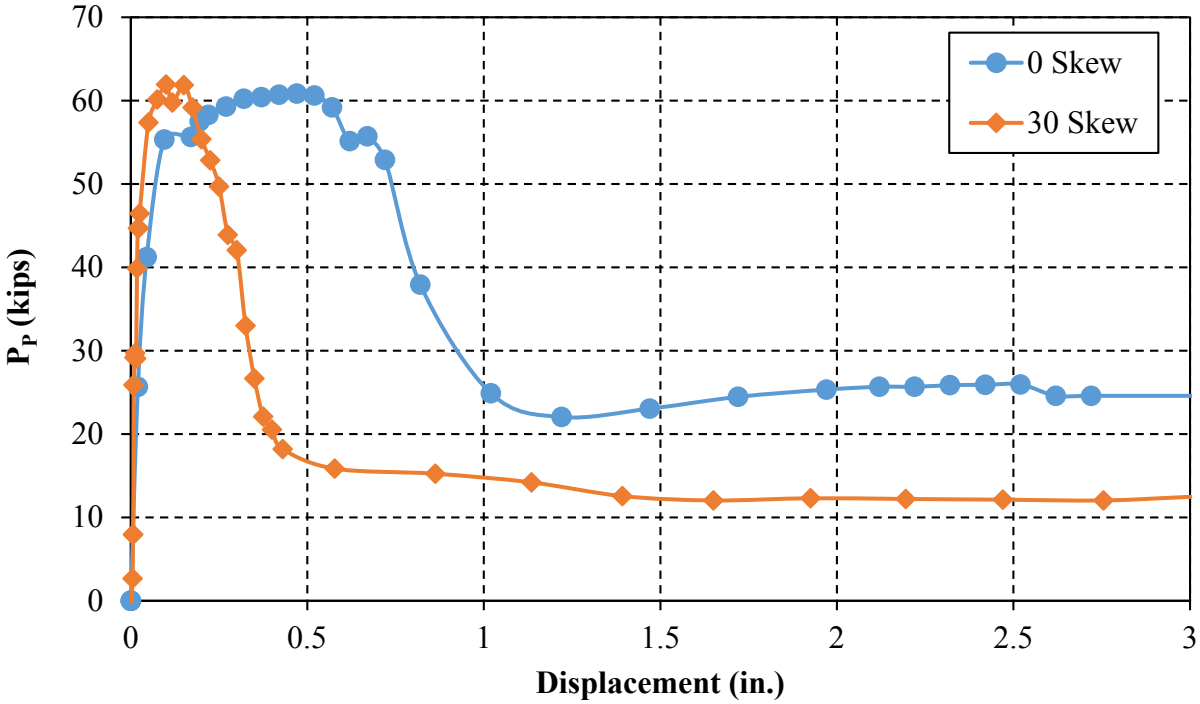

Figure 4-3. Passive force versus displacement.

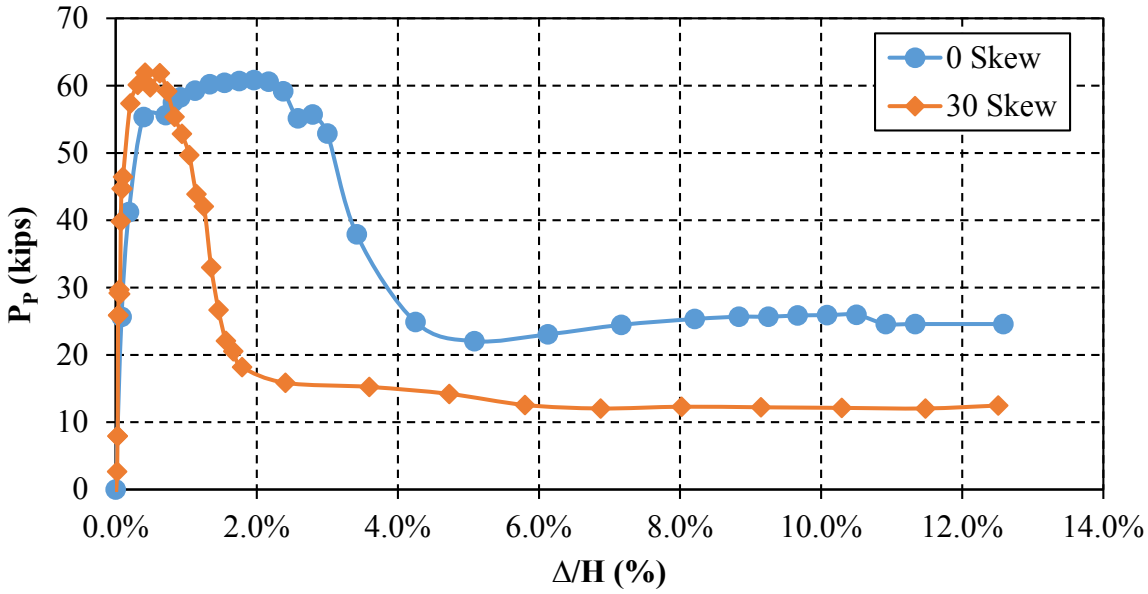

Figure 4-4. Passive force versus normalized displacement.

The plots in Figures 4-3 and 4-4 show that the peak passive pressure occurred with less displacement for the 30° skew test than for the 0° skew test. The UCS of the CLSM backfill was higher for the 30° skew test than for the 0° skew test, so the stiffness, or modulus, was likely higher. This is apparent from the initial slope of the passive force-displacement curves, in that the slope was slightly steeper for the stronger CLSM used in the 30° skew test. However, the stiffness values were quite similar for the two tests when compared with their corresponding UCS. The stiffness, k, was estimated from the preceding passive force-displacement curves as the initial slope of the curve. K was estimated as 1900 kip/in (3.3 MN/cm) for the 30° skew test and approximately 1300 kip/in. (2.3 MN/cm) for the 0° skew test. The UCS of each corresponding test was divided by these approximate stiffness values, and the ratios for the two tests are very similar. The UCS/k (psi/kip/in.) ratio expressed as a percentage was 3.5% for the 0° skew test and 3.2% for the 30° skew test. Thus, the average k can be approximated using Equation 4-1, which is given as

$$k\left(\frac{kip}{in}\right) \approx 30 * UCS\ (psi) \quad (4\text{-}1).$$

The higher magnitude of stiffness for the CLSM used in the 30° skew test likely caused it to fail at a smaller displacement than for the 0° skew test. The displacement required to reach the peak passive force for the CLSM backfill used in the 0 and 30° skew tests was approximately 2.0 and 0.75% of the backwall height, respectively. This agrees with research done on soil-cement material which reported strains less than 1% to reach the peak UCS in their testing (Filz 2015, Kitazume and Terashi 2013). On average displacement required to reach the peak passive pressure for the CLSM material used in these two tests was approximately 1.4% of the backwall height. Previous research has agreed that displacements of approximately 3-5% are typically required to reach peak passive pressures using conventional backfill materials (Rollins and Cole 2006, Rollins and Jessee 2013). The smaller displacement in the CLSM tests was likely due to the brittle nature of the CLSM. It has a higher modulus than conventional backfill, so smaller strains have a much more pronounced effect on CLSM.

The passive force-displacement relationship follows the hyperbolic shape suggested by Duncan and Mokwa (2001), but the initial slope was nearly linear. Using Equation 2-2, the peak passive forces were estimated for the two different CLSM batches. The inputs for Equation 2-2 were the average unit weight, UCS, wall width, wall height, and cohesion. The cohesion was assumed to be 50% of the average UCS of the CLSM. Table 4-1 shows the inputs for predicting the peak passive force, and the results of the predicted versus measured peak passive forces are shown in Table 4-2.

Table 4-1. Equation 2-2 Input Parameters

	0° Skew Test	30° Skew Test
γ_m (pcf)	122.0	112.5
B (in)	49.5	49.5
H (ft)	2	2
UCS (psi)	45.23	58.75
c (psf)	3257	4230

Table 4-2. Measured and Predicted Peak Passive Forces

	P_p max		
Test	Measured	Predicted	Error
0° Skew	60911	54740	10.1%
30° Skew	62740	70723	-12.7%

It can be seen that there is very good agreement with the prediction given by Equation 2-2 and the measured peak passive forces. The error ranges from a 10% underestimate for the 0° skew test, to a 12.7% overestimate for the 30° skew test. These results suggest that the average resistance is appropriately estimated using the Rankine equation for passive force. Using the peak predicted passive forces, the passive force data were normalized and plotted against displacement in Figure 4-5. Figure 4-6 shows the normalized passive force versus normalized displacement curve.

Figures 4-5 and 4-6 also show the residual strength of the CLSM, and the displacement required to reach the residual strength. For the 0° skew test, the residual strength was

approximately 40% of the predicted peak passive force, and approximately 20% of the peak for the 30° skew test. The displacement required to reach the residual strength was approximately 4-5% for the CLSM used in these two tests. These results are in agreement with results found when testing soil-cement materials which were stated to also have residual strengths of 20% of their UCS within strains of 3-5% (Filz et al. 2015, Kitazume and Terashi 2013).

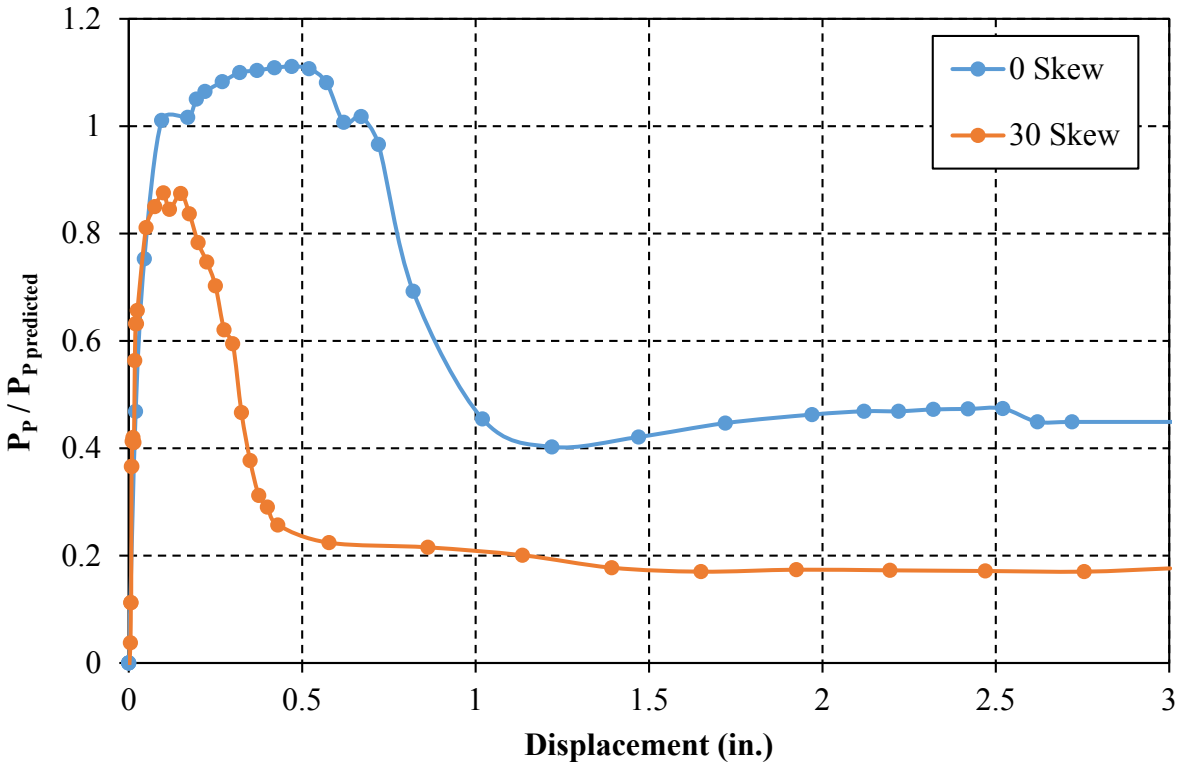

Figure 4-5. Normalized passive force-displacement curve.

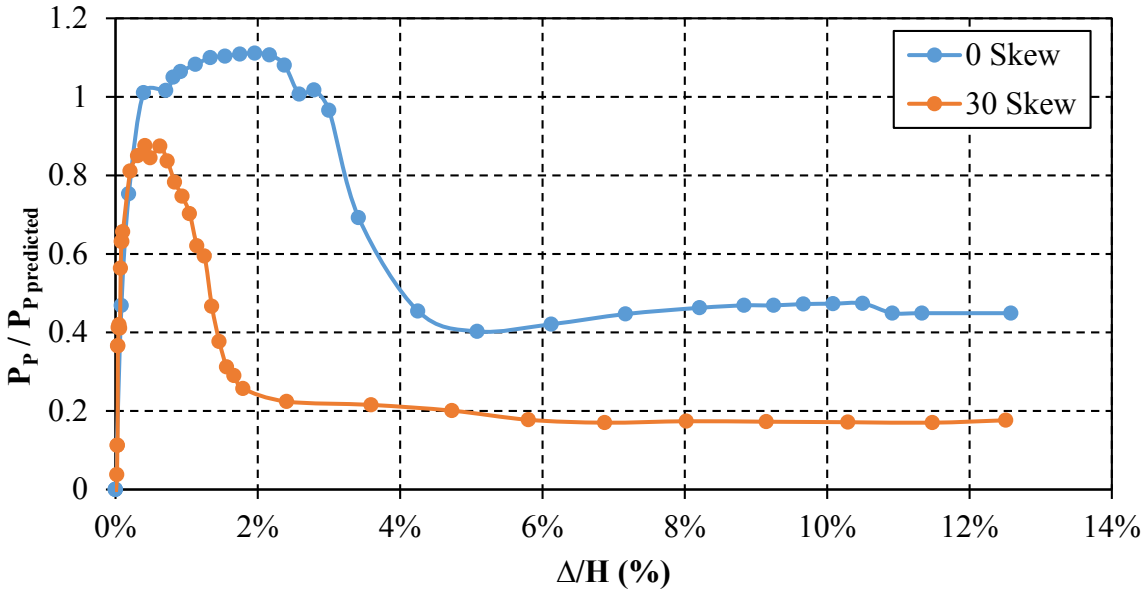

Figure 4-6. Normalized passive force vs. normalized displacement.

The residual strength for CLSM as a percentage of the peak passive strength is much lower than the reported 60% for dense compacted sand (Rollins and Jessee 2012). Once the cementitious bonds are broken, the cohesive strength is reduced significantly. The weight of the soil and the reduced cohesion are the two contributors to the residual passive force calculated in Equation 2-2. In Table 4-3, the fraction of the maximum cohesive strength that was required to calculate the observed residual strengths was back-calculated. The fraction of the peak cohesive strength that produced the residual strength ranged from 17% for the 30° skew test to 43% for the 0° skew test. If these are taken as the extreme cases, then the average amount of cohesive strength required to develop the ultimate or residual strength is 30% of the CLSM's maximum cohesion strength. This is attributable to the significant loss in strength observed in the passive force-displacement curves.

Table 4-3. Percent of Unconfined Compressive Strength Required for Residual Strength

					Contributions to Eqn 2-2			
Test	$P_{p\,measured\,peak}$ (lbs)	γ (pcf)	P_{ult}/P_p	P_{ult} (lbs)	Soil Weight (lb)	Cohesion (lb)	$UCS_{measured}$ (psi)	$UCS_{req'd}$ (%)
0^0 Skew	60911	122	40%	24364	1008	23357	45.23	43%
30^0 Skew	62740	112.5	20%	12548	929	11619	58.75	17%
							AVERAGE:	30%

4.2 Backwall Movement and Rotation

String potentiometer data that displayed both the transverse and vertical backwall displacement was examined for both tests to find the maximum displacement for each direction. Table 4-4 shows the maximum transverse and vertical backwall displacements for each test. To summarize, the maximum displacements in the transverse and vertical directions were 0.16 in. (4.06 mm) and 0.14 in. (3.56 mm), respectively. Contrary to typical skewed abutment test results, the transverse displacement was in the direction of the obtuse side of the backwall for the 30° skew test. The maximum vertical displacement was upward for the 0° skew test. The high shear resistance of the CLSM on the backwall made it reasonable to see the 30° skew test's transverse displacement in the direction of the obtuse side of the backwall. Also, the movement was so small it was nearly insignificant. Furthermore, it was expected that the lighter backwall used in the 0° skew test would be displaced vertically more easily than the heavier 30° skewed backwall, and this was the observed result.

Table 4-4. Maximum Backwall Movements

Backwall Movement (in.)		
Test	Transverse Displacement	Vertical Displacement
0° Skew	0.07	0.14
30° Skew	0.16	0.06
Max:	**0.16**	**0.14**

Despite the stiffness of the actuator-backwall loading system, there was differential displacement in each direction. The differential displacement resulted in rotation about each axis. Each of the transverse, longitudinal, and vertical axes are displayed in Figure 4-7.

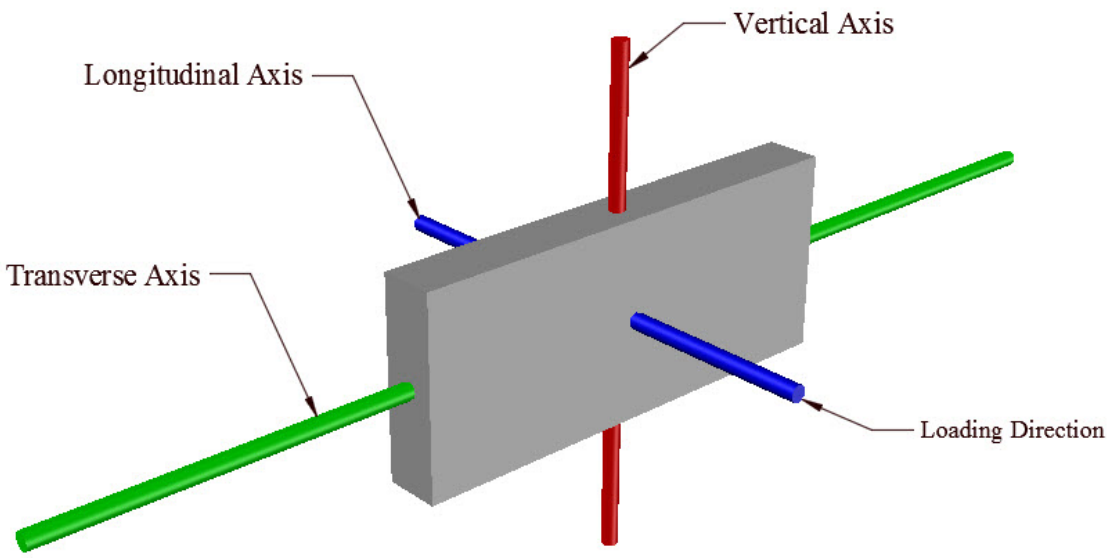

Figure 4-7. Backwall axes of rotation.

The maximum rotations about each axis are listed in Table 4-5. To summarize, the maximum rotation about the transverse axis, caused by differential longitudinal displacement at the top and bottom of the backwall, was 1.92°. In both tests, longitudinal displacement was greater at the bottom than at the top. Rotations about the longitudinal and vertical axes were considerably less. The maximum rotation about the longitudinal axis was due to differential transverse displacement, and was 0.34°. Maximum rotation about the vertical axis was due to differential longitudinal displacement on the right and left sides of the backwall, and resulted in a 0.22° rotation. The rotation about the vertical axis was maximum with a skewed backwall. The rotation was in the direction of the obtuse side of the 30° skewed backwall, which is in agreement with the results discussed in Section 2.4 by Sandford and Elgaaly (1993). However, rotations about each axis were very small.

Table 4-5. Maximum Backwall Rotations

	Backwall Rotation (°)		
Test	Transverse Axis Rotation	Longitudinal Axis Rotation	Vertical Axis Rotation
0° Skew	-1.92	-0.16	+0.12
30° Skew	-1.15	+0.34	-0.22
Max:	**-1.92**	**+0.34**	**-0.22**

4.3 Variations of Forces with Skew Angle

The forces P_L, P_P, P_T, and P_R that were defined in Section 2.3 were plotted against backwall skew angle and the results are shown in Figure 4-8. The longitudinal force, P_L, was simply the load output from the actuator load cell. P_P, the passive force, was calculated using

Equation 2-5. The transverse shear force, P_T, which was applied on the backwall-backfill interface was calculated with Equation 2-6, and the shear resistance, P_R, of the backfill was determined using Equation 2-7. In Figure 4-8, the forces are normalized by the corresponding predicted peak passive forces shown in Table 4-2 for each test. They are then normalized again by the longitudinal force/predicted peak passive force ratio so that the plot starts at 1.

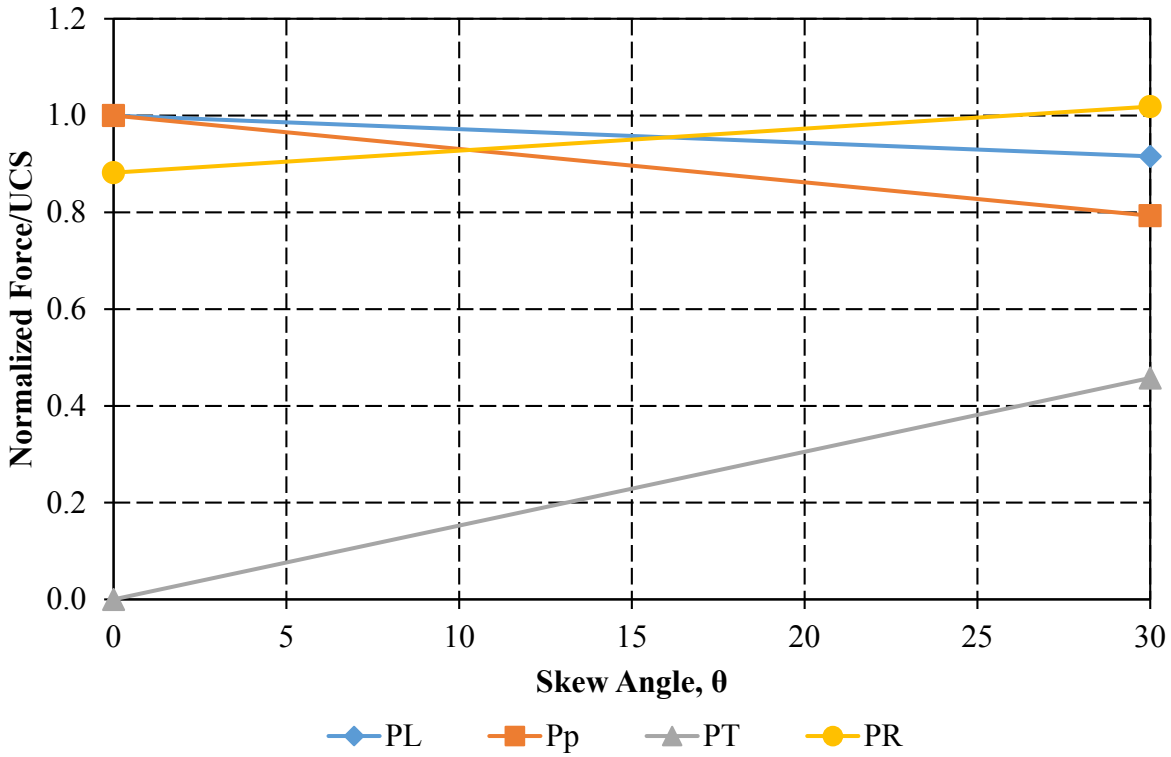

Figure 4-8. Normalized longitudinal, passive, transverse shear, and shear resistance forces vs. skew angle.

It can be seen in Figure 4-8 that the backwall skew angle may have caused a slight reduction in the peak longitudinal and passive forces if it is assumed that the lower passive force is due to skew rather than variation in the UCS. In the worst case, the reduction in peak passive

force would be approximately 20% for a skew angle of 30°. This is much less of an influence than predicted by previous research done on conventional backfill material, which suggests a reduction of peak passive force of approximately 53% for the same skew angle (Rollins and Jessee, 2012).

Furthermore, it was noted that the shear resistance increased with skew angle. Shear resistance, P_R, was calculated using Equation 2-7, but with the zero friction angle assumption the shear resistance was simplified to be cohesion multiplied by the backwall surface area. The surface area increased with skew angle because the length of the backwall-backfill interface was longer for the skewed backwall. This resulted in the shear resistance increasing with skew angle despite the apparent decrease in passive force, P_p. The transverse shear force, P_T, started out at zero with the 0° skew test (as it is a function of the skew angle, θ) and increased for the 30° skew test. However, the shear resistance force, P_R, was still much greater than the transverse shear force, P_T. The very large shear resistance relative to the imposed shear stress explains why the backwall transverse displacements were negligible for both tests.

4.4 Failure Surface Geometries

The failure surface geometries varied for the 0 and 30° skew tests. In both tests, the failure planes weren't manifested on the surface until the peak passive force had been reached and passed. They appeared when the loads were decreasing towards the residual shear strength and the displacements were high. The following subsections will describe and illustrate the failure surface geometries of the two tests.

4.4.1 Zero Degree Skew Failure Surface Geometry

The 0° skew test failure surface included two failure planes that appeared at the surface as shown in Figure 4-9 (Note: each surface square is 6 in. x 6 in.). The first failure plane occurred at approximately 4 ft from the backwall, and it was relatively parallel to the transverse axis. The second failure plane occurred at an angle of approximately 25° relative to the transverse axis. It started along the south wall approximately 5 ft from the backwall face. As the backwall displacement fully mobilized the CLSM failure wedge, the failure surface propagated at the aforementioned angle to a distance of 7 ft from the wall face. From the center of the wall to the failure surface was approximately 6 ft. The failure surface was anticipated to appear nearly parallel to the transverse axis. The rotation about the vertical axis mentioned in Table 4-5 was 0.12° in the counterclockwise direction. This rotation forced the backwall to displace at a slight skew angle with the north side of the backwall slightly ahead of the south side. The diagonal nature of the failure plane may be explained partially by this rotation. Furthermore, the CLSM itself was very stiff and cohesive, so it is possible that the true failure plane was actually closer to parallel with the transverse axis than shown in Figure 4-9. The diagonal portion of the failure plane along the north side could be just a shallow section of still in-tact CLSM that branched off the true failure plane. Either the rotation of the backwall or the nature of the CLSM itself may have contributed to the diagonal nature of the failure plane.

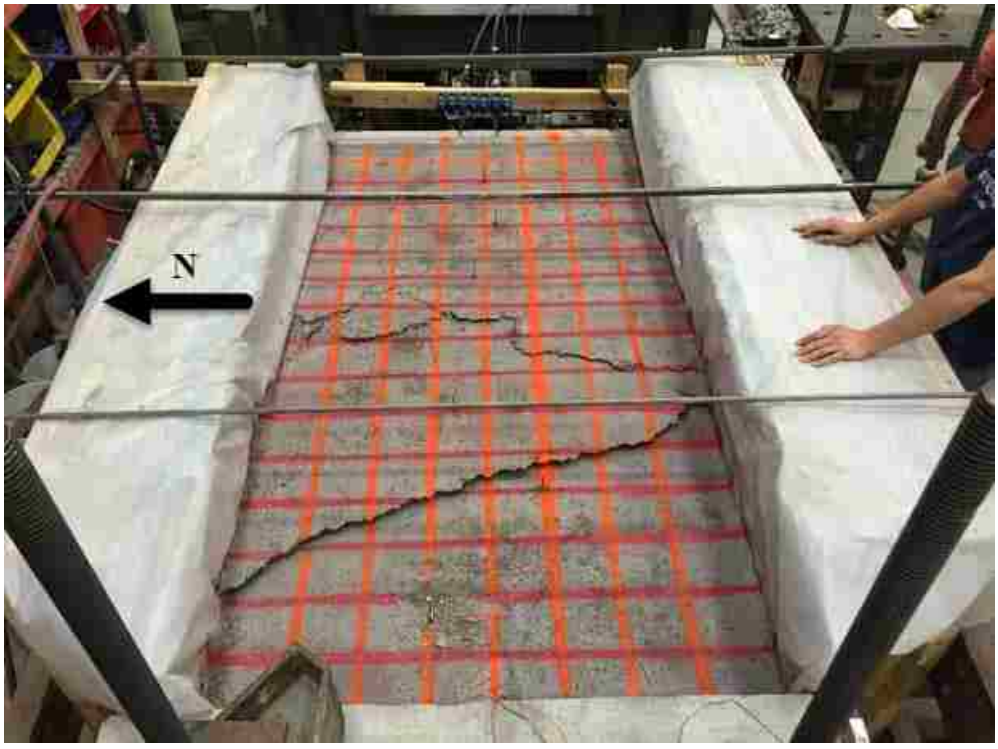

Figure 4-9. Failure surface geometries at ground surface for 0° skew test.

The frame that was built to restrain the actuator and the CLSM required a great deal of labor to install because of space constraints in the laboratory. Consequently, it was left intact after the 0° skew test was concluded to avoid any set up alterations to the 30° skew test. This, however, prohibited examination of the failure surface profile propagating through the CLSM backfill. Hand removal of the backfill required percussion hammer equipment, shovels, and pick axes. The violence of the hand removal process crumbled the brittle CLSM as it was removed, so that no subsurface failure planes could be examined.

4.4.2 Thirty Degree Skew Failure Surface Geometry

Unlike the 0° skew test, the 30° skew test only had one failure plane manifest itself at the surface. It began approximately 3.5 ft from the acute point of the abutment backwall and continued towards the obtuse side at an angle of approximately 20° relative to the transverse axis as shown in Figure 4-10. In the center of the shear area, the failure plane is about 6.0 ft behind the backwall face, which is the same distance where the failure plane ultimately daylighted for the 0° skew.

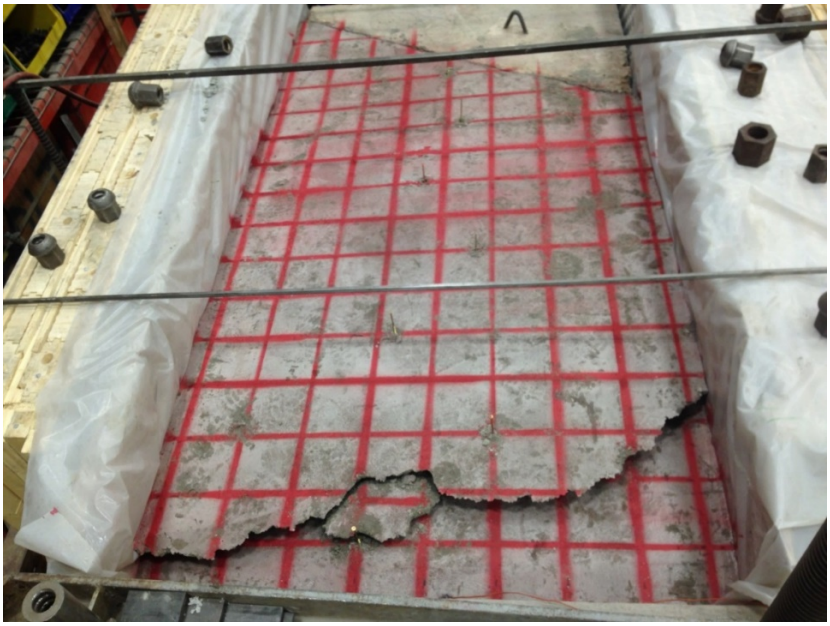

Figure 4-10. Failure surface geometries at ground surface for 30° skew test.

With no further scheduled tests, one side of the reaction frame was removed to examine the failure surface profile propagating through the backfill. The failure surface did not extend below the bottom of the backwall as the Log Spiral lateral earth pressure theory predicts. Instead,

Figure 4-11 shows that the failure plane was nearly linear at an inclination of approximately 23°. With the 0° friction angle assumption, the angle of inclination would be expected to be 45°. The variation in the failure plane inclination could be attributed to the anisotropy of the aggregate in the CLSM mix. The variation of strength depending on the aggregate orientation may have contributed to the difference in the failure plane angle of inclination.

Figure 4-11. Failure surface profile.

Figure 4-12 shows the internal cracks and failure plane with markers placed to highlight them. The middle set of markers is the assumed failure plane, and the top set of markers outlines a crack that propagated off the failure plane. The horizontal set of markers along the bottom show the crack that is evidence of the CLSM being displaced as a block before the failure developed fully. Figure 4-13 shows an isometric view of the described cracks and failure plane.

Figure 4-12. Highlighted failure planes.

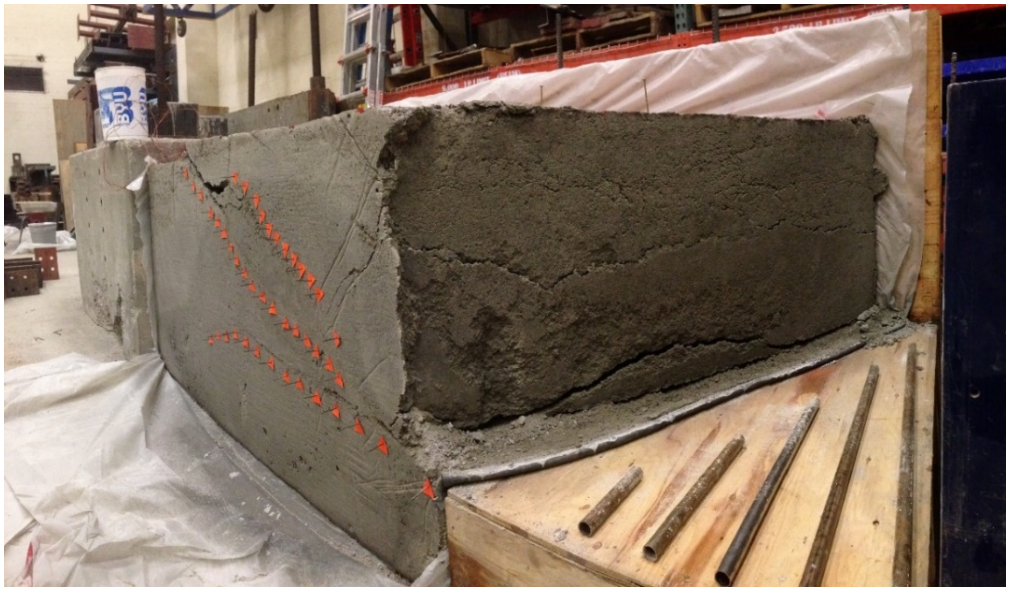

Figure 4-13. Isometric view of the failure planes.

After the failure planes were examined, the hardened CLSM was removed using a forklift and an overhead crane. The forklift forks were inserted in the failure plane then were used to lift the backfill above the failure plane enough to get rigging underneath it so that the crane could remove large blocks of the upper segment CLSM above the failure surface. Once the upper portion was removed, the three-dimensional view of the failure plane could be observed as shown in Figures 4-14 and 4-15.

Figure 4-14. Photograph of the three-dimensional failure surface from the south side.

Figure 4-15. Photograph of the failure wedge from the front or East side.

From the shape of the failure plane, it appears that the skew failure wedge was pushed like a block with no skew. A triangular wedge adjacent to the obtuse side of the wall appears to have moved with the wall and then the failure plane sheared in more of a two-dimensional plane beyond this triangular wedge. As mentioned previously, the shear resistance, P_R, along the backwall was much higher than the applied transverse force, P_T, and this likely caused the CLSM trapped against the obtuse side of the backwall to act as an effective extension of the backwall, which created an effective skew angle closer to 0°. Figure 4-16 shows an illustration of this theory where a triangular block moves longitudinally along with the backwall and reduces the effective skew angle.

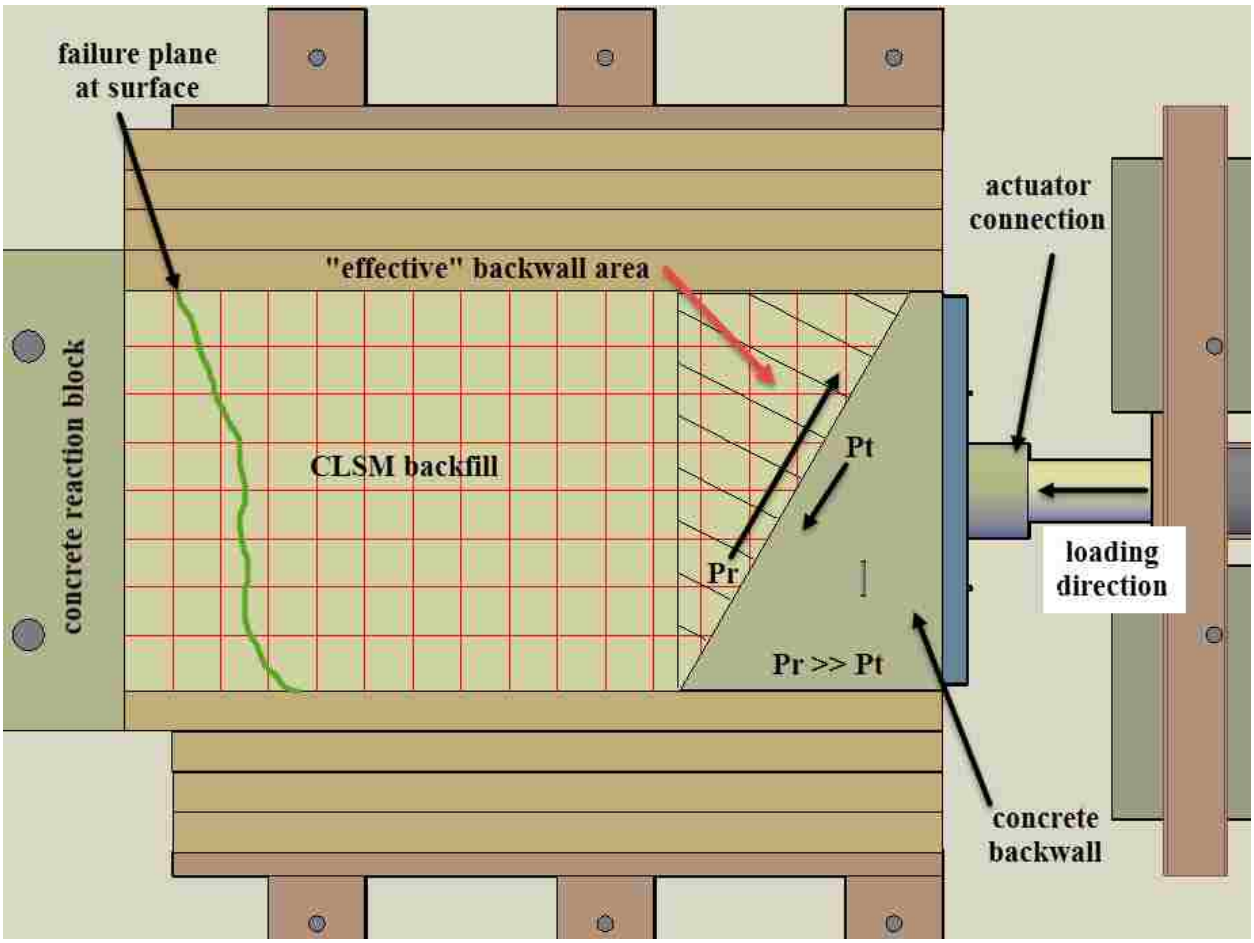

Figure 4-16. CLSM acting as an extension of the backwall.

4.5 Displacement and Strain within Failure Wedge

As mentioned in Section 3.2.2, seven longitudinal string potentiometers were installed at 1 ft (0.3 m) increments to monitor the displacement on the ground surface at different distances from the backwall face. The distance from the backwall face was measured at the ground surface from the center of the backwall-backfill interface. Figure 4-17 is a plot of the normalized displacement as a function of the normalized distance from the backwall face. The maximum displacement at each distance was normalized by the maximum longitudinal displacement of the backwall. The longitudinal distance from the backwall was normalized by the height of the wall.

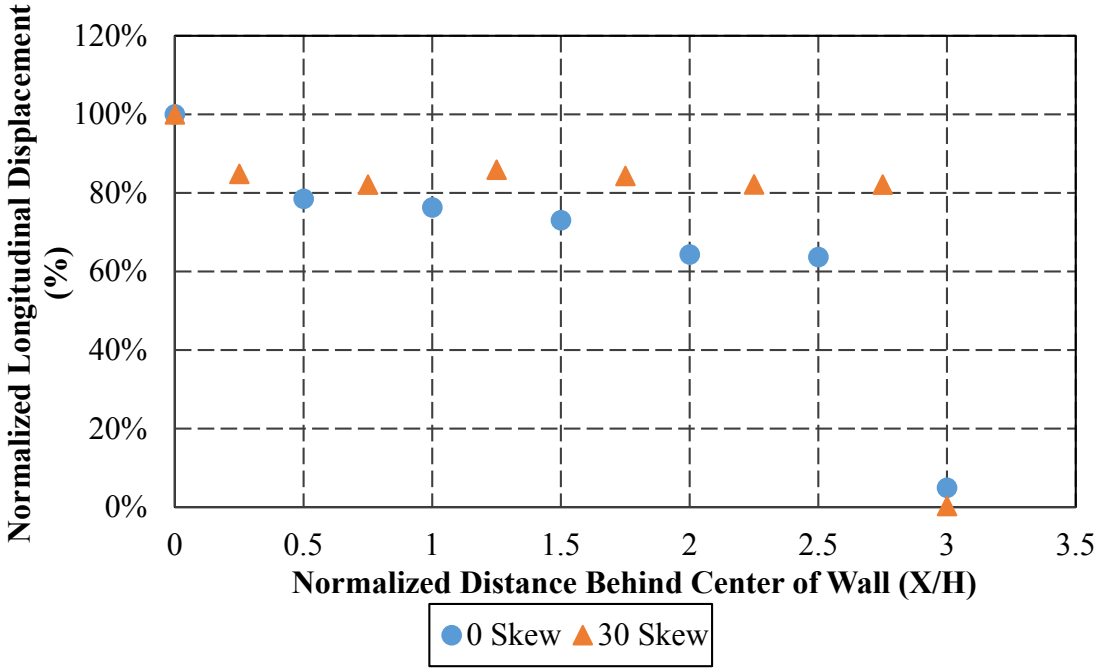

Figure 4-17. Distance from backwall relative to wall height (X/H) versus normalized ground surface displacement.

As can be seen in Figure 4-17, the normalized displacement at a small distance from the backwall face was slightly reduced from the maximum displacement of the wall for both tests. It was reduced to about 85% for the 30° skew test at a distance of 6 in. (0.15 m) from the backwall face, and 80% for the 0° skew test at a distance of 1 ft (0.30 m) from the backwall face. For the 30° skew test, the normalized displacement at greater X/H ratios remained almost constant near 80%. This indicates that the failure wedge moved like a stiff or rigid mass and that the compressive strains within the failure wedge were very low. However, the difference in longitudinal displacements at various X/H ratios was more apparent for the 0° skew test, and thus the results showed more compressive strain within the failure wedge than for the 30° skew test. It should be noted that the normalized displacement in Figure 4-17 decreased to nearly zero once the X/H ratio was beyond where the failure plane reached the surface. This result shows

that there was essentially no movement in the CLSM beyond the failure surface. This occurred at an X/H ratio of approximately 3.0 for both tests. So, both tests' failure planes reached the surface at a distance of approximately three times the wall height from the center of the backwall.

The compressive strain at each point was calculated as the difference in displacement between two adjacent points divided by their initial separation of 1 ft (0.3 m). Figure 4-18 is a plot of the compressive strain as a function of distance from the center of the backwall.

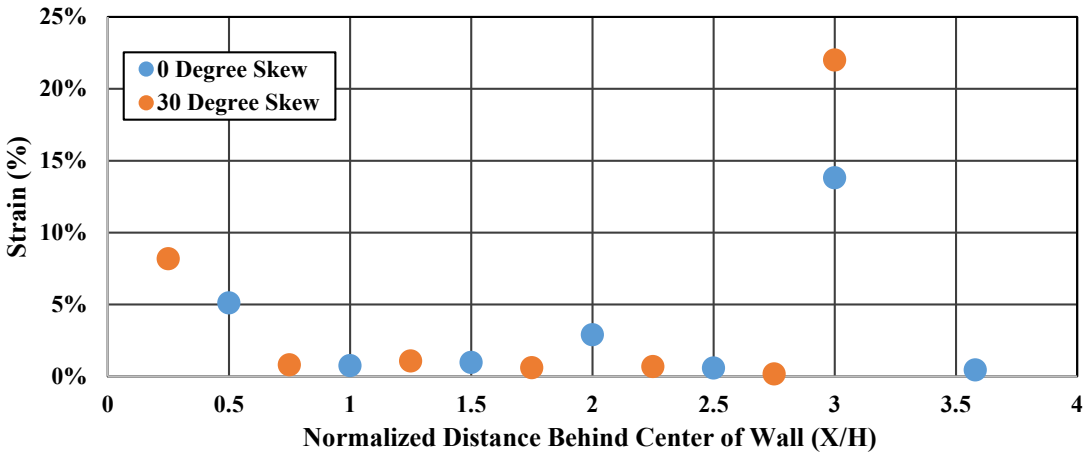

Figure 4-18. Distance from backwall relative to wall height (X/H) versus compressive strain.

The plot shows how the strain variation was very similar for the two tests. The zone nearest to the backwall experienced strains of approximately 5 and 8% for the 0 and 30° skew tests, respectively. Then, the strains decreased significantly through the middle of the failure wedge (typically 1% or less) as it moved more like a block. Once a failure plane developed, the differential movement on either side of the failure plane was significant. This caused the string potentiometer data to calculate high strains where the failure planes appeared at the surface. The

strain values at X/H equal to 3.0 in Figure 4-18 are very high, and likely represent only the strain on the surface but not through the entire wedge. Again, it is interesting to note that the failure surface for both cases appears to be located at about the same normalized distance behind the backwall face.

4.6 CLSM Backfill Surface Heave

A 6 in. x 6 in. (0.15 m x 0.15 m) grid was surveyed with a level promptly before and after the passive force tests were completed. Heave was calculated at each grid point as the difference in the measured elevations before and after the test. The grid point data were input to ArcMap to interpolate heave between grid cells and create the heave contours. Surface heave was greatest where the failure planes cracked the top of the backfill surface. When displacements were large, there was a significant change in elevation at these cracks on the surface. The contours shown in Figures 4-19 and 4-20 show the surface heave from the top view for the 0 and 30° skew tests, respectively. It is worth noting that the surface heave in the triangular area at the obtuse side of the backwall in Figure 4-20 is very low. This strengthens the hypothesis described in Figure 4-16 that the CLSM in this zone acted as an effective extension of the backwall. It should be pointed out that some of the grid points near the surface cracks were actually covered by the displaced failure wedge, so the survey was taken at the closest possible point to the covered grid point. However, in the zone beyond these surface cracks there was almost always nearly zero measured heave. This explains why some of the contours for the 0° skew test in Figure 4-19 show zero heave right along the surface crack. Generally, the contours show the locations of the failure planes fairly well and illustrate the two-dimensional failure surface parallel to the transverse axis.

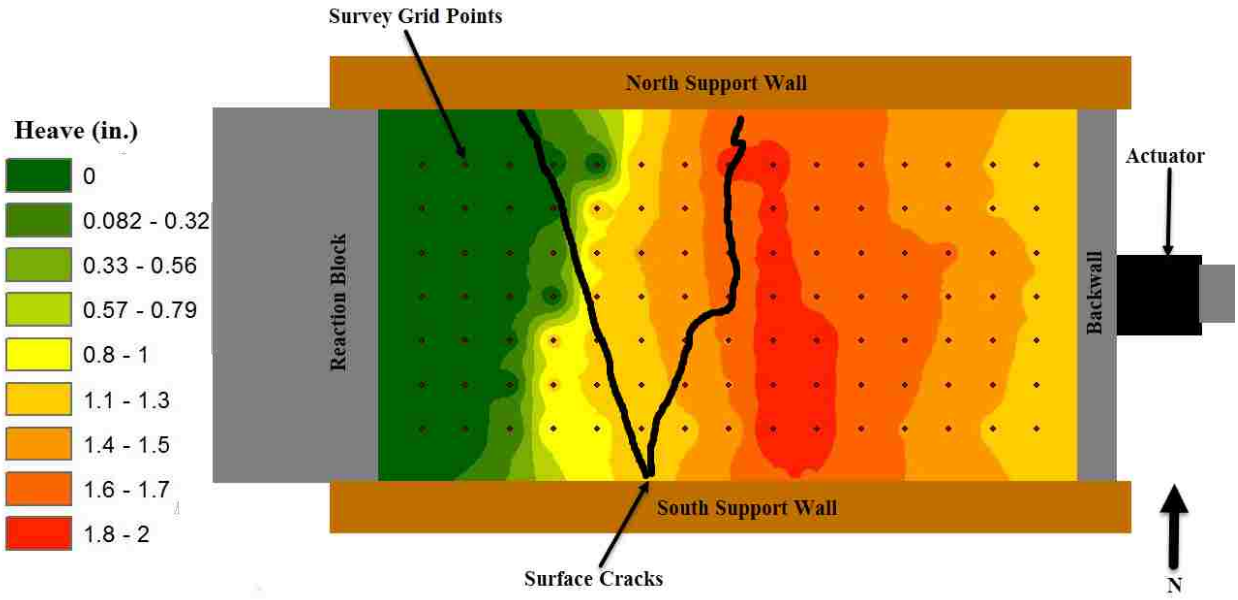

Figure 4-19. Surface heave contours for the 0° skew test.

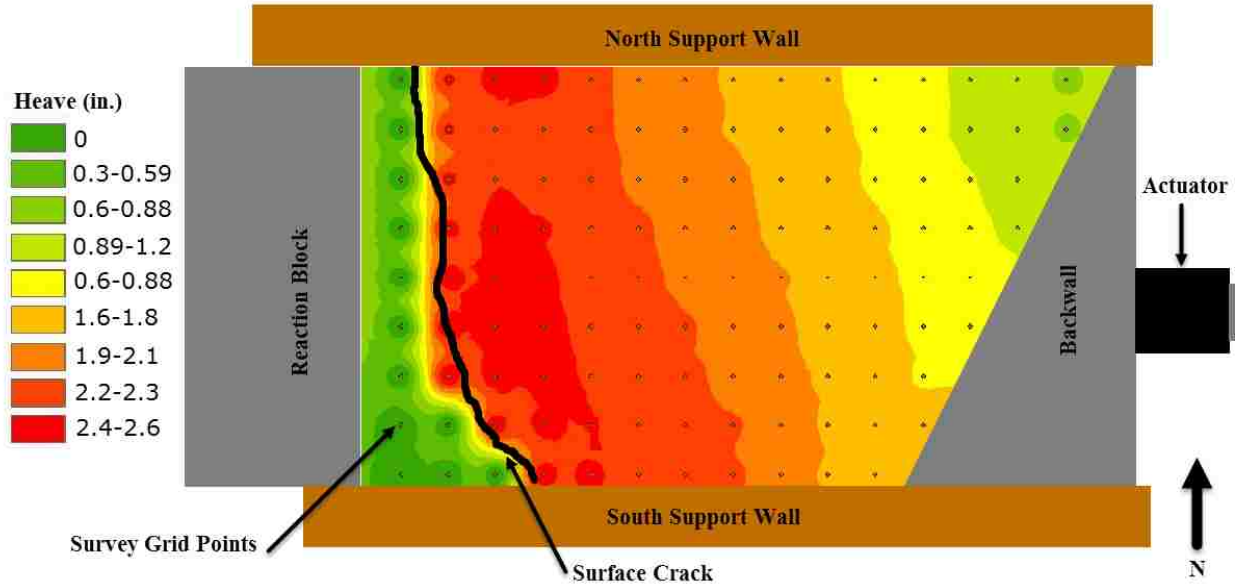

Figure 4-20. Surface heave contours for the 30° skew test.

5 ANALYSIS OF TEST DATA

The passive force-displacement curves were generated using the program PYCAP (Duncan and Mokwa 2001). The program uses the Log Spiral method to predict the curves, but with the assumption that the friction angle of the CLSM is 0°, the passive earth pressure coefficient, K_p, is equal to 1.0 regardless of the method used. Thus, the Rankine, Coulomb, and Log Spiral methods all predict the same passive earth pressures based on Equation 2-2. This chapter describes the input parameters used in the analysis and compare the results from PYCAP to the results measured in the actual tests.

5.1 Computer Program Input Parameters

Table 5-1 summarizes the input parameters used to calculate the passive force-displacement curves in PYCAP. Many of the inputs were found using trial and error within the program to get the best agreement with the measured passive force-displacement curves. The estimates of the spring constant, k, from Section 4.1 were used to provide initial soil modulus estimate values for the two tests. Moduli values of 2500 ksf (120 MPa) and 3100 ksf (148 MPa) for the 0 and 30° skew tests, respectively, were found to give the best agreement with the measured curves. The UCS for the 30° skew test was higher than for the 0° skew test, so it is reasonable that the modulus would be somewhat higher. The cohesion values were simply taken as 50% of the measured UCS as previously discussed. The major difference between

conventional materials and the CLSM was the input for Δ_{max}/H (displacement to reach the peak passive resistance). Duncan and Mokwa (2001) recommend a Δ_{max}/H of 3-4%. This parameter is what governs how much displacement is required for the hyperbolic passive force-displacement curve to reach its peak. Using the recommended range of Δ_{max}/H for conventional, compacted soils produced curves with initial slopes that were much too low and did not peak until the measured curves had nearly reached their residual strengths. The Δ_{max}/H that gave the best agreement with the measured curves was 0.5%. The Poisson's ratio of the CLSM was input as 0.15 as is typical for cement-treated base used in concrete pavement design (Huang 2003).

Table 5-1. PYCAP Input Parameters

Input Parameters		Test	
		0° Skew	30° Skew
cap width,	**b (ft)**	4.13	4.13
cap height,	**H (ft)**	2	2
embedment depth,	**z (ft)**	0	0
surcharge,	**q_s (psf)**	0	0
cohesion,	**c (psf)**	3257	4230
soil friction angle,	**ϕ (deg.)**	0	0
wall friction,	**δ (deg.)**	0	0
initial soil modulus,	**E_i (kip/ft^2)**	2500	3100
poisson's ratio,	**ν**	0.15	0.15
soil unit weight,	**γ_m (pcf)**	122	112.5
adhesion factor,	**A**	1	1
Displacement,	**Δ_{max}/H**	0.005	0.005

5.2 Analysis of Computer Program Results

The passive force-displacement curves computed by PYCAP are plotted together with the measured curves in Figure 5-1. The results show that there is good agreement between the PYCAP prediction and the measured results until the peak is reached. In the measured passive force-displacement curves, the strength dropped to a residual or ultimate value very quickly after peaking, but the PYCAP spreadsheet, which uses a hyperbolic curve to model the passive force-displacement curve, cannot account for this drop in strength. The resulting spring constant, k, values for the 0 and 30° tests were 1500 kip/in (2.6 MN/cm) and 1890 kip/in (3.3 MN/cm), respectively. The initial estimates of k from the measured data were approximately 1300 kip/in (2.3 MN/cm) for the 0° skew test and 1900 kip/in (3.3 MN/cm) for the 30° skew test. There was good agreement between the PYCAP computed stiffness values and the measured values.

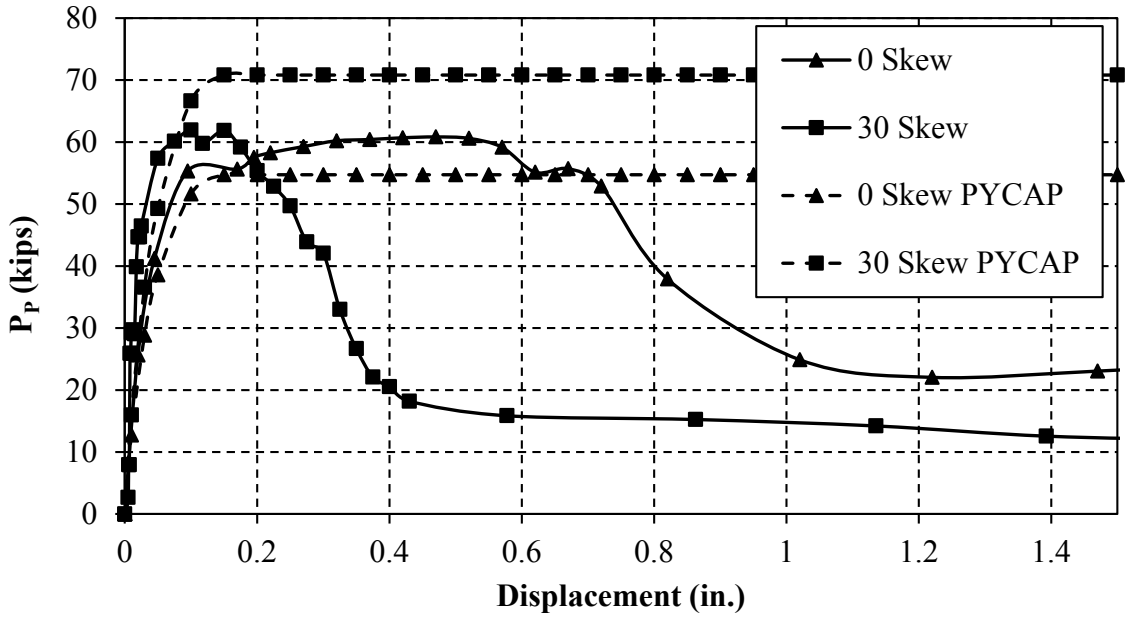

Figure 5-1. PYCAP vs. measured passive force displacement curves.

The stiffness for the CLSM is much higher than for typical sand and gravel backfill materials. Table 5-2 is reproduced from Duncan and Mokwa (2001) and it shows the recommended initial moduli, E_i, values for sands and gravels at shallow depths.

Table 5-2. Typical Modulus Values for Sands and Gravels (Duncan and Mokwa 2001)

Density	D_r	N_{60}	Normally Loaded	Preloaded or Compacted
Loose	40%	3	E_i = 200 - 400 ksf	E_i = 400 - 800 ksf
Medium	60%	7	E_i = 300 - 500 ksf	E_i = 500 - 1000 ksf
Dense	80%	15	E_i = 400 - 600 ksf	E_i = 600 - 1200 ksf

Table 5-2 shows that the modulus values of 2500-3100 ksf (120-148MPa) that were used as the input parameters in PYCAP were approximately two to three times the highest modulus recommended by Duncan and Mokwa for even dense, compacted sand or gravel. This high stiffness and small displacement to reach the peak passive force are signs of the brittle nature of CLSM. The ratio of the UCS of the CLSM to the modulus value computed in PYCAP was nearly identical for the two tests. On average the UCS/E ratio was 0.27% for the two tests. Equation 5-1 relates the modulus value to UCS in a linear form, but Equation 5-2 relates the two parameters using the square root format commonly used for structural concrete. The linear equation

$$E\ (psi) \approx 375 * UCS\ (psi) \tag{5-1}$$

approximates the modulus when the CLSM still has a relatively low UCS strength. This value agrees very well with the correlations made for soil-cement materials of E_{50} approximately 300-380 times the UCS (Filz et al. 2015). However, it is likely more appropriate to approximate the

non-linear behavior of the modulus at higher UCS strengths using the square root equation

$$E(psi) \approx 2696 * \sqrt{UCS(psi)} \quad (5\text{-}2).$$

5.3 Analysis of Skew Effects

The reduction of passive force for CLSM backfill caused by the backwall skew angle is much less than the reduction for conventional backfill materials previously reported (Rollins and Jessee 2012, Marsh 2013). Figure 5-2 shows the normalized displacement versus the normalized passive force. As previously discussed, the passive force was normalized by the peak predicted passive force for each test. With the 0° friction angle assumption, the predicted passive forces were the same for the Rankine, Coulomb, and Log Spiral methods. This caused the two normalized curves in Figure 5-2 from PYCAP to be the same and to peak at exactly 1.0, because PYCAP predicted the same peak passive force as Equation 2-2.

Figure 5-2 shows that the passive force reduction from the 30° skew angle is minimal compared to the results of previous research on conventional granular materials (Rollins and Jessee 2012, Marsh 2013, Franke 2013, Rollins et al. 2015). It is possible that the reduction was not due to the skew angle whatsoever, but that it was actually due to errors in the assumptions made about the CLSM backfill. Assuming that the cohesion was equal to 50% of the UCS and that the backfill cohesion was perfectly represented by the measured strength of the test cylinders may have been the actual contributors to the apparent reduction of passive resistance for the 30° skew test.

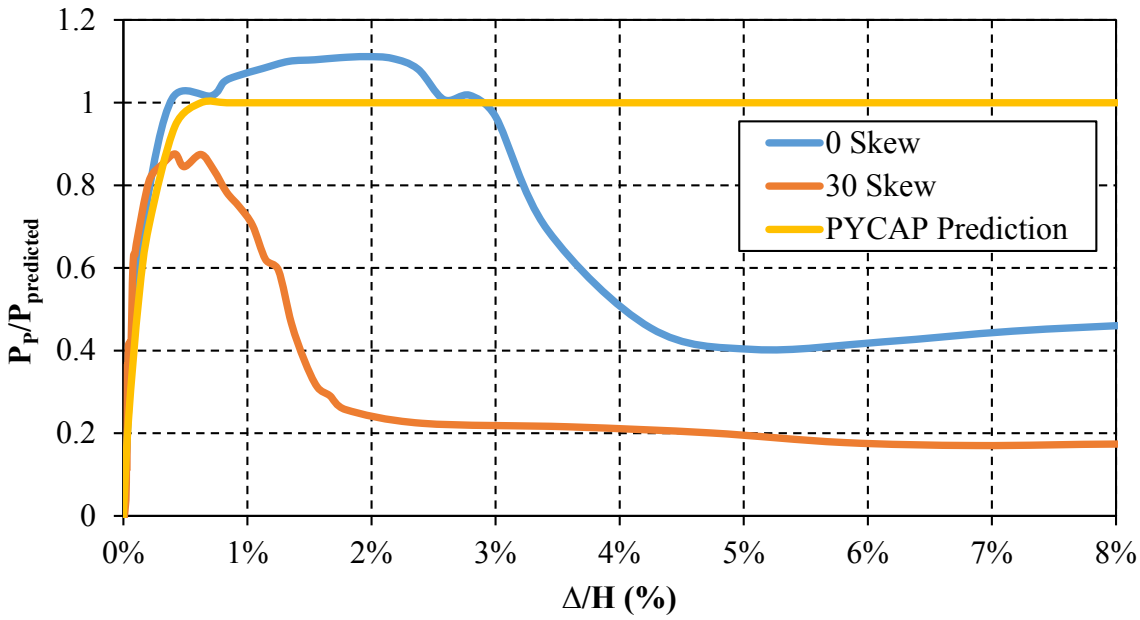

Figure 5-2. Normalized passive force vs. normalized displacement curves.

Figures 5-3 and 5-4 show the measured passive force displacement curves plus three different curves computed by PYCAP. The figures plot the computed curve from PYCAP shown in Figure 5-1, and they also plot the computed curves assuming a 10% increase and decrease in UCS. Figure 5-3 shows that the 10% overestimate agrees very well with the measured passive force-displacement curve for the 0° skew test, and Figure 5-4 shows that the 10% underestimate agrees very well with the measured passive force-displacement curve for the 30° skew test. This agreement shows that predicting the passive force-displacement curves for CLSM should account for a 10% variation in strength.

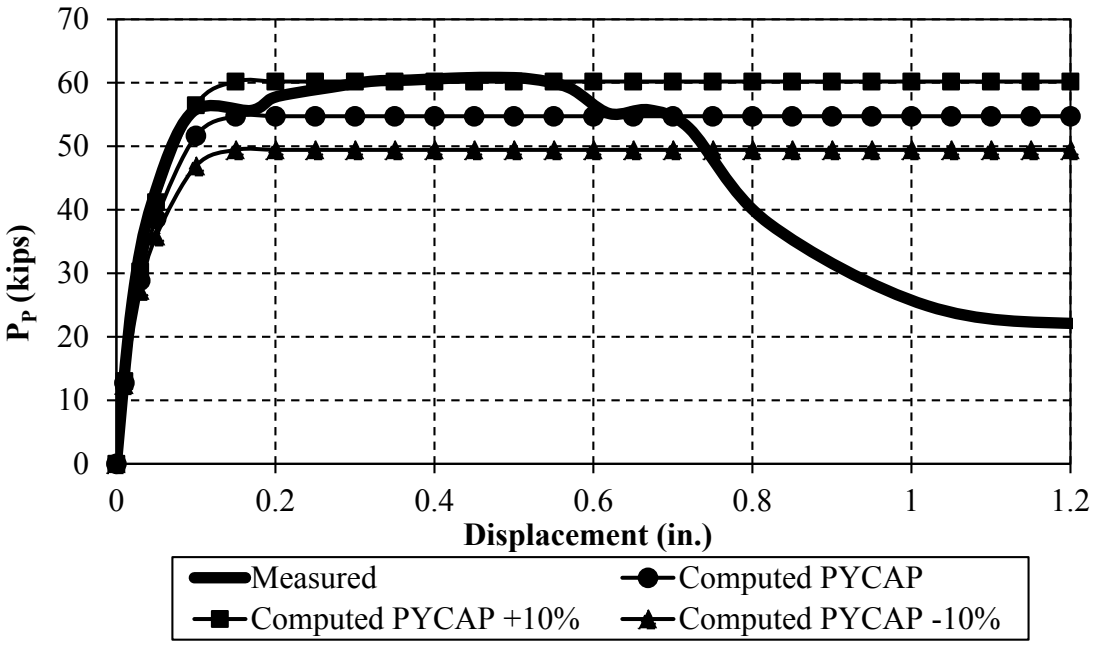

Figure 5-3. Measured and computed passive force-displacement curves for 0° skew test.

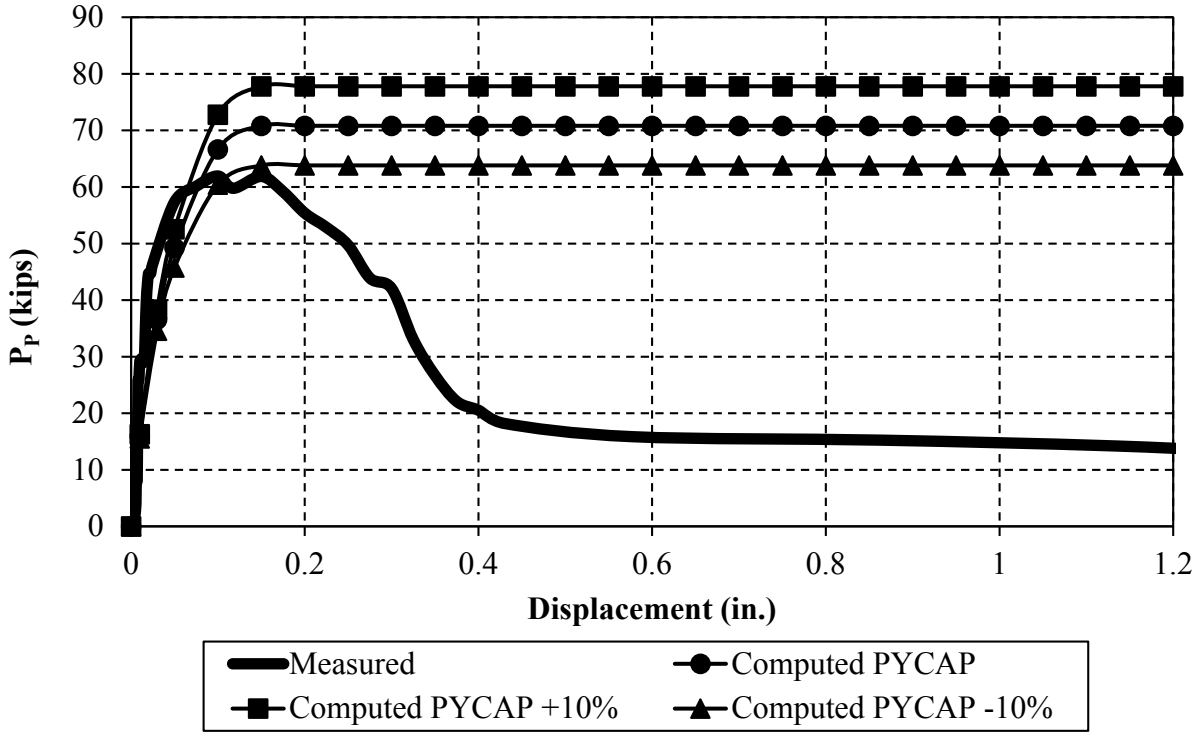

Figure 5-4. Measured and computed passive force-displacement curves for 30° skew test.

5.4 Prediction of Passive Force-Displacement Relationship

Figure 5-5 shows an attempt to empirically model the passive force-displacement relationship for CLSM. Equations were derived and their results plotted to give a visual representation of the equations. The data were limited to only two tests, but Equations 5-3 and 5-4 can provide a very crude estimate of the passive force-displacement curves for abutment backwalls displaced into CLSM.

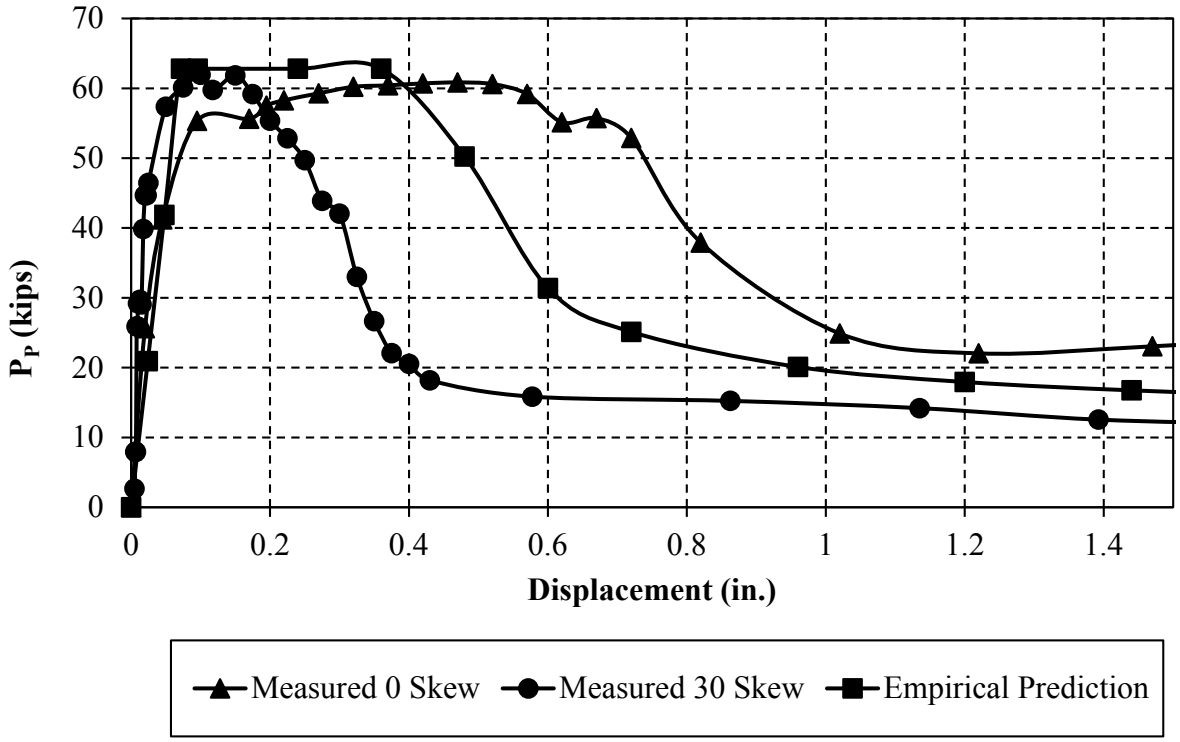

Figure 5-5. Measured and empirically estimated curves.

As shown in Figure 5-5, the empirical curve is made up of three segments: one linear portion, the plateau, and one asymptotic portion. The linear portion of the curve was used from X/H of 0-0.003 and is given as

$$y = A * X/(0.003H) \quad (5\text{-}3)$$

where

$A = P_p \; from \; Equation \; 2-2,$

$X = displacement \; in \; inches,$ and

$H = height \; of \; the \; backwall.$

The inputs used in Equation 2-2 when creating the empirically estimated curve in Figure 5-5 were the average of the two tests' unit weights and cohesion measurements. The width and height remained the same for both.

The plateau portion of the curve is used from X/H of 0.003-0.015. The 1.5% of the wall height was the average displacement required for failure for the two tests. However, the length of this plateau section is the variable with the least clarity. The passive resistance along the plateau was simply the constant value given by Equation 2-2, once again using the average unit weights and cohesion values for the two tests.

The asymptotic portion of the curve is used from X/H of 0.02 and beyond and is given as

$$y = (0.2 * A * X)/(X - 0.015H) \quad (5\text{-}4),$$

and the inputs are the same as for Equation 5-3. The 0.2 factor in Equation 5-4 is what determines the residual strength. This value was found using trial and error with the measured curve. It also corresponds with the observed residual strength of the 30° skew test. It should be

noted that between X/H of 0.015 and 0.02 is where the asymptotic portion of the curve approaches infinity, so it was chosen to start the asymptotic curve x/H of 0.2 and create a smooth curve from X/H of 0.015-0.20.

Though the effect of skew angle was minimal on passive force reduction, it appears to have had a negative impact on the residual strength of the CLSM. These curves and equations provide very crude estimates for the passive force-displacement relationship when using CLSM backfill and their results should be confirmed with further testing. As a whole, the CLSM may provide a good alternative to conventional backfill materials.

6 CONCLUSIONS AND RECOMMENDATIONS

6.1 Summary

The passive force-displacement relationship at the backwall-backfill interface is an important parameter in the design of bridge abutments for seismic loads as well as thermal expansion. Increasing the skew angle of the abutment backwall has been shown to cause a reduction in the peak passive resistance for conventional backfill materials. However, no research had been done to examine the passive force-displacement relationship, nor the effect of skew angle on this relationship, when using CLSM as a backfill material. Two large-scale lateral load tests were performed using a 4.13 ft (1.26 m) wide by 2 ft (0.61 m) tall concrete backwall with skew angles of 0 and 30°. The resisting backfill material was CLSM with an average UCS of 45.2 psi (312 kPa) for the 0° skew test and 58.7 psi (405 kPa) for the 30° skew test. The assumptions made about the CLSM were that it had a friction angle of 0°, that the shear strength was due entirely to the cohesion of the cemented CLSM, and that the cohesion was equal to one half of the UCS. Using 50% of the UCS as the approximate cohesion, the cohesion was 3257 psf (156 kPa) for the 0° skew test and 4230 psf (203 kPa) for the 30° skew test.

6.2 Observations and Conclusions

Several conclusions can be made from these lateral load tests using CLSM and they are listed in the following discussion.

1. The effect of the backwall skew angle had much less of an influence on the peak passive resistance in the CLSM backfill as compared to conventional backfill. Though the CLSM may reduce the negative impact of skew angle on passive resistance, the CLSM had a very significant drop off to residual strength. The residual strength was generally 20-40% of the peak passive force, whereas conventional backfill materials have a much less significant drop off to its residual strength.
2. The displacements required to mobilize the peak passive resistance of the CLSM backfill were from 0.75-2% of the wall height. This is much lower than the anticipated 3-5% displacement suggested in the literature for peak passive resistance in a backfill consisting of conventional backfill material.
3. The passive force-displacement relationship was hyperbolic in shape up to the peak resistance. Both tests showed a similar shaped curve where the load climbed almost linearly with little displacement until it reached the peak passive resistance. The load then dropped off significantly to its residual or ultimate strength. The residual strength was generally reached within displacements of 4-5% of the wall height.
4. The assumption that the shear strength of the CLSM was due entirely to cohesion (the cohesion being approximated as 50% of the UCS) with a friction angle of 0° predicted peak passive pressures that were within ±10-12% of the measured values. It was concluded that the cohesion equal to 50% of the UCS is a good approximation for characterizing the shear strength of the CLSM backfill. This conclusion is consistent with experience for soil-cement materials and other cemented soils.
5. The greatest compressive strain in the failure wedge was apparent very close to the backwall face, but it decreased to a constant of approximately 1-2% throughout the

majority of the wedge until the failure surface daylighted. This indicates that the failure wedge moved rigidly with little internal compressive strain.

6. The spring constant or stiffness, k, was calculated as the initial slope of the passive force-displacement curve. The lateral load test data gave stiffness values of approximately 1300 lb/in. (2.3 MN/cm) and 1900 lb/in. (3.3 MN/cm) for the 0 and 30° skew tests respectively. Using PYCAP to match the measured curves gave back-calculated initial moduli values, E_i, of 2500-3100 ksf (120-148 MPa). This is two to three times the stiffness expected for a dense, compacted conventional backfill. The ratio of UCS to modulus was almost identical for the two tests. The relationship was derived to be calculated as $E\ (psi) = 2696 * \sqrt{UCS\ (psi)}$, or $E\ (psi) = 375 * UCS\ (psi)$.
7. Both tests had failure planes that exited the CLSM fill at a distance from the center of the backwall of approximately 6 ft (1.8m). This gives a distance to backwall height ratio, X/H, equal to 3.0. From observation of the 30° skew test failure wedge, it was noted that the angle of inclination was much flatter than the expected 45° with the 0° friction angle assumption.

6.3 Recommendations for Future Research

To supplement the results of the tests conducted in this study, further research should be done to verify the results and increase the understanding of CLSM even further. First, only two lateral load tests were performed at skew angles of 0 and 30°, so the effect of skew angle on the passive force-displacement relationship when using CLSM as a backfill should be examined at more skew angles. Furthermore, the laboratory tests were constrained to fail in a two-dimensional manner, so tests performed with a backfill zone wider than the abutment will allow

for study of the three-dimensional effects on the passive force–displacement relationship for CLSM. The results from this study should also be verified with lateral load tests simulating a full-scale bridge abutment backwall to evaluate any potential scale effects that might need to be considered.

Laboratory testing of the CLSM should be more in depth. Strain should be monitored during the UCS tests. Also, the anisotropy of the CSLM should be considered by testing the compressive strength in perpendicular directions. Furthermore, the shear strength of the CLSM should also be examined in a triaxial compression test to further examine the frictional versus cohesive strength characterization. The characterization of residual strength due to internal friction could also be analyzed using a critical state soil mechanics model. More precise calculation of the CLSM's modulus value should be verified using a free-free resonant column test that calculates the modulus based on p-wave velocity. Also, the CLSM mix design could include polypropylene fibers to examine how the fibers can increase the amount of strain before failure of the CLSM. Lastly, moisture content should be examined with depth within the backfill zone to monitor the uniformity of curing process

REFERENCES

AASHTO. (2011). Guide Specifications for LRFD Seismic Bridge Design, 2nd Edition.

ACI. (2005). "Controlled low strength material." *Reported by ACI Committee 229*, ACI-229R-99

Brinch Hansen, J. (1966). "Resistance of a rectangular anchor slab." Copenhagen: Danish Geotechnical Institute.

Burke, M. P. (1994). "Semi-Integral Bridges: Movements and Forces." *Transportation Research Record: Journal of the Transportation Research Board*, 1460, 1-8.

CALTRANS. (2010). Seismic Design Criteria, ver. 1.6: CALTRANS, Division of Engineering Services, Office of Structure.

Caquot, A., and Kérisel, J., (1948). *Tables for the calculation of passive pressure, active pressure and bearing capacity of foundations*. Gautier-Villars, Paris.

Cole, R. T., and Rollins, K. M. (2006). "Passive Earth Pressure Mobilization during Cyclic Loading." *J. Geotech. Geoenviron. Eng. Journal of Geotechnical and Geoenvironmental Engineering*, 132(9), 1154–1164.

Coulomb, C. A. (1776). *Essai sur une application des règles de maximis & minimis à quelques problèmes de statique, relatifs à l'architecture*. De l'Imprimerie Royale, Paris.

Das, B. M. (2010). *Principles of geotechnical engineering*. Thomson, Toronto, Ont.

Duncan, J. M., and Mokwa, R. L. (2001). "Passive Earth Pressures: Theories and Tests." *J. Geotech. Geoenviron. Eng. Journal of Geotechnical and Geoenvironmental Engineering*, 127(3), 248–257.

Elnashai, A. S., Gencturk, B., Kwon, O.-S., Hashash, Y., Roesler, J. R., Kim, S. J., Jeong, S.-H., Dukes, J., and Valdivia, A. (2010a). "The Maule (Chile) Earthquake of February 27, 2010: Consequence Assessment and Case Studies." MAE Center Report No. 10-04,

MidAmerica Earthquake (MAE) Center, Department of Civil and Environmental Engineering, University of Illinois at Urbana-Champaign.

FHWA. (1997). “User guidelines for waste and byproduct materials in pavement construction.” *FHWA Publication,* FHWA-RD-97-148.

Filz et al. (2015). “Material properties for analysis of deep mixing support systems.” *Deep Foundations Institute*

Franke, B. (2013). "Passive Force on Skewed Abutments with Mechanically Stabilized Earth (MSE) Wingwalls Based on Large-Scale Tests." M.S. Thesis, Department of Civil and Environmental Engineering, Brigham Young University, Provo, UT. 171

Gabr, M. (2000). “Controlled low-strength material using fly ash and AMD sludge.” *Journal of Hazardous Materials*, 76(2-3), 251–263.

Howard, A. K. (1998). *The design and application of controlled low-strength materials (flowable fill)*. ASTM, West Conshohocken.

Huang, Y. H. (2004). *Pavement analysis and design*. Pearson/Prentice Hall, Upper Saddle River, NJ.

Kitazume, M., and Terashi, M. (2013). *The Deep Mixing Method.* CRC Press/Balkema, Leiden, The Netherlands.

Kumar, J., and Rao, K. S. S. (1997). “Passive pressure coefficients, critical failure surface and its kinematic admissibility.” *Géotechnique*, 47(1), 185–192.

Lemnitzer, A., Ahlberg, E. R., Nigbor, R. L., Shamsabadi, A., Wallace, J. W., and Stewart, J. P. (2009). “Lateral Performance of Full-Scale Bridge Abutment Wall with Granular Backfill.” *J. Geotech. Geoenviron. Eng. Journal of Geotechnical and Geoenvironmental Engineering*, 135(4), 506–514.

Marsh, A. (2013). "Evaluation of Passive Force on Skewed Bridge Abutments with Large-Scale Tests." M.S. Thesis, Department of Civil and Environmental Engineering, Brigham Young University, Provo, UT. 3291

NRMCA. (2015). “Guide specification for controlled low strength material (CLSM).”

PCA. “Controlled Low-Strength Material.” <http://www.cement.org/cement-concrete-basics/products/controlled-low-strength-material> (Feb. 18, 2016).

PLAXIS. (2004). Plaxis V8, R. B. J. Brinkgreve, and W. Broere Eds., Delft, The Netherlands.

Potyondy, J. G. (1961). “Skin Friction between Various Soils and Construction Materials.” *Géotechnique*, 11(4), 339–353.

Puppala, A. J., Balasubramanyam, P., and Madhyannapu, R. S. (2007). “Experimental investigations on the properties of controlled low-strength material.” *Proceedings of the ICE - Ground Improvement*, 11(3), 171–178.

Rajendran, N. (1994) “Contolled Low Strength Materials (CLSM).” *Reported by ACI Committee 229*, ACI-229R-94.

Rankine, W. J. M. (1857). “On the Stability of Loose Earth.” *Philosophical Transactions of the Royal Society of London*, 147, 9–27.

Rollins, K. M., and Cole, R. T. (2006). “Cyclic Lateral Load Behavior of a Pile Cap and Backfill.” *J. Geotech. Geoenviron. Eng. Journal of Geotechnical and Geoenvironmental Engineering*, 132(9), 1143–1153.

Rollins, K. M., and Jessee, S. J. (2013). “Passive Force-Deflection Curves for Skewed Abutments.” *J. Bridge Eng. Journal of Bridge Engineering*, 18(10), 1086–1094.

Rollins, K.M., Palmer, K., and Fredrickson, A., “Reduced Passive Force-Deflection Behavior for Skewed Bridge Abutments.” *Proceedings of the 10th National Conference in Earthquake Engineering, Earthquake Engineering Research Institute, Anchorage, AK,* 2014.

Rollins, K. M., and Sparks, A. (2002). “Lateral Resistance of Full-Scale Pile Cap with Gravel Backfill.” *J. Geotech. Geoenviron. Eng. Journal of Geotechnical and Geoenvironmental Engineering*, 128(9), 711–723.

Sandford, T. C., and Elgaaly, M. (1993). “Skew effects on backfill pressures at frame bridge abutments.” *Transportation Research Record: Journal of the Transportation Research Board*, 1415, 1-11.

Schmitz, M., Parsons, R., Ramirez, G., and Zhao, Y. (2004). “Use of controlled low strength material as abutment backfill.” *Kansas Department of Transportation.,* K-TRAN: KU-02-6.

Shamsabadi, A., Kapuskar, M., and Zand, A. (2006). “Three-Dimensional Nonlinear Finite Element Soil-Abutment Structure Interaction Model for Skewed Bridges.” *Paper presented at the Fifth National Seismic Conference on Bridges & Highways, San Francisco, CA*.

Soubra, A.-H. (2000). “Static and seismic passive earth pressure coefficients on rigid retaining structures.” *Canadian Geotechnical Journal Can. Geotech. J.*, 37(2), 463–478.

Steinberg, E., Sargand, S. M., and Bettinger, C. (2004). “Forces in Wingwalls of Skewed Semi-Integral Bridges.” *J. Bridge Eng. Journal of Bridge Engineering*, 9(6), 563–571.

Terzaghi, K. (1943). *Theoretical soil mechanics*. J. Wiley and Sons, Inc., New York.

Terzaghi, K., and Peck, R. B. (1996). *Soil mechanics in engineering practice, 3rd Editon*. Wiley, New York.

Toro, Felipe, et al. (2013) "Statistical Analysis of Underpasses Damaged During 2010 Chile Earthquake." *Seventh National Seismic Conference on Bridges and Highways, Paper B3-1*

Türkel, S. (2007). “Strength properties of fly ash based controlled low strength materials.” *Journal of Hazardous Materials*, 147(3), 1015–1019.

Wilson, J., (1999) “Flowable fill as a Backfill for Bridge Abutments.” *Wisconsin Department of Transportation.*

Zhu, D.-Y., and Qian, Q. (2000). “Determination of passive earth pressure coefficients by the method of triangular slices.” *Canadian Geotechnical Journal Can. Geotech. J.*, 37(2), 485–491